‘Influence of 2D and 3D schematizations of heterogeneous subsurface in the modelling of critical groundwater conditions under dikes’

An assessment in relation to the safety of the dike section between Wijk bij Duurstede and Amerongen (The Netherlands)

Ylva Veldhuis

Utrecht University

‘Influence of 2D and 3D schematizations of the heterogeneous subsurface in the modelling of critical groundwater conditions under dikes: an assessment in relation to the safety of the dike section between Wijk bij Duurstede and Amerongen (The Netherlands)'

MSc Thesis
September 2019 – April 2020

Author: Ylva Veldhuis
Students number: 4142918
E-mail: y.n.veldhuis@students.uu.nl

First supervisor: Rens van Beek
Second supervisor: Teun van Woerkom

MSc Programme Earth Surface and Water
Faculty of Geosciences
Department of Physical Geography
Utrecht University, the Netherlands

Abstract

In low-lying areas such as the Netherlands the land is protected from floods and high tides by a flood protection system. The safety of the dikes part of this system are threatened by collapse, which can be caused by the dikes structural integrity under the increased loads imposed on it during a high water event. In particular, increased groundwater flow can lead to the formation of critical pore pressures that can either lead to internal erosion resulting in undermining of the dike by piping, or to slips in the inner or outer slopes of the dike. In order to assess the stability of dikes, information on groundwater flow patterns is thus essential. Under the imposed gradients, these patterns are strongly dependent on the geological structure and hydraulic properties of the subsurface. The variation in thickness of the subsurface layers and the continuity of these layers affect the pore pressure and the seepage of the groundwater.

This research investigates how the groundwater flow conditions around and underneath dikes, with a highly heterogeneous subsurface, influence the hydraulic head under normal and high water conditions in the river. Subsequently, the hydraulic head of the 3D model can be compared to the hydraulic head of the 2D model, which schematization has the same boundary conditions and input values as the 3D model. The aim of this research is to explore differences between 3D and 2D modelling in hydraulic heads and groundwater flow paths around a dike during characteristic conditions and a high water event. The investigation takes place on the dike between Wijk van Duurstede and Amerongen. The tool that will be used in this research is a 3D groundwater model in iMOD which is reduced to two dimensions.

The results indicate strong differences between the 3D groundwater model and 2D groundwater model. The hydraulic head distribution shows different behaviour in terms of dimensions:

- The behaviour changes with the distance from the river. A higher difference between the models is observed in the hinterland compared to the river.
- The higher the discharge, the more the behaviour can change around the river as well.
- The depth at which the results are observed show a higher difference deeper into the subsurface.
- The longer the model runs the higher the differences can become. This is mainly in the hinterland.

In terms of underestimation of the 2D model, which can provide false safety if used for dike stability assessments, the following findings were observed:

- Underestimation is highest in the aquifer on days with the high discharge.
- Impermeable clay with an hydraulic conductivity of 0.002 [m/d] has influence on the underestimation of the 2D model.

Concluded can be that a 2D groundwater model mainly overestimates which is OK for dike stability assessments. But the influence of the lithology on the underestimation of the 2D model has not yet been thoroughly determined therefore 3D groundwater model gives a better representation of the hydraulic head prediction in response to the influence in heterogeneity near and under river dikes than a 2D model.

Keywords: Dike stability, groundwater modelling, iMOD, 2D, 3D.

CONTENTS

FIGURES

TABLES

1 INTRODUCTION

1.1 BACKGROUND

In low-lying areas such as the Netherlands the land is protected from floods and high tides by a flood protection system. This system consists of dike rings, a set of dikes, dunes and structures along the coast and rivers to protect the land behind it (hinterland) (Van Der Most et al., 2014). To warrant the safety of these protected areas, each dike has to pass certain safety standards to prevent overtopping and collapse during and following high water events. The height of a dike, required to avoid overtopping, is obtained from the maximum expected water height, and needs to withstand floods with a discharge that can only occur once every 100 to 100.000 years depending on the location of the dike (Lambert et al., 2015; Slijkhuis et al., 2001; Van Der Most et al., n.d.). A future increase in water height needs to be taken into account due to climate change (Lambert et al., 2015), as extreme weather events become more frequent, leading to more recurrent and intensified high water events (Brandl & Szabo, 2013).

As mentioned before, the safety of a dike is also threatened by collapse, which can be caused by the dikes structural integrity under the increased loads imposed on it during a high water event. In particular, increased groundwater flow can lead to the formation of critical pore pressures that can either lead to internal erosion resulting in undermining of the dike by piping, or to slips in the inner or outer slopes of the dike. In short, enhanced groundwater flow and elevated pore pressures occur during a high water event as the water level in the river rises, creating a larger difference between the river head and the polder head. This difference causes more groundwater to seep into the ground under the dike and flow towards the polder situated behind the dike, resulting in an increase in pressure in the ground (de Groot, 2016; Pham-Van et al., 2011).

Not only the magnitude of the high water event is important, also the duration has influence on hydraulic dike failure. Long-lasting high water events show a high potential for hydraulic dike failure, such as piping or internal erosion. Periodic short water events with high loads can cause dike failure by internal erosion on the long term. The aquifer or the top layer can be gradually eroded during these loads. It can be difficult to determine the cause of dike failure because several groundwater processes might be involved, such as seepage, which do not show any external evidence, in addition to form outside invisible structural instabilities (Brandl & Szabo, 2013).

In order to assess the stability of dikes, information on groundwater flow patterns is thus essential. Under the imposed gradients, these patterns are strongly dependent on the geological structure and hydraulic properties of the subsurface. The variation in thickness of the subsurface layers and the continuity of these layers affect the pore pressure and the seepage of the groundwater (Polanco & Rice, 2014; Sloff et al., 2013; Winkels et al., 2018).

Big geological structures can be found in the Rhine-Meuse delta, the Netherlands. The geological layers in this area which are relevant for dike stability have been deposited in the Quaternary period. These layers are a permeable Pleistocene sand layer covered by a less permeable Holocene clay top layer. Due to the geological evolution of this delta, the lithology of the sub-soil shows large variation within the Pleistocene and Holocene layers, thus within the sand and clay layers. Several generations of sandy channel belts can be found in the subsurface due to the influence of sea-level rise, sediment supply and tectonics (Berendsen & Stouthamer, 2002; Sloff et al., 2013). These processes have resulted in an extremely heterogenic subsurface, which is not as straightforward as the schematizations the dike stability assessments often use.

Lithology has a large effect on the groundwater flow pattern and it is important to examine the hydrological impacts of the lithological heterogeneity near and underneath a dike. Under high river water levels, the groundwater often follows similar pathways, divided in three different zones. 1) In the Holocene top layer, groundwater flows gradually from the river towards the toe at the inner side of the dike. The head gradually decreases from the river side to the inner toe side. In the

Pleistocene sand layer there is a larger permeability causing a weaker decreasing gradient of the head than in the Holocene top layer from the river to the inner toe of the dike (Dorst, 2019; Hoffmans & Van Rijn, 2018).

2) The weaker gradient creates a transition zone in the lower part of the Holocene top layer, because the head differs between the layers. This head difference leads to seepage flow. Seepage flow can transport particles within a dike or its base leading to internal erosion, which induces dike failure. Seepage is a three-dimensional (3D) process. Pipes that are created as a result of this process are irregular in shape, they can have a meandering or braided pattern (Hoffmans & Van Rijn, 2018).

3) The head in the lower Pleistocene layer influences the head in the Holocene top layer. When the Pleistocene sand layer has a hydraulic connection with the river and the water level rises, an uplifting pressure is created beneath the impermeable Holocene layer. The increase in pressure in the ground due to groundwater will reduce the friction between the clay and sand layer, which can also lead to dike failure (Allersma & Rohe, 2003). Therefore, the Pleistocene layer must be considered in this research as well.

1.1 Problem statement

By nature, groundwater flow is three-dimensional (3D), 3D should thus be the preferred modelling dimension as water flow in 3D has impact on the stability of the dike (Vandenboer et al., 2014). Still, often 2D models are adopted to assess dike stability for practical reasons and expediency. The direction of the 2D cross-section coincides with the dominant gradients: between the river stage and polder level for groundwater flow and the between the major and minor principal stress in the soil. Therefore, 2D models often suffice to assess stability from a geo-mechanical point of view. Groundwater flow however is controlled by the subsurface structure and properties that vary in three dimensions and that can only be approximated in 2D.

This research will investigate how the groundwater flow conditions around and underneath dikes, with a highly heterogeneous subsurface, influence the hydraulic head under normal and high water conditions in the river. Subsequently, the hydraulic head of the 3D model can be compared to the hydraulic head of the 2D model, which schematization has the same boundary conditions and input values as the 3D model. This comparison aids to analyse the added value of a 3D model in comparison to the 2D model, regarding its importance for dike stability calculations.

1.2 Objectives and research questions

The objective of this research is to quantify information for dike stability assessments. Therefore, this research will simulate pore pressures under dikes under different conditions and model complexities. The aim of this research is to explore differences between 3D and 2D modelling in hydraulic heads and groundwater flow paths around a dike during characteristic conditions and a high water event. This research investigates these differences on dike between Wijk van Duurstede and Amerongen. The tool that will be used in this research is a 3D groundwater model in iMOD which can be reduced to two dimensions.

This research will answer the following research question:

- Does a 3D groundwater model give a more realistic representation of the hydraulic head prediction in response to the influence of heterogeneity near and under river dikes for dike stability assessments compared to a 2D model?

Sub-research questions:

- What input parameters are at least required for an accurate schematization of the subsurface under a dike for a 3D groundwater model?
- What is the hydraulic head distribution under a dike in a 3D groundwater model?

- What is the hydraulic head distribution under a dike in a 2D groundwater model?
- What is the difference in hydraulic heads under and near a dike in space and time between the 2D and the 3D groundwater model?

2 LITERATURE REVIEW

This chapter summarizes the background information. First, the different failure mechanisms due to groundwater flow are discussed. Followed by an elaboration of the soil characteristics and hydraulic properties in the study area. After that the groundwater model schematization and parametrization is explained, and different groundwater models are discussed. The last section gives an overview of the study area.

2.1 FAILURE MECHANISMS

Statistical analyses show that the most common dike failure mechanisms are overtopping and internal erosion (Brandl & Szabo, 2013). Internal erosion occurs when particles within a dike are carried downstream by groundwater flow and is the general term to describe erosion of the soil by groundwater (Hoffmans & Van Rijn, 2018; Polanco & Rice, 2014).

One of the failure mechanisms related to groundwater is sliding of the inner or outer slopes of the dike. Sliding can occur in two ways. Firstly, when the dike is saturated due to high water, and the water in the river falls again, groundwater in the dike cannot drop as fast as the water level in de river because the dike is constructed on less permeable soils such as clays. An over-elevated pore pressure is created which triggers surface sliding on the waterside slope of the dike (Figure 1) (Finsbury et al., 2013, p.1071). Secondly, when the soil is weathered and softened, the cracks that are formed in summer will create a pathway for water in winter. This softening process will lead to surface sliding on the landside slope of the dike (Figure 2) (Finsbury et al., 2013, p.170).

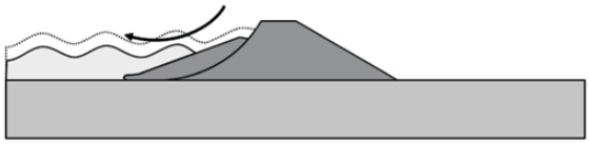

Figure 1: Shallow rotational sliding of the waterside of a dike (Finsbury et al., 2013)

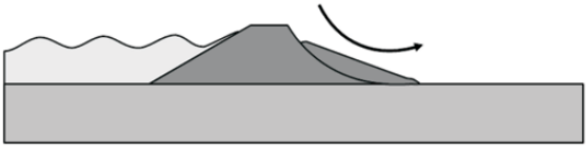

Figure 2: Shallow rotational sliding of the landside of a dike (Finsbury et al., 2013)

When the river is in connection with the permeable lower sand layer, a rise in water level in the river creates an increasing uplifting pressure underneath the impermeable upper clay layer. The pore pressure is increased in the permeable sand layer and the friction between the sand and clay layer will diminish leading to failure of the dike by the uplifting mechanism. In addition, these elevated pore pressures could ultimately lead to piping and undermining (Figure 3) (Allersma & Rohe, 2003).

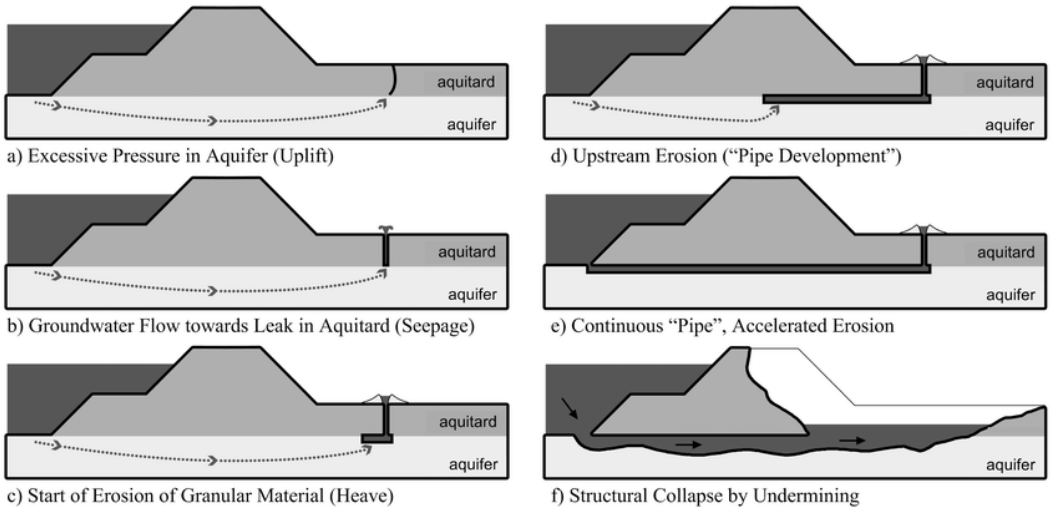

Figure 3: Phases of piping (Schweckendiek et al., 2014).

2.2 GROUNDWATER AND HYDRAULIC CHARACTERISTICS OF THE SOIL

2.2.1 PORE PRESSURE, POROSITY, AND PERMEABILITY

In this section the following characteristics of the soil, relevant for this research, are explained: pore pressure, porosity, and permeability.

The pore pressures, as showed in the previous section, are a main driver for dike failures. Pore pressure occurs as a result of water that is stored within the pores of the soil. The capacity for storing water is defined as porosity. Porosity is a property of the material, and is defined as the percentage of pores in a unit volume. Permeability is related to porosity, it indicates how well pores are interconnected . So clay can have high porosity (up to 90%) but a low permeability, meaning that there is a large capacity for storing water but the water cannot be transmitted easily (Ge & Gorelick, 2015).

The pore pressure can increase or decrease on the basis of groundwater flow. Flow in a saturated zone is guided by pressure differences. In the dike profile and the subsurface layers there is a water level difference from the river to the ditch, with a high river water level and a low inland water level. This difference causes a flow through the dike from the river to the ditch.

The width and the permeability of the dike also plays a part in the vertical cross section of the flow lines. Because of the low permeability of the clay layer located on the top of the natural subsurface the flow is gradual and slow. Due to this low permeability in the top layer there is potential build-up of water pressure in the layer underneath the clay (Polanco & Rice, 2014).

2.2.2 HYDRAULIC CONDUCTIVITY

Because water is the only fluid used in this research the permeability and hydraulic conductivity are used synonymous. Hydraulic conductivity is the ability of the soil to transmit fluid. Where permeability is only a property of the soil, hydraulic conductivity is a property of the soil and the fluid (Dorst, 2019). Hydraulic conductivity depends on the size and shape of the soil particle and often decreases when the grain size of the particle decreases (Hoffmans & Van Rijn, 2018). Often the hydraulic conductivity is equal in the x and y direction meaning the soil is isotropic. The hydraulic conductivity can change in the vertical direction due to vertical difference in texture, structure and porosity of the sediments (Stoop, 2018). Horizontal and/or vertical variability of hydraulic conductivity means that the soils is heterogeneous.

2.2.3 STORATIVITY

In relation to porosity, the amount of water that can be stored in a soil layer can be described by storativity (Ge & Gorelick, 2015). When calculating groundwater fluxes over time, the storativity of the subsurface is important to take into account. Storativity is generally high for sand and gravel, and decreases with increasing clay content.

In confined aquifers the storativity can be described by equation [2]. In unconfined aquifers the storativity is equal to the specific yield (Sy) (Roover, 2015).

$$S = Ss * b \quad [2]$$

S =	Storage coefficient	[-]
Ss =	Specific storage	[m^{-1}]
b =	Layer thickness	[m]

2.2.4 HYDRAULIC HEAD

Hydraulic head is used to describe a groundwater system. It is defined as the mechanical energy per unit weight of fluid. The hydraulic head can be divided into the pressure head and the elevation head. Pressure head is the energy due to pore pressure, elevation head is the energy arising from elevation (Ge & Gorelick, 2015). Water flows along a gradient from high to low hydraulic heads. This hydraulic gradient is the driving force behind groundwater flow. This is proved by Darcy's law equation [1] (Harbaugh, 2005) (Ge & Gorelick, 2015). In equation [1] also the hydraulic conductivity, explained before, is present. The material of the soil is thus leading in the way the groundwater flows.

$$Q = KA \frac{(h1-h2)}{L} \quad [1]$$

Q =	Volumetric flow	[m^3/s]
K =	Hydraulic conductivity	[m/s]
A =	Cross sectional area perpendicular to flow	[m^3]
h1-h2 =	Head difference	[m]
L =	Length	[m]

The hydraulic head can be modelled by several numerical techniques, the finite difference and finite element methods are common techniques for groundwater modelling. Both methods use approximations for boundary conditions and the flow domain is bounded. The two methods have the advantage that the hydraulic conductivity can easily be varied throughout the model system. They are also capable of modelling transient flow.

2.3 SOIL AND SUBSOIL CHARACTERISTICS

Because the safety of a dike is threatened by its structural integrity, it is important to know the exact and complex lithology underneath dikes. The outcome of this research is universal, but there has been chosen to implement lithology of the Netherlands in this research, because a lot of data is available about the paleogeographic evolution of the Rhine-Meuse delta.

2.3.1 PALEOGEOGRAPHIC EVOLUTION OF THE RHINE-MEUSE DELTA

The subsurface of the Rhine-Meuse delta is highly heterogenic and shows large variations in sand and clay layers due to the geological evolution of this area. Due to the influence of sea-level rise, sediment supply and tectonics, several generations of sandy channel belts can be found in the subsurface (Berendsen & Stouthamer, 2002; Sloff et al., 2013). The evolution of the Rhine-Meuse delta will be discussed with a focus on the formations in the study area.

During the quaternary period, in the Pleistocene and Holocene epochs, geological layers important for assessing dike stability have been deposited (Figure 5). In the Pleistocene epoch, during the middle Pleistocene, very coarse sand with gravel was deposited, this sand is highly permeable thus an important groundwater reservoir (Stouthamer & Van Asselen, 2015). During the cold Plen iglacial and Younger Dryas, the Rhine-Meuse delta was dominated by braided channels (Figure 4) depositing coarse to very fine sand (Stouthamer & Van Asselen, 2015). At the end of the Pleistocene epoch a flat, generally westward dipping sand layer existed in the Rhine-Meuse delta.

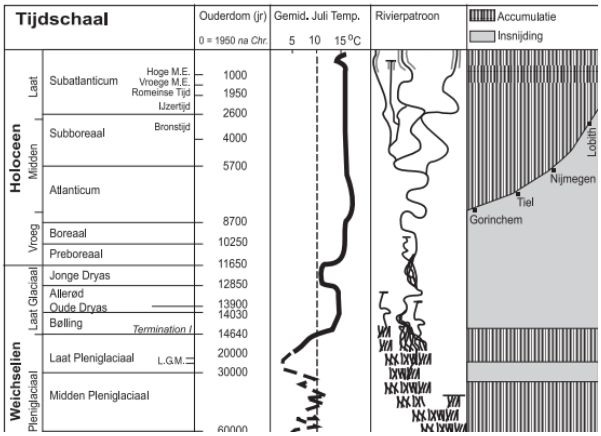

Figure 4: River pattern and climate change in late glacial and Holocene (Cohen, 1994).

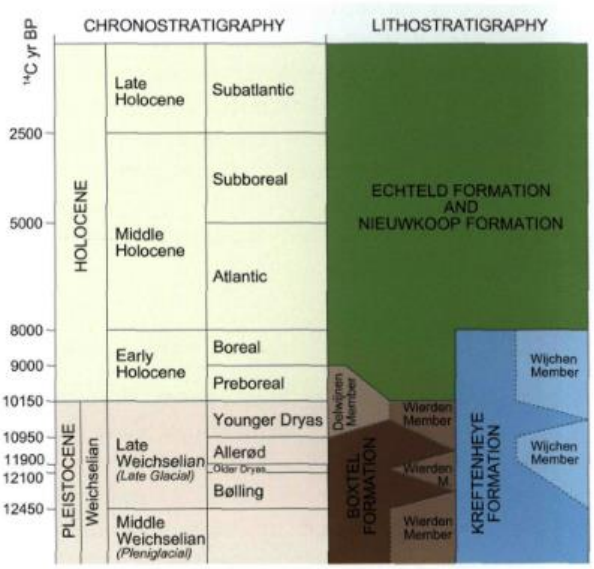

Figure 5: Chronostratigraphy and lithostratigraphy of the Rhine-Meuse delta (Gouw & Erkens, 2007).

During the start of the Holocene epoch the climate warmed causing several events. i) melting ice sheets lead to sea-level rise, due to which the groundwater level in the Rhine-Meuse delta rose as well, creating an area where peat could develop. ii) restoration of vegetation leading to a decrease of peak discharge, creating a change in river pattern from braided to deep incising meandering (Figure 4) (Berendsen & Stouthamer, 2002).

2.3.2 *Variability of the hydraulic conductivity / permeability in the Rhine-Meuse delta*

The events in the Holocene epoch resulted in large variations in grain size and layer properties. All clastic fluvial deposits in the Rhine-Meuse delta from the Holocene epoch are part of the Echteld formation. This formation is divided into 6 units which differ in lithology and geometry, i) channel-belt deposits, consisting of fine to coarse sand, ii) natural dike deposits, consisting of silty and sandy clay, iii) crevasse-splay deposits, consisting of very fine to coarse sand and silty, sandy clay, iv)

channel-fill deposits, consisting of clay, v) flood basin deposits, consisting of clay embedded with peat layers, and vi) dike-breach deposits (Figure 6) (Gouw & Erkens, 2007).

In the Pleistocene layer, located underneath the impermeable Holocene clay layer, the permeability is higher due to the braided river deposits of mainly sand and gravel, meaning that more water can go through in a certain amount of time.

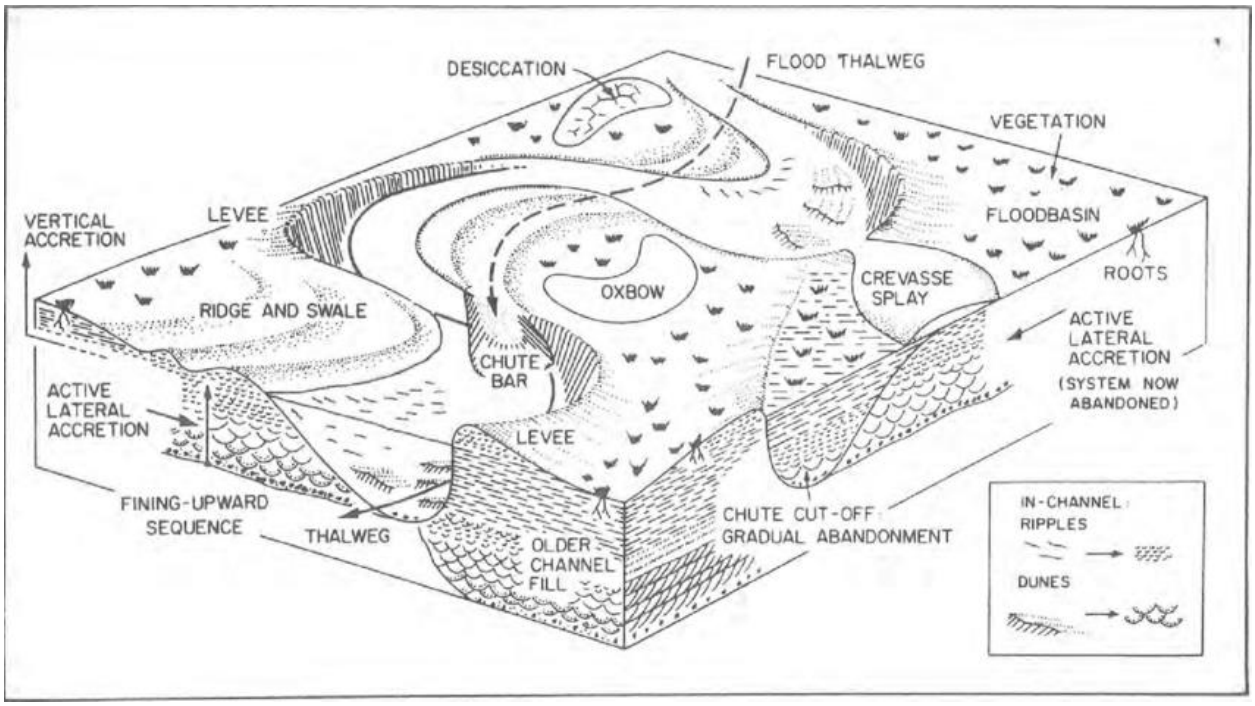

Figure 6: Cross section of a meandering river, showing different morphological elements (Davies, 1991).

3 STUDY AREA

3.1 DESCRIPTION OF THE STUDY AREA

The research is conducted around the dike between Wijk bij Duurstede (x-coordinate: 151.000 y-coordinate: 443.000, RD coordinate map) and Amerongen (x-coordinate: 160.000 y-coordinate: 445.000, RD coordinate map). This dike is located in the Netherlands in the central part of the Rhine-Meuse delta, and stretches for 11 km along the river 'Lek'. The dike is a primary flood defence and is called the 'Lekdijk', and is located between pole 0 and 105 (Figure 7). A dike has been at this location for approximately 1000 years.

90% of the area is below 6 m+NAP, the current river stage in the 'Lek'. A collection of small channels behind the dike controls the water system by weirs and pumps.

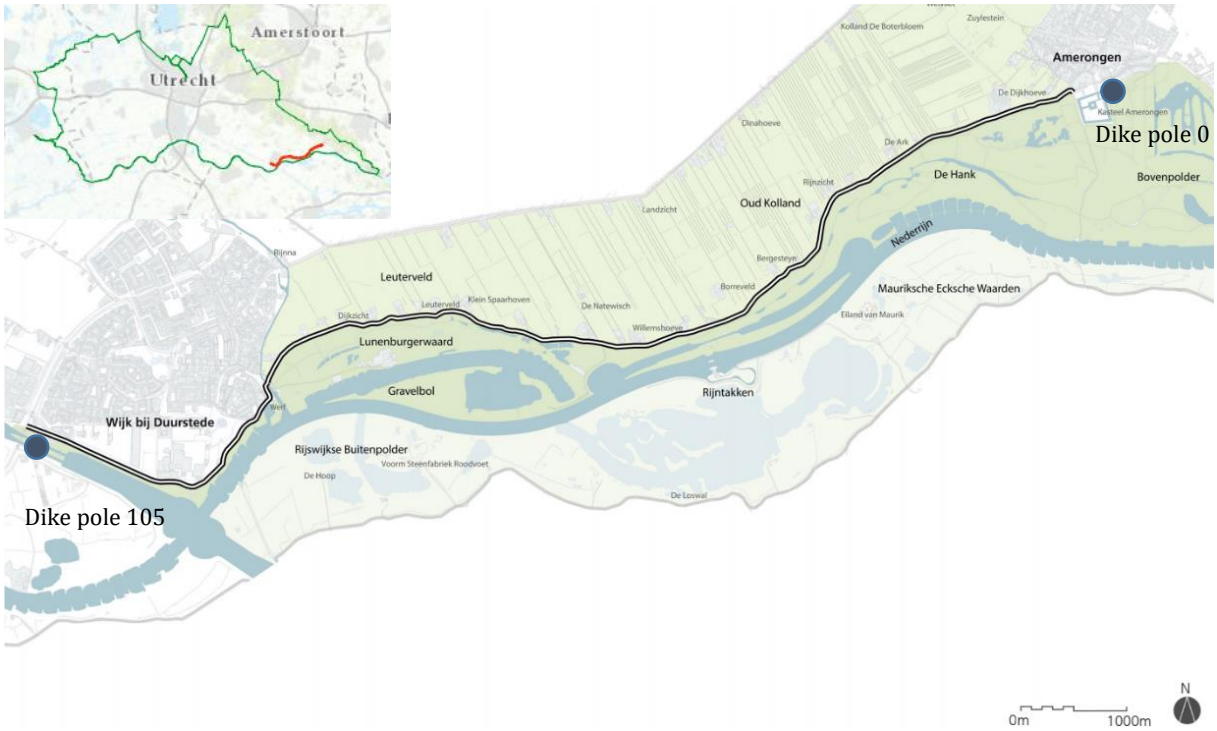

Figure 7: An overview of the study area (WAM rapport, 2018).

Outside the dike near Wijk bij Duurstede at the Lunenburgerwaard are some houses, a marina with a parking lot and an old sand pit located. The floodplain is mostly in use for agricultural purposes. Inside the study area some farms are located, the buildings are all a sufficient distance from the dike, more than 60m. At pole 105 the Prinses Irelensluis is located and at pole 45 'Sluis Amerongen'.

In the surface around this trajectory old dikes and dams can be found, also remnants of dike related structures are present. Near pole 40 two dike breaches have occurred, one of these breaches occurred in 1277, reason unknown (Oudhouten, n.d.) and near pole 5 one dike breach has occurred in the past. These spots are generally weak spots. Near Wijk bij Duurstede and Amerongen the density of the cables and pipes increases.

The dike between Wijk bij Duurstede and Amerongen is part of the 'Sterke Lekdijk' project which started in 2017, in which 55 km of dike is reinforced to meet the new safety standard for dikes. The dike and project are managed by 'Hoogheemraadschap de Stichtse Rijnlanden' (HDSR). The safety of the dike has recently been assessed by HDSR in 2019. The dike has been tested on three failure mechanisms, piping, stability and height of the dike (Figure 8). Almost the whole dike failed for the test of piping. Slumping of the polder-facing side of the dike (binnendijks) failed on between

the poles 14, 42-62, 74-87 and 99-106. The dike does not meet the current standards against overtopping around pole 53-58 and 61-63 (HDSR, 2019).

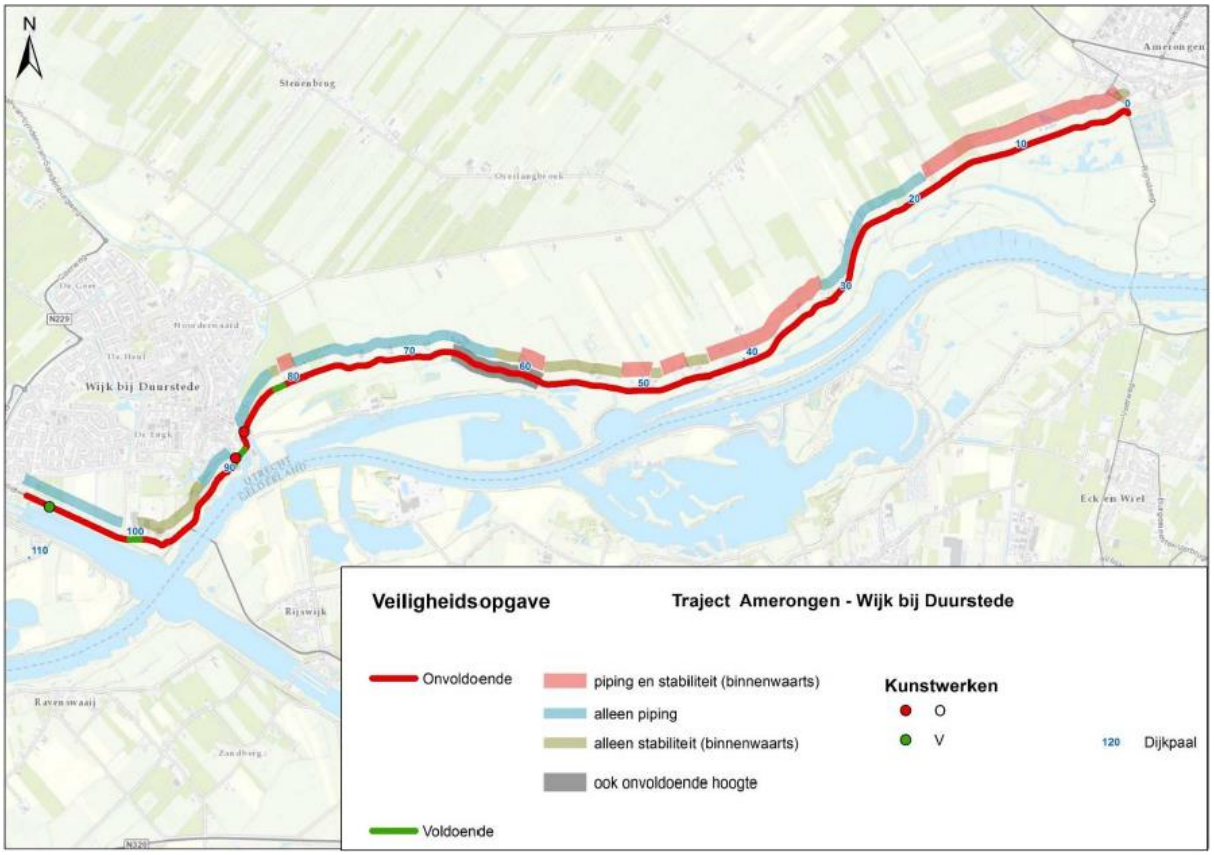

Figure 8: Dike safety analysis performed by HDSR between Wijk bij Duurstede and Amerongen. (HDSR, 2019). ***Onvoldoende = insufficient, voldoende = sufficient.***

3.2 SOIL PARAMETER DATA IN THE STUDY AREA

The large variation in processes during the Pleistocene and Holocene played a role resulted in deposition of various geological units and corresponding subsurface materials in the study area. Their local characteristics and the implications for this study will be explained in this section using the 3D subsurface model GEOTOP developed by TNO. GEOTOP is a 3D database of the Dutch subsoil up to -50m with a resolution of 100 m horizontally and 0.5 m vertically. It includes the lithology and chronostratigraphy (Figure 5) of the subsoil which are determined on the base of corings and cone penetration tests (Sloff et al., 2013).

Two cross-sections are chosen to display the data for the geology and lithology in the study area. The cross-sections are chosen based the past river activity (Figure 9). At cross-section B-B' an old channel belt is located in the inside bend of the present day river. This indicates that a lot of sand has been deposited there and an aquifer is possibly present for my study. The same is for cross-section A-A'. Another reason these two cross-sections have been chosen is for their location in the study area, at the outer side and in the middle of the study area.

The data in cross section A-A' (Figure 10) shows that the Pleistocene sand deposits start a depth of 8 m below NAP (Normaal Amsterdams Peil), NAP is a Dutch ordnance surey datum, which continues until approximately 34 m below NAP. The top half of this sandy material is from the Kreftenheye formation, which has finer sediments at the top and coarser sediments below. In this formation also thin peat layers occur. These deposits contain very little to no clay which creates a low variability between vertical and horizontal permeability (de Groot, 2016). The bottom half consists of the Sterksel formation. At even greater depths clayey deposits of the Waalre formation

are present. At the top the impermeable Holocene deposits are presents, indicated by the different Echteld deposits. These impermeable deposits are present from the surface down to -4 m+NAP.

The data in cross section B-B' (Figure 11) shows that the Pleistocene sand deposits start a depth of 4 m below NAP, which continue until approximately 12 m below NAP. This sandy material is from the Kreftenheye formation. The Sterksel formation is not present in this cross section. At approximately 12m below NAP the Waalre formation is present. At 50m below NAP an impermeable layer of clay is present in the Waalre formation. Because the impermeable characteristics inhibit groundwater flow, this clay layer will serve as boundary for the model domain. Again at the top the impermeable Holocene deposits are present, indicated by four different Echteld deposits, these deposits range from the surface down to -2 m+NAP to -6 m+NAP.

Although these two cross-sections are chosen to display an as accurate as possible idea of the lithology of the study area, it has to be taken in mind that the thickness of these formations such as the Kreftenheye and Sterksel formation change in thickness over the whole study area and may even disappear as you can see from the differences between cross-section A-A' and B-B'. The extent of the different lithological layers may seem random but the reason the different layers of sand are deposited as they are, is all because of the past evolution of the delta. Because of the different kind of deposits in the Echteld formations, the heterogeneity in the top layer is large.

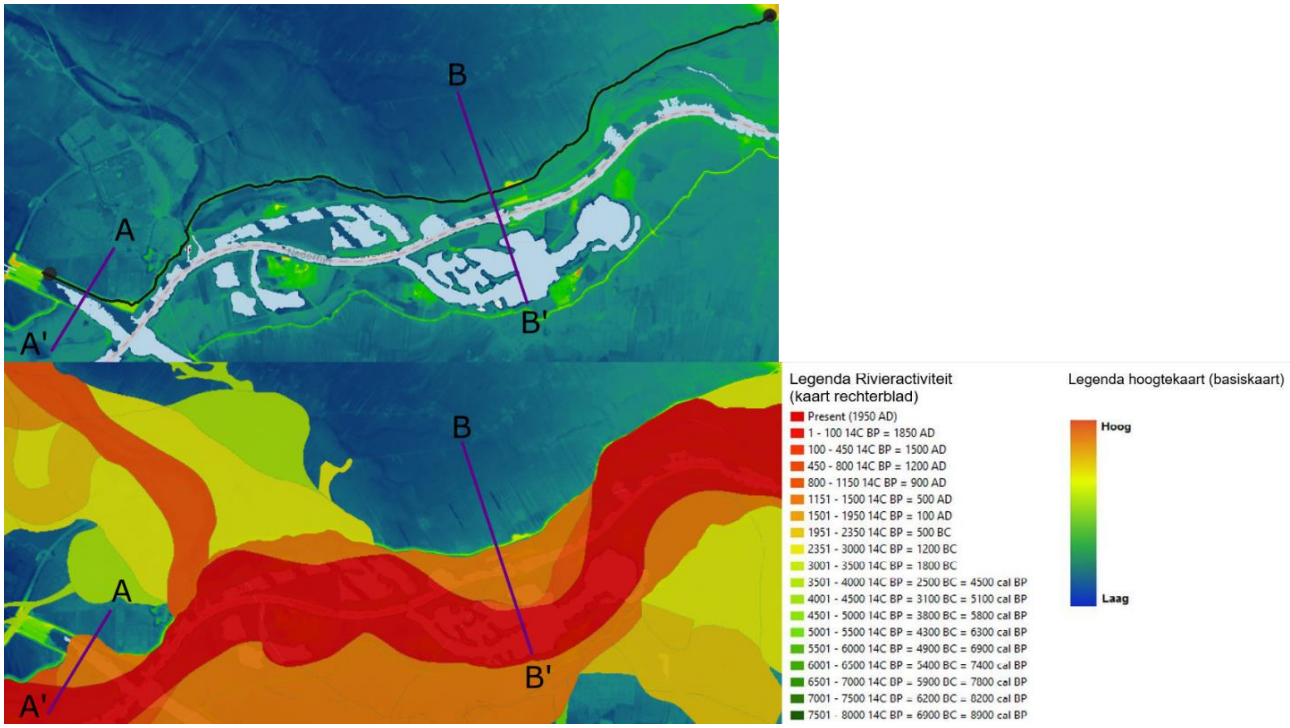

Figure 9: Cross sections used for lithology and geology in figure 6,7. I) top view of the dike trajectory and river. ii) top view of aast river activity (HDSR, n.d.)

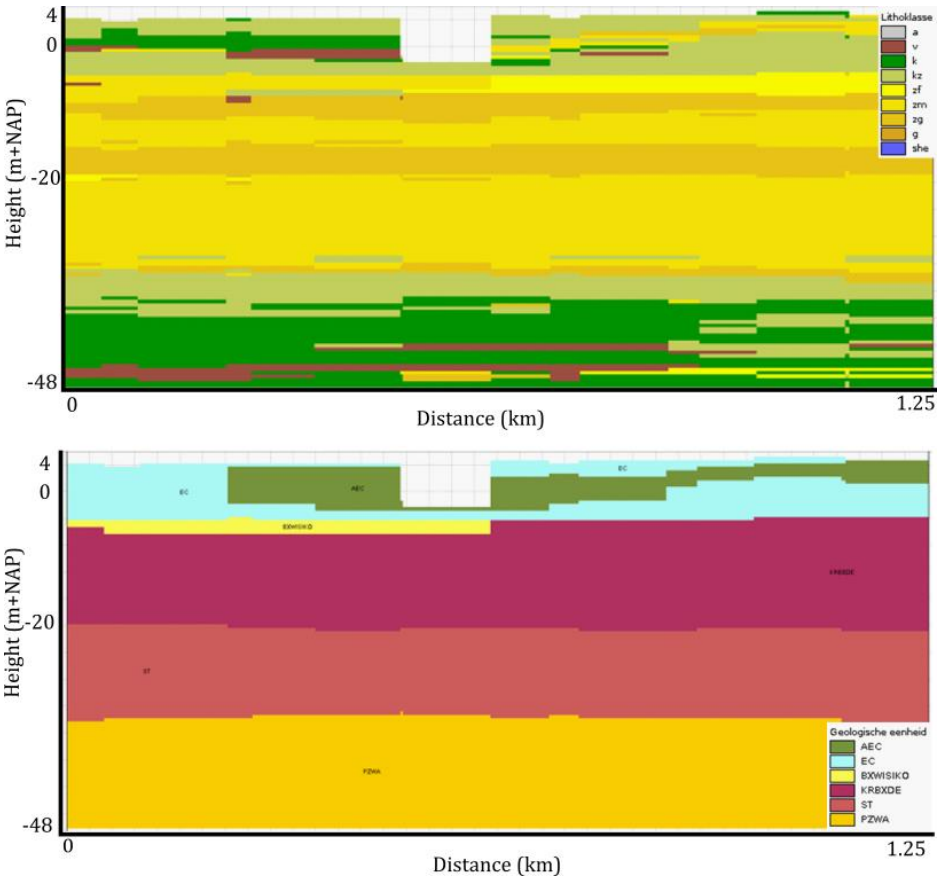

Figure 10: i) Lithology, ii) Geology of cross section A-A'(GeoTOP). AEC and EC are different Echteld formation deposits. BXWISIKO is the Boxtel formation. KRBXDE is the Kreftenheye formation. ST is the Sterksel formation. PZWA is the Peize and Waalre formation.

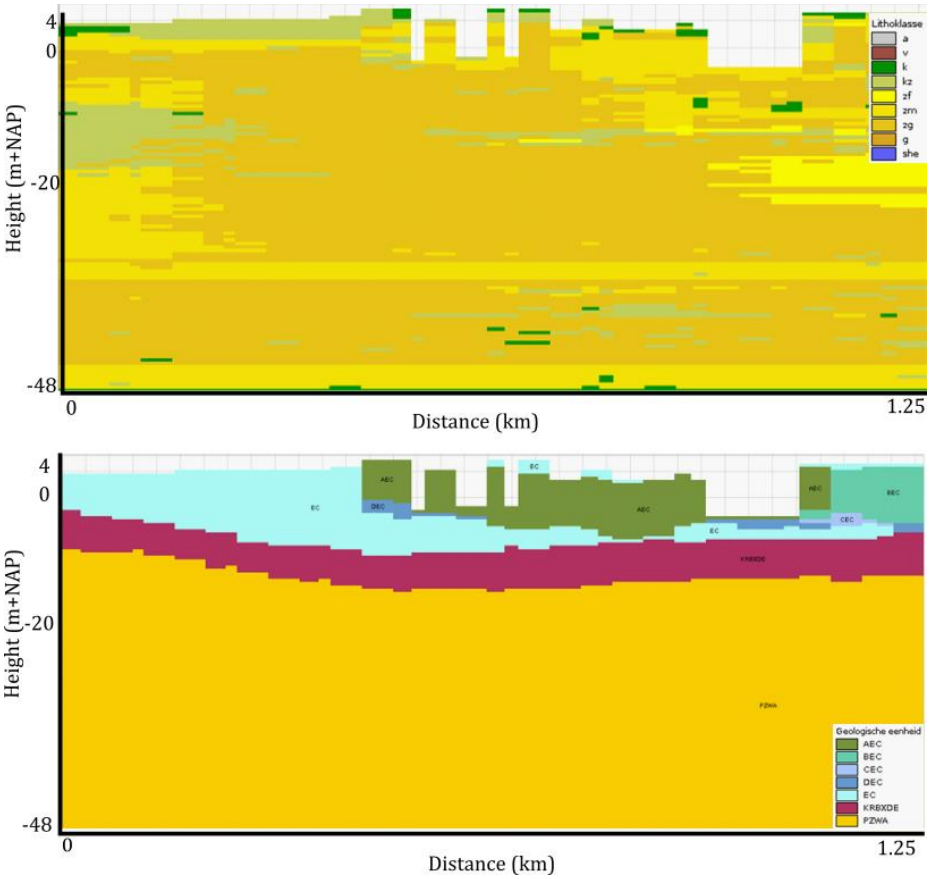

Figure 11: i) Lithology, ii) Geology of cross section B-B' (GeoTOP). AEC, BEC, CEC, DEC, and EC are different Echteld formation deposits . KRBXDE is the Kreftenheye formation. PZWA is the Peize and Waalre formation.

4 MATERIALS & METHODS

This chapter explains the software that is used in this research, shows how the 2D and 3D models are schematized and what input parameters are needed for the schematizations. After that the scenarios for the daily water levels in the Lek are shown. An area of interest is chosen and further zoomed in to.

4.1 IMOD

The software iMOD (interactive MODelling) is used in this research to simulate the subsurface and to calculate the groundwater flow. iMOD is a supra-regional groundwater model that simulates and visualizes the subsurface in 3D (Vermeulen et al., 2013). To execute the groundwater calculations, the software uses MODFLOW. MODFLOW bases its calculations on Darcy's law and the volumetric budget using the finite difference approach.

4.2 SCHEMATIZATIONS

The input parameters were schematized towards the 3D and 2D model. The 3D and 2D models use the same input parameters, the difference between the models are the size of the dimensions.

4.2.1 SCHEMATIZATION OF THE 3D MODEL

The dimensions of the 3D model are 10 000m (width) x 4 000m (length) (Table 1), with a voxel size of 20m x 20m x thickness of model layer indicated in table 2 (depth) (Figure 12).

Table 1: Dimensions of the groundwater models

Dimension	2D model	3D model
1st dimension (length)	4.000 m	4.000 m
2nd dimension (depth)	60 m	60 m
3th dimension (width)		10.000 m

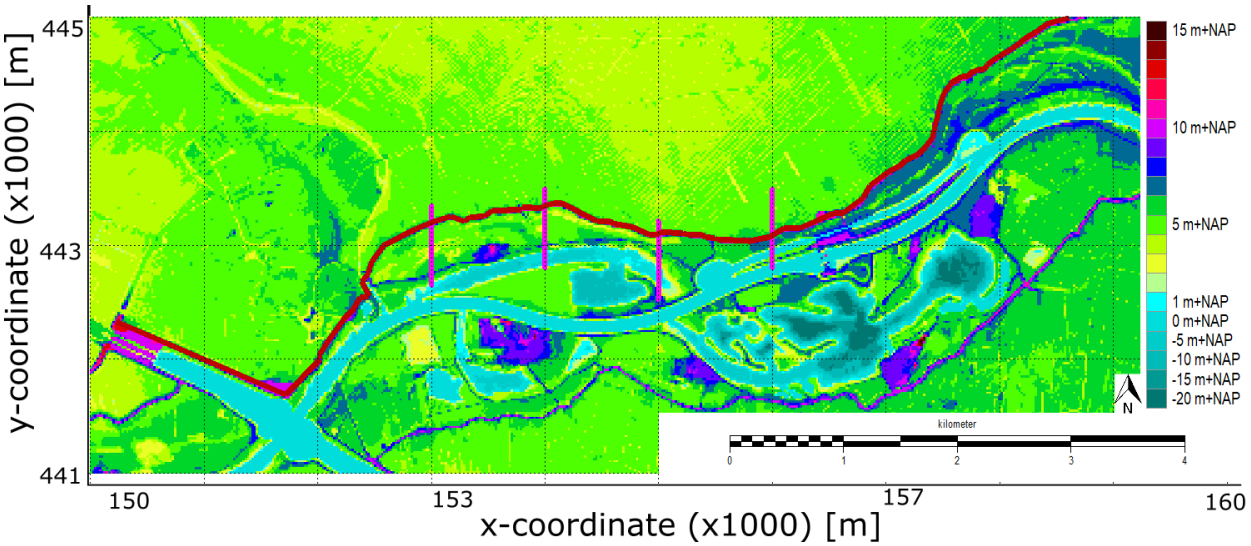

Figure 12: AHN of the 3D model with in red the dike, bathymetry not included. Purple lines indicate the transects used in results.

4.2.2 SCHEMATIZATIONS OF THE 2D MODELS

The dimensions of the 2D models can be found in Table 1, with a voxel size of 20m x 20m x thickness of model layer indicated in table 2 (depth). The 2D model is thus 1 cell wide. The 2D models are vertical cross sections through the study area as depicted in Figure 13.

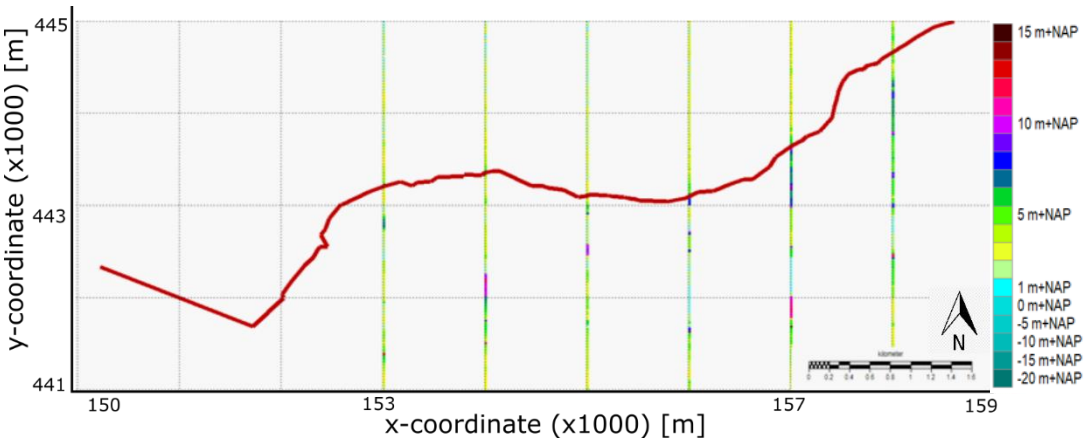

Figure 13: Location of the 6 2D models with in red the dike, visualized with the AHN. Red line indicates the dike.

4.3 INPUT PARAMETERS

The iMOD model needs several input parameters in order to create a model of the subsurface, the information of these parameters is stored in the Input Data File (IDF). The IDF is a raster file and contains the input data for every hydrological and soil parameter at every raster point, more information about the input parameters can be found in the next section. These IDF files are coupled to a parameter in the project manager, creating a project (PRJ) file. This PRJ file can be transformed into a RUN file which refers to the input data and is needed to run the simulation.

iMOD can run two types of simulation, a steady-state and a transient simulation. A steady-state simulation runs until an equilibrium is established in the system. A transient simulation runs over a period of time and observes the changes of patterns during that period. The output of iMOD is one or multiple IDF files, depending on the type of simulation.

In this research the river package (RIV) is used to simulate a river with the surface water higher than the surface level. The drainage package (DRN) is used to simulate the drainage in the polder situated behind the dike. A more detailed explanation of these packages is described in the iMOD manual (Vermeulen & Minnema, 2019).

The first input parameters are the top and bottom values of the model layers. To capture the information with a vertical resolution of 0.5 m from the GEOTOP data base, a subsurface database managed by the Netherlands Organization for Applied Scientific Research (TNO). By the 25 model layers that are adopted in iMOD for computational expediency, the subsurface information is generalized when adjacent materials are similar (similar to a low-pass filter) while at the same time maintaining those materials that stand out from the surrounding areas (similar to a high-pass filter). The schematization of the model layers is achieved using a combination of the 'patatsnijder' and 'dunschiller' approaches (Figure 14). For the top of the first model layer a base file for the 'Actueel Hoogtebestand Nederland' (AHN) is used.

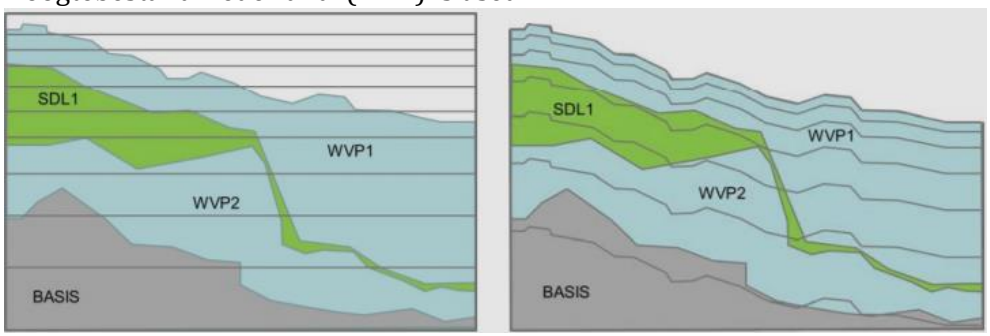

Figure 14: 'Patatsnijder' method (left) vs 'dunschiller' method (right) (Deltares, 2015).

The subsurface of the Netherlands is very complex and it consists of thinning layers, and layers that disappear. MODFLOW takes a long computation time to calculate thinning layers and does not work when model layers have a thickness of 0 m. Therefore, the models are layered by using the

'patatsnijder' method (Figure 14), creating a voxel model. This method uses straight model layers; all layers have a constant distance to a horizontal plane. The advantage of this method is that the modelling grid is consistent. As the model represent a medium sized area, this method can be easily used. Another method which is better for larger models, is the 'dunschiller' method (Figure 14). This method uses model layers with a constant distance from the surface (Deltares, 2015). Due to the fact that iMOD cannot run with model layers with no value for top elevation and bottom elevation, the first seven model layers are a combination of the two methods. See appendix A for an example of the composition of the layers.

The upper 7 model layers all have a thickness of 1 m because the focus of this research is on the upper 20 m. To make the upper layers 1 m thick, the model creates more detailed hydraulic head predictions for these layers. To decrease the computation time, the thickness of model layers increases with depth so that the model consists of less layers. The details of each model layer is listed in Table 2.

Table 2: Details of the model layers in iMOD model.

Model Layer	***Top [cm]***	***Bottom [cm]***	***Thickness of layer***	***Structure of model layer***
1	AHN	600		Dunschiller
2	600	500	1	Dunschiller
3	500	400	1	Dunschiller
4	400	300	1	Dunschiller
5	300	200	1	Dunschiller
6	200	100	1	Dunschiller
7	100	0	1	Dunschiller
8	0	-100	1	Patatsnijder
9	-100	-200	1	Patatsnijder
10	-200	-300	1	Patatsnijder
11	-300	-400	1	Patatsnijder
12	-400	-550	1.5	Patatsnijder
13	-550	-800	2.5	Patatsnijder
14	-800	-1100	3	Patatsnijder
15	-1100	-1250	1.5	Patatsnijder
16	-1250	-1600	3.5	Patatsnijder
17	-1600	-1900	3	Patatsnijder
18	-1900	-2250	3.5	Patatsnijder
19	-2250	-2800	5.5	Patatsnijder
20	-2800	-3400	6	Patatsnijder
21	-3400	-3750	2.5	Patatsnijder
22	-3750	-4150	4	Patatsnijder
23	-4150	-4750	6	Patatsnijder
24	-4750	-4950	2	Patatsnijder
25	-4950	-5000	0.5	Patatsnijder

4.3.1 SOIL PARAMETERS

The parameters of each lithological unit can be described by several parameters (Figure 15: Lithology of the top layer in top view, and the lithology in 3D perspective. The red line indicates the dike.). The location of lithological units are based upon GEOTOP. The parameters of the lithological units are horizontal and vertical permeability (KH & KV) (m/d), transmissivity (KDW) (m^2/d), vertical resistance (VCW) (d) and storage coefficient / specific yield (STO) (-). The soil is assumed to be isotropic, meaning that the horizontal and vertical permeability (Table 3) are the same and based on the values in appendix 1. The values in this research are based on the values used in the Thesis of

Stoop (2018). The Dutch soil is highly variable within and between soil layers. Therefore, the permeability is difficult to determine. Stoop (2018) has done extensive research on the permeability of the soil and used many sources and the hydrogeological model of TNO (REGIS) to determine the permeability in the Dutch soil (Appendix A). The values that Stoop (2018) determined for the Dutch soil are therefore considered reliable and is used in present research. The layer underlying the model domain is considered as an aquitard for modelling purposes, and is therefore assumed to consist solely on clay which is impermeable.

The transmissivity is based on the horizontal permeability and the top and bottom values per model layer. iMOD calculates the values for transmissivity. The vertical resistance is based upon the vertical permeability between model layers and also determined by iMOD (Vermeulen & Minnema, 2019).

The storage coefficient (STO) is the amount of water that can be stored in a cell (Table 2). STO can range from $1x10^{-5}$ to $1x10^{-3}$ [-] (Dorst, 2019; Vermeulen & Minnema, 2019). Specific yield is the storage coefficient for unconfined layers (Table 3).

Table 3: Parameters of lithological units.

	Permeability [m/d]	Storage coefficient [-]	Specific yield [-]
Anthropogenic	0.1	0.0001	0.3
Peat	0.35	0.0001	0.1
Clay	0.002	0.0001	0.1
Sandy clay	0.5	0.0001	0.1
Fine sand	2	0.0001	0.1
Medium sand	5	0.0001	0.1
Coarse sand	25	0.0001	0.1
Gravel	250	0.0001	0.1
Shells	-9999.99	-9999.99	-9999.99

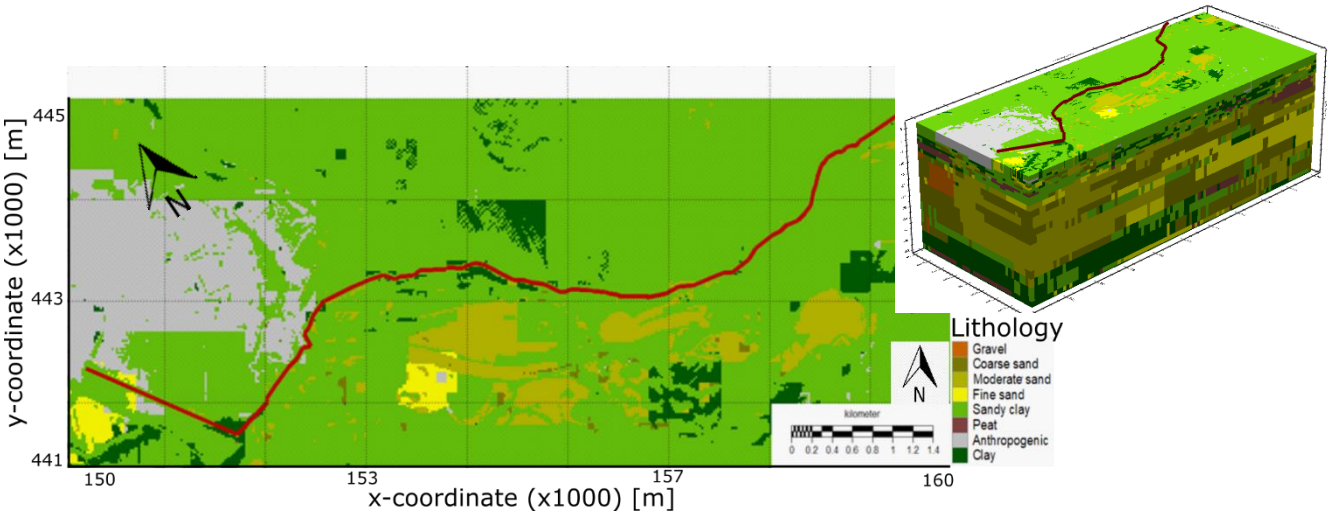

Figure 15: Lithology of the top layer in top view, and the lithology in 3D perspective. The red line indicates the dike.

4.3.2 BOUNDARY CONDITIONS

The needed boundary conditions are a starting head, river properties including water level and drain properties. The latter two are managed by the river package and the drainage package respectively. The starting head is the initial hydraulic head, thus the hydraulic head at the beginning of the simulation period. The starting head used in the steady-state simulation is set to 3m+NAP in the polder areas. The starting head in the transient simulations is the hydraulic head resulting from the steady-state simulation. A transient simulation is a simulation whereby the changing input

parameters, such as river stage, change daily/monthly/yearly. A steady state simulation has fixed parameters and runs infinitely until a steady state is reached.

To simulate river water levels the following parameters are needed: infiltration, river stage, bathymetry, and conductance. River stage is based on data from Rijkswaterstaat (RWS) (Figure 16); river bottom, is based on the bathymetry; river conductance, which has a higher value for the river than the side channels, is based on values from the iMOD tutorial (Vermeulen & Minnema, 2019) (Figure 15); river infiltration is set to a positive value, when positive infiltration takes place when the water head in the cell is lower than the water level.

To simulate drainage, water level in the polder and conductance is needed. Water level in the polder is based on the data of the water board HDSR (Figure 17). Conductance is based on the data in the iMOD tutorial, a low value has been chosen (Vermeulen & Minnema, 2019).

The area that is excluded from the simulations is the area south of the middle of the river (Figure 18). To give an idea of the area the dike is shown in red.

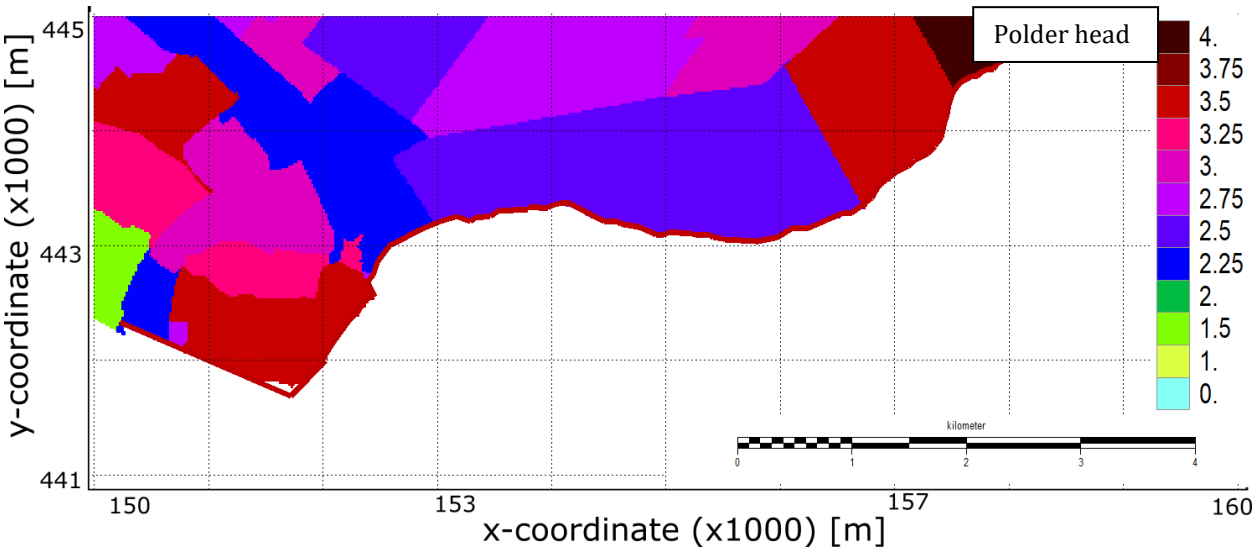

Figure 16: Water level of polder in iMOD (HDSR, 2019)

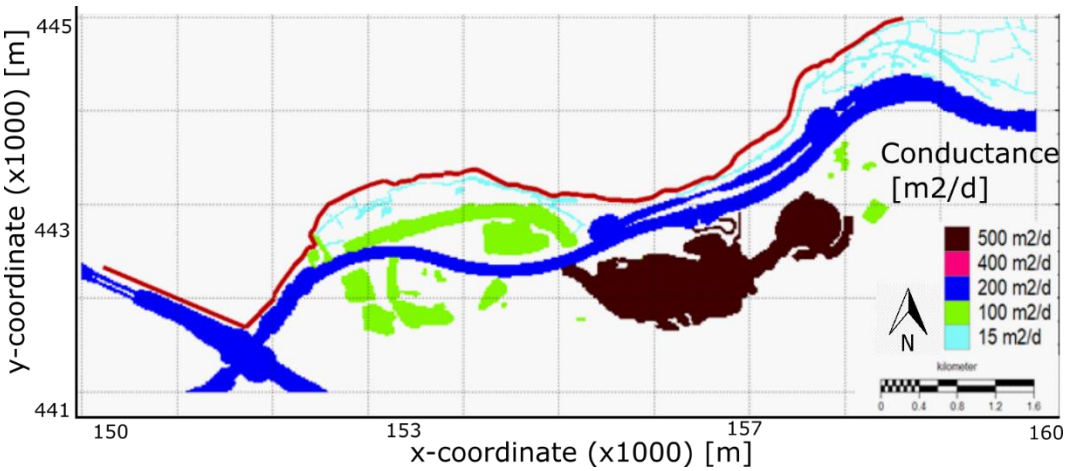

Figure 17: Values for the conductance of the river and canals. The red line indicates the dike.

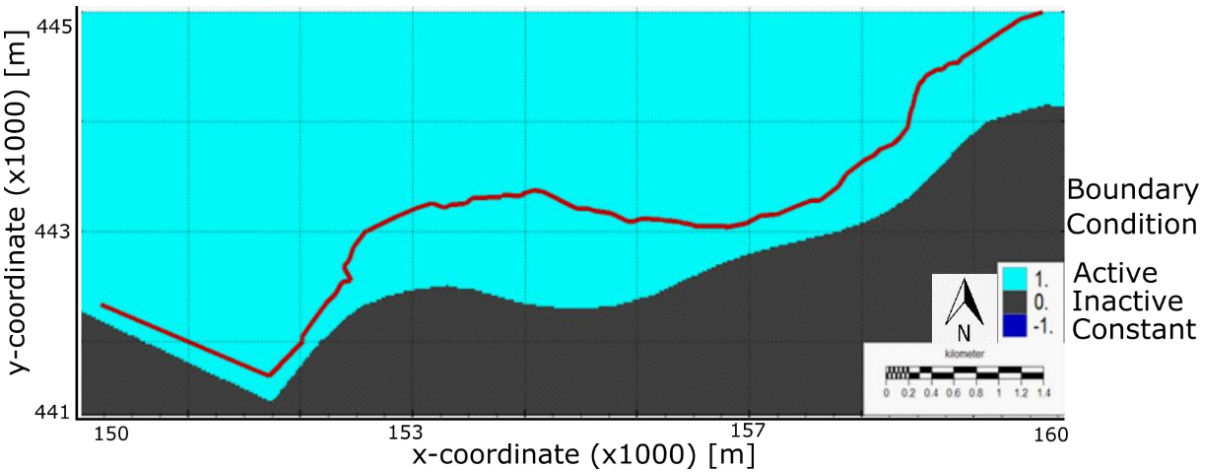

Figure 18: Boundary conditions of the model. Red line indicates the dike. Grey areas are not included in the model simulation.

4.4 Scenario's

This study explores two scenarios of varying river stages, which are prescribed to the model in the transient simulation with a daily temporal resolution in a period of 31 days. The first scenario is based on the river stages in January 2019, of the data of Rijkswaterstaat (Figure 20). The 2019 scenario is used for the validation of the model, because the river stages are stable which create a stable model output. The second scenario is based on the data from January 2018 (Figure 19). The 2018 scenario is used in this research for the results because there are two peak discharge moments in this scenario.

The water level in the river changes daily. The water level in the canals located along the river (buitendijks) and after the weir are assumed to have the same level as the main river after the weir. The water level in the canals located along the river (buitendijks) and before the weir are constant and assumed to be 4.5m+NAP

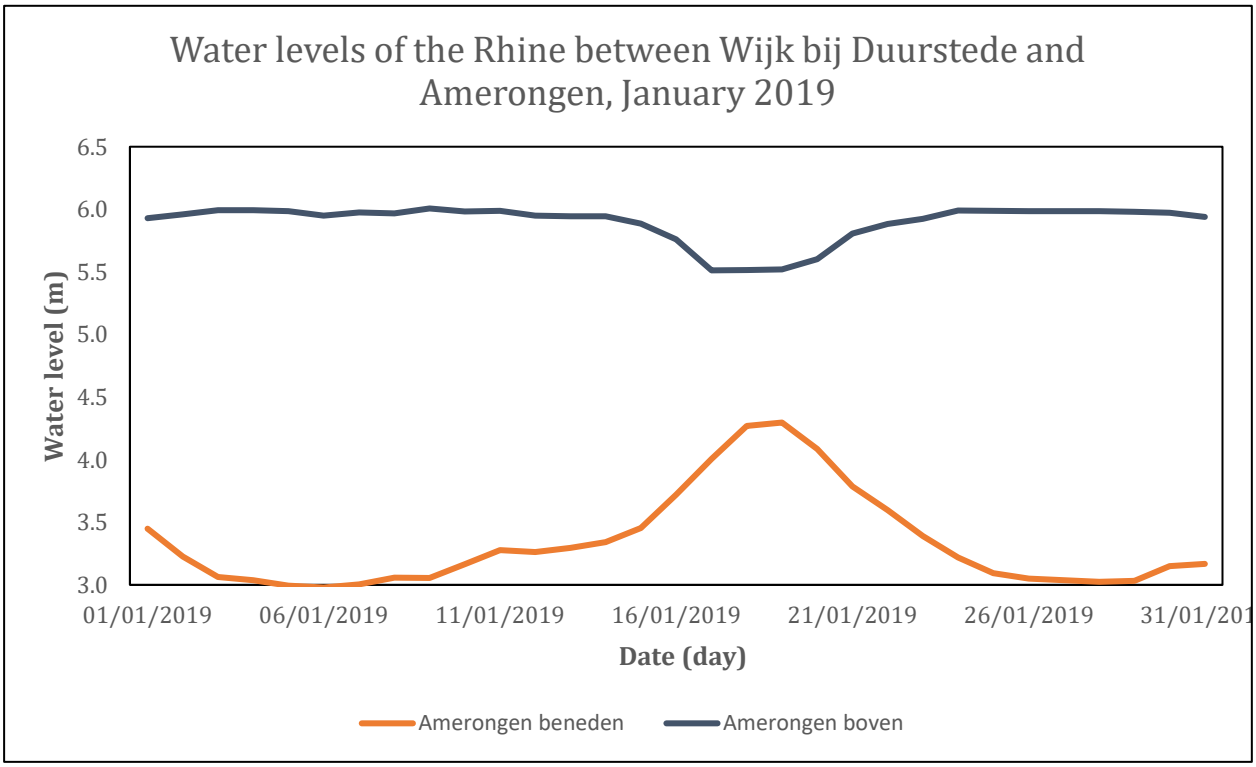

Figure 19: Water levels [m+NAP] of the Lek, January 2019 (RWS).

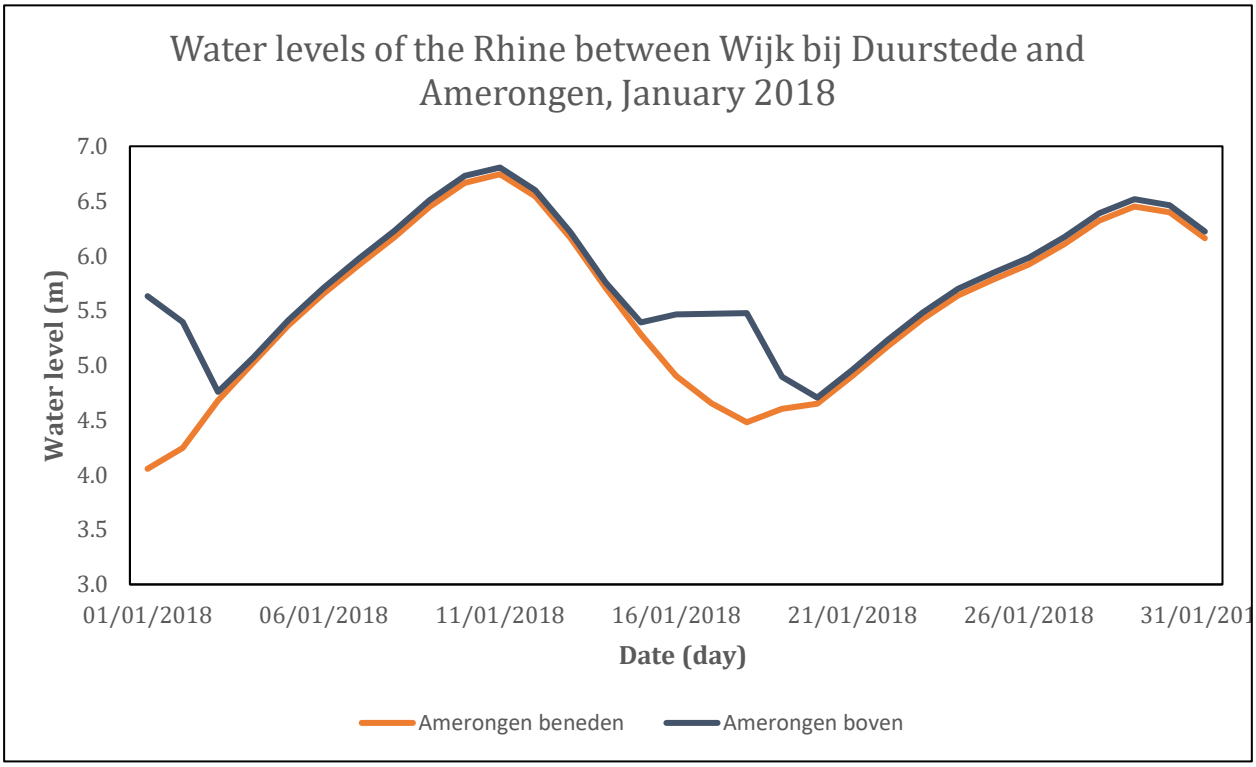

Figure 20: Water levels[m+NAP} of the Lek, January 2018 (RWS).

4.5 AREA OF INTEREST

For the presentation of the results an area of interest is chosen. This area is situated behind the weir at x-coordinate 156.500, to create coherence of river stage for the results. The area is not situated around the two towns because at these locations the upper layers consist of anthropogenic material. Furthermore, the amount of cables and pipes increases near towns which are not simulated in this model. The area of interest is situated behind the weir at x-coordinate 156.000 until x-coordinate 153.000 at which the anthropogenic lithology has not started yet, (between dike poles 45 and 75) (Figure 21). Four transects with a length of 700 m have been made. The transects are located exactly 1000 m apart from each other.

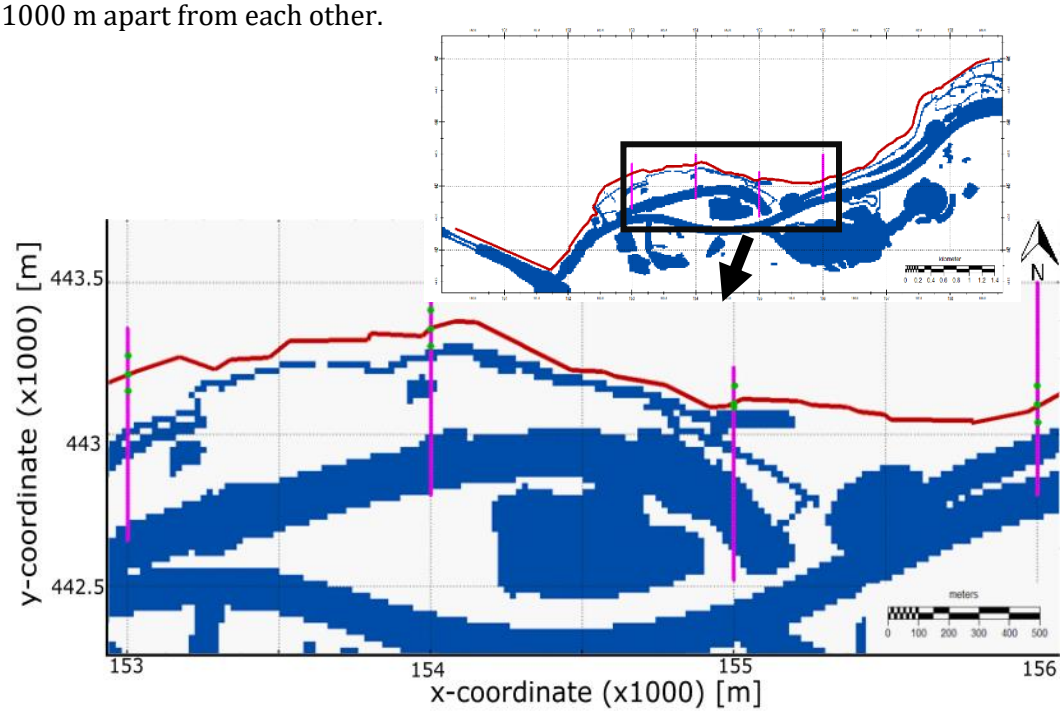

Figure 21: Location of the four transects in the area of interest. Red line is the dike. Four purple lines are the transects. : Location of the data points in the hinterland, dike and foreland are depicted by green dots.

The transects are numbered 153 till 156. At transect 153 the dike safety test of HDSR has failed on slumping of the landside and piping (Figure 8). At transect 154 the test failed on piping. At transect 155 the test failed on slumping of the landside, piping and the dike was not high enough. Transect 156 failed on slumping of the landside and piping.

4.5.1 LITHOLOGY IN AREA OF INTEREST

As mentions in section 3.2 the subsurface in the study area is highly heterogenous. The lithology of each of the four transects is visualized in Figure 22 to Figure 25. The lithology is shown in a voxel model, to a depth of -50 m+NAP. In each transect the top layer, the confining layer is clearly visible consisting of sandy clay and clay. Below the confining layer the aquifer can be found consisting of coarse to medium sand. The transects differ in the amount of aquifers they contain and the occurrence of clay or not in the confining layer.

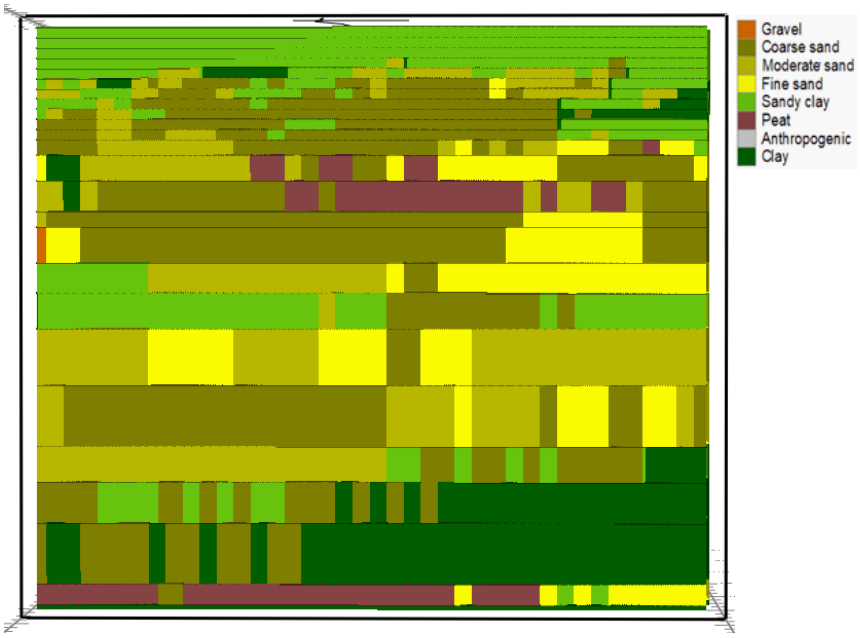

Figure 22: Lithology in transect 153.

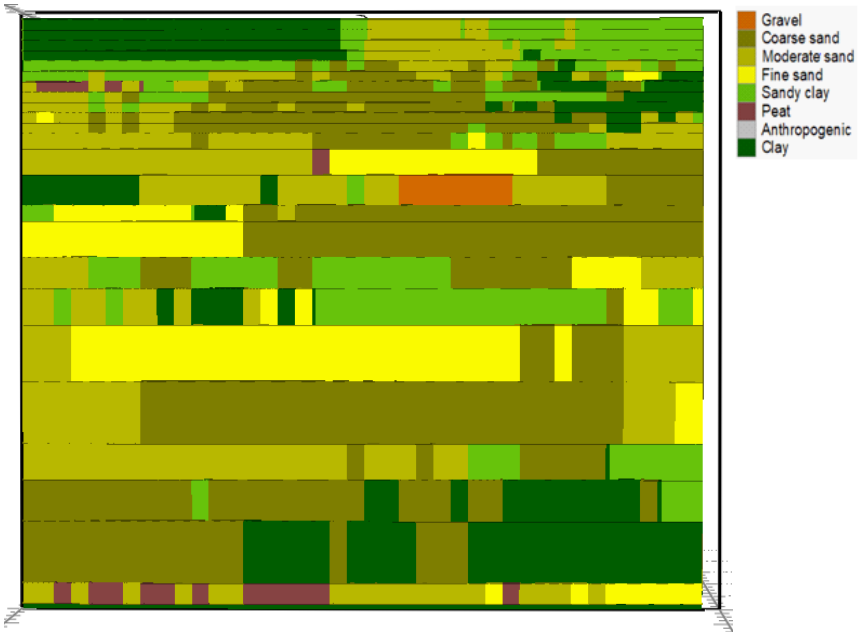

Figure 23: Lithology in transect 154,

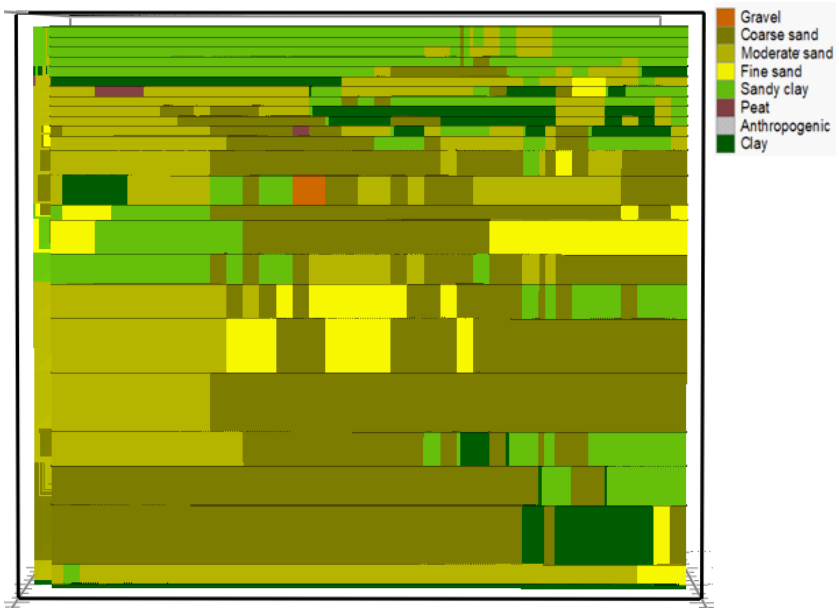

Figure 24: Lithology in transect 155

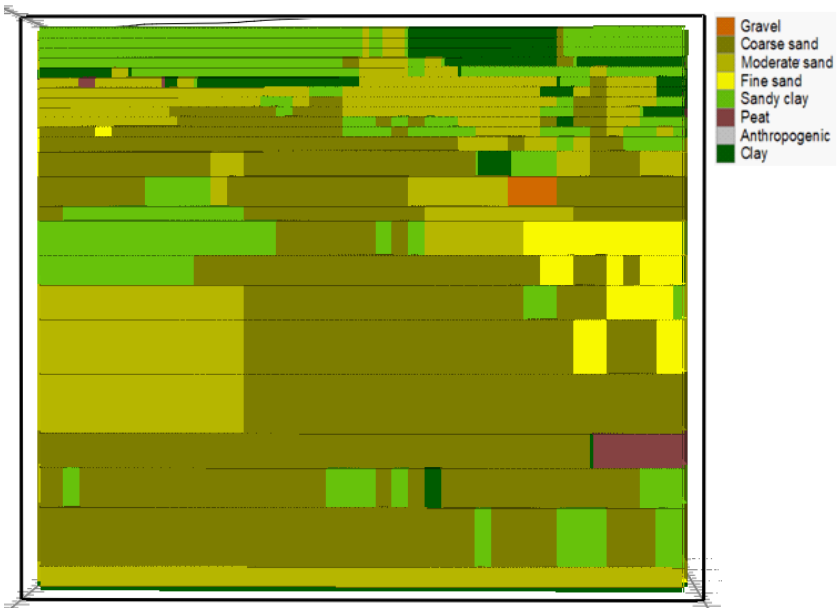

Figure 25:Lithology in transect 156

4.6 HYDRAULIC HEAD DISTRIBUTION

I have looked at the temporal distribution of calculated hydraulic heads at each of the four transects across the dike (Figure 21). The transects are each divided in three sections: Outside of the dike, underneath the dike and inside of the dike. Values 60 meters inside and outside of the dike are found to be representative for the respective sections. At each location, the hydraulic head is sampled from the dike (model layer 1) or the confining layer (model layer 1 to 4) and from the upper aquifer (model layer 7 to model layer 18) (Figure 26). The used model layer depends on which transect is looked at and in which model layer the sections are present. For the representation of the model layers, see method section 1.3. The hydraulic head distribution is analysed in reference to the river stage (Figure 20). The hydraulic head distribution is displayed in section 5.5.

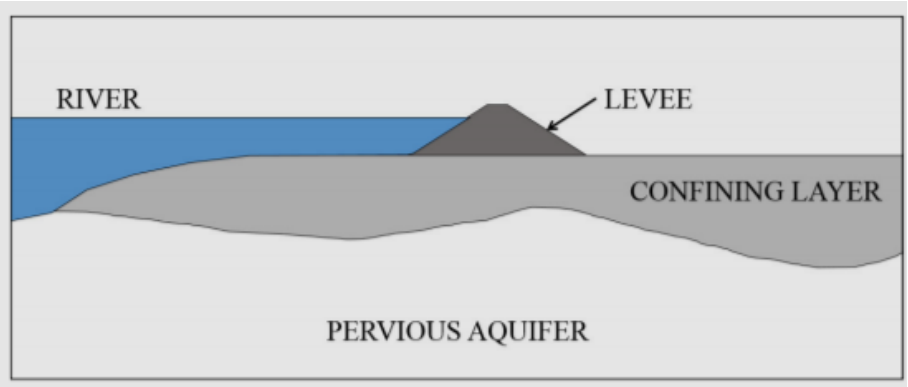

Figure 26: Geological cross section common of dikes (Robbins et al., 2016).

4.7 RESULT ANALYSIS

For dike stability assessments it is valuable to know when a 2D model over or underestimates. Especially underestimations of a 2D model can become very dangerous, because insufficient steps will be taken to warrant the safety of a dike.

Too look at the over and underestimation of the 2D model, the 2D and the 3D model have been compared and the difference between the models has been calculated. The values of the 2D model for the hydraulic head have been subtracted from the hydraulic head values of the 3D model. This has been done per cell, per time step, per model layer. Positive difference means the 2D model underestimates, negative values mean the 2D model overestimates.

After that the mean of the difference between the models is calculated per time step, per model layer and a pattern is detected. Also the maximum and minimum difference per time step, per model layer is calculated to check for a systematic error in the 2D model.

5 RESULTS

This section describes the output data of the iMOD model, the hydraulic head and the pressure head in different model layers. The focus of the displayed results is of the top 14 metres of the model, model layer 1 (AHN) to model layer 11 (-4 m+NAP). The results are displayed in figures with the top view of the study area, in graphs and in 2D-cross-sections.

The validation of the model is discussed first after which the maximum hydraulic head in the study area is described. Followed by the hydraulic head distribution in the foreland, hinterland and under the dike in the area of interest. This sections ends with the result analysis of the hydraulic head and pressure head, per cross-section, per model layer.

5.1 VALIDATION OF THE MODEL

Hoogheemraadschap De Stichtse Rijnlanden (HDSR) has provided data obtained at several piezometer locations along the dike trajectory Amerongen – Wijk bij Duurstede (Figure 27). These piezometers provide data of the hydraulic head in the aquifer from 2019 up to present.

For the validation of the model scenario 2019 is used, with a duration of 31 days. 17 piezometer locations were chosen which had data for 10 or more days in the range of the 31 chosen days. Each piezometer collects data on a certain depth, depending on where the bottom of the filter is located. This location is known. In the 3D model the locations of the 17 piezometers are determined by the use of coordinates (Figure 27). At these 17 locations the hydraulic head is identified in the model layers which correspond with the depth of the filter of the piezometer.

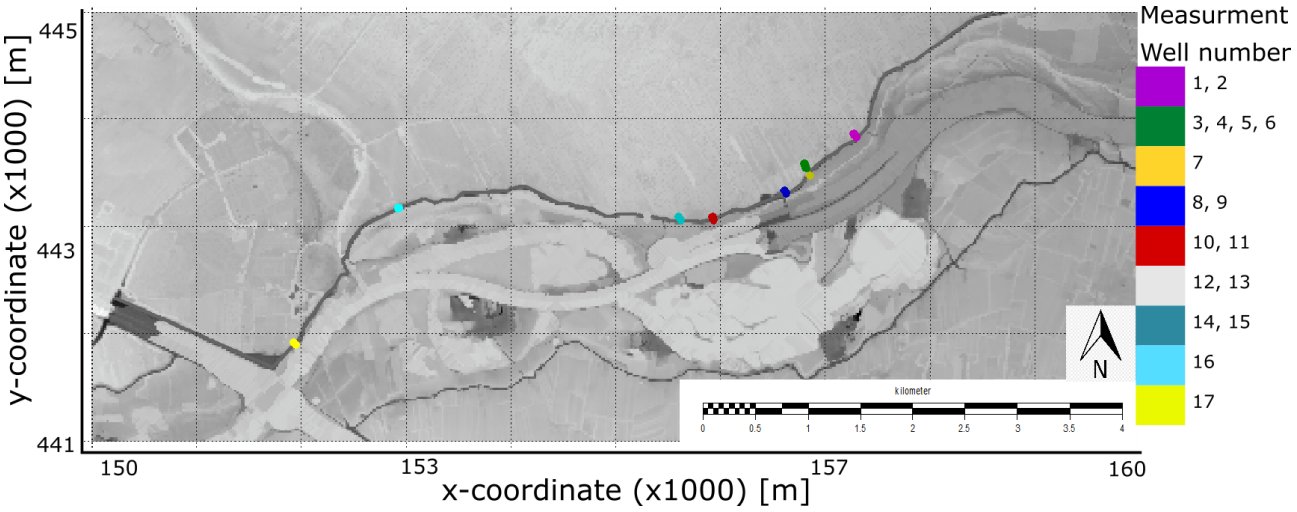

Figure 27: Location of the piezometers used for validation.

The difference of the modelled (3D model) and the empirical values (Xi-Xobs) of the hydraulic head in the aquifer is determined. Negative values mean the modelled hydraulic head is lower than the empirical hydraulic head. Figure 28 provides an overview of the difference between the modelled and the empirical values of the hydraulic head in the aquifer. On the y-axis the modelled values (Xi) are subtracted from the empirical values (Xobs). This is done to obtain an overview for the difference between the modelled and empirical value per piezometer location.

The graph shows in blue the empirical values on the zero-line, the average over time of the modelled values at the same data point are plotted in yellow above or below the zero-point. When the modelled value is below the zero-point is means that the modelled value is lower than the empirical value at that location. In orange the maximum and minimum value of the difference between the modelled and empirical value is plotted.

5.1.1 *RESULT OF THE VALIDATION*

Figure 28 shows a large difference (average of -0.7 m to -0.9 m) between the modelled and empirical hydraulic heads at the upstream side of the model (location 1-2). The hydraulic heads in the middle of the study area, location 3 till 15, differ on average between -0.5 m to -0.1 m. The hydraulic heads at the west side of the project area, at data point 17 (at the downstream side of the model) show a higher hydraulic head (0.05 m) for the model than in the empirical situation. This contrast in average difference between the locations occurs because of the river stage that is set in the model. Location 1 to 7 have a higher river stage than location 8-17, because of the weir that regulates the river stage. High river stages seem to have a large influence on the model. The model cannot increase the hydraulic head fast enough. Observed is that the first day (01-01-2019) has the lowest hydraulic head in these locations and the last day (31-01-2019) has the highest hydraulic head. This probably has to do with the starting head condition that is set, this is probably to low at these locations.

The range of difference of the modelled (3D model) and the empirical values (Xi-Xobs), is low around location 3 to 7 (0.17 m) and lower around location 14 to 17 (0.10 m). The range at the other locations is around 0.50 m. Observed is that the first day (01-01-2019) has the lowest hydraulic head in these locations and the last day (31-01-2019) has the highest hydraulic head. The range is high at these locations because of the explanation above.

The total average over time over locations of the modelled and the empirical values is -0.37 m. Which means that this model is not good enough to provide further analysis for dike stability. It is good enough to check for differences between the 2D model and the 3D model, because the empirical hydraulic heads do not have influence on this difference.

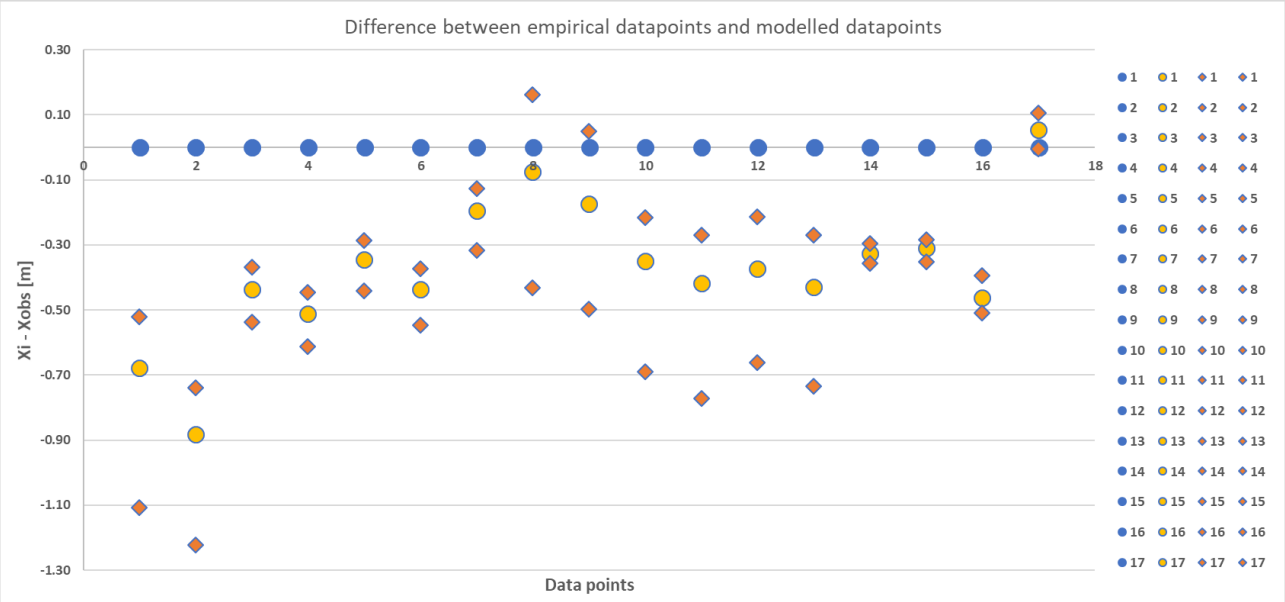

Figure 28: Difference between empirical and modelled values for the hydraulic head.

5.2 VISUAL REPRESENTATION OF THE FLOWLINES

Flowlines going through different types of subsurface layers are interesting to look at, because show flowlines where groundwater flows to and how fast. Especially for this research it is crucial to know in which direction the groundwater moves to. In the field the direction of the flow can be assessed by the use of piezometers. The model has an option to calculate and display the flowlines. Both are displayed in this section.

The piezometers in transect 154 (Figure 29) show that the hydraulic head in the aquifer, starting from 3 m+NAP, decreases further away from the main river. As the seepage of groundwater

is always from a higher to a lower hydraulic head. The seepage, meaning flow path of the groundwater, is from the aquifer into the confining layer given that the hydraulic head in the confining layer is lower than in the aquifer. In location B the seepage is from the confining layer into the aquifer.

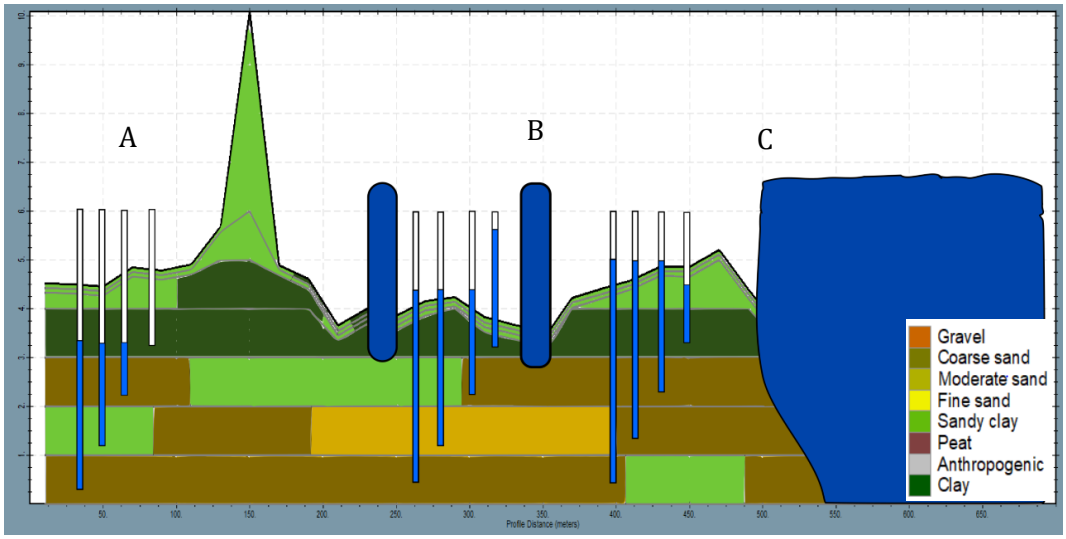

Figure 29: Cross-section of transect 154, with the dike at x=150 m. Visualization of the hydraulic head in observation pipes in transect 154 with lithology on day 10 (January 10th). A Hinterland, B and C foreland. Blue shapes indicate the position of the river and the height of the river on day 10.

The flow lines around transect 154 flow from south to north in Figure 30. They do not flow perpendicular on the dike, they have a slight deviation to the north-west. Especially in the hinterland the flow lines flow north-west.

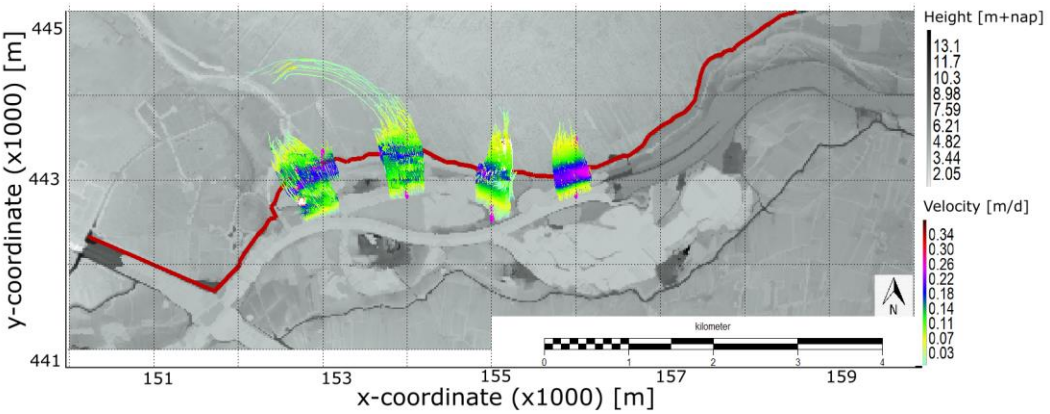

Figure 30: Top view of the flow lines started in the river and canal situated around transect 153, 154, 155 and 156. Background image of the AHN of the study area. The velocity is in the direction of the flow.

Figure 31 shows that the water particles flow fast in coarse sand and slow in sandy-clay. The flow lines come till a depth of -40 m+NAP. The flow lines tend to go around the clay, sandy clay and peat layers. In iMOD the flowlines in an aquifer are programmed to flow horizontal and in an aquitard to flow vertical.

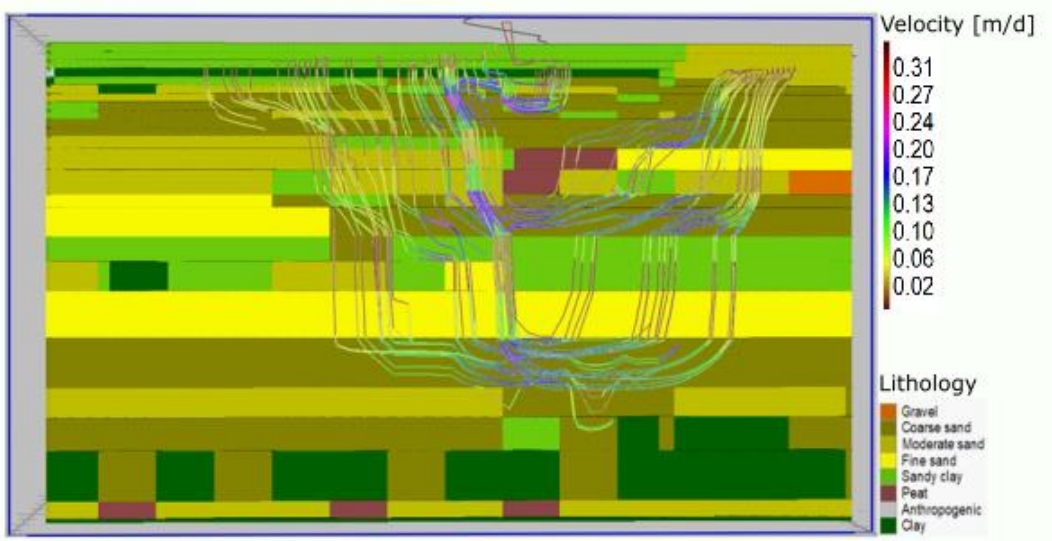

Figure 31: Front view of the flow lines around transect 154 with the lithology.

The observation pipes in transect 155 show in Figure 32 that the hydraulic head in the aquifer, starting from 3 m+NAP under the river and at 0 m+NAP under the hinterland, decreases further away from the main river. At location A, the groundwater flows from the lower model layers into the upper model layers. At location B there is no seepage up or down, the same at location C. Here the water travels mainly towards the left.

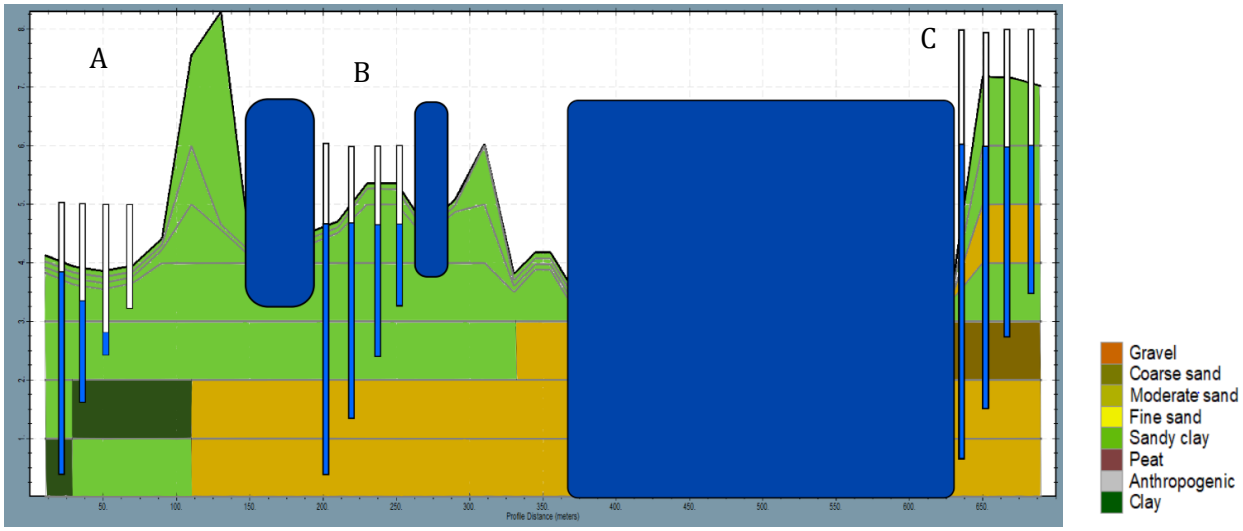

Figure 32: Visualization of the hydraulic head in observation pipes in transect 155 on day 10 (January 10th).

The flow lines in Figure 30 around transect 155 flow from south to north. They do flow perpendicular on the dike. They have a slight deviation to the north-east in front of the dike and a slight deviation to the north-west in the hinterland.

The front view of the flow lines in Figure 33 inside the lithology of the transect 155 show that the water particles flow fast in coarse sand and slow in fine sand and sandy-clay. The flow lines come till a depth of -40 m+NAP. The flow lines tend to go around the clay and sandy clay layers.

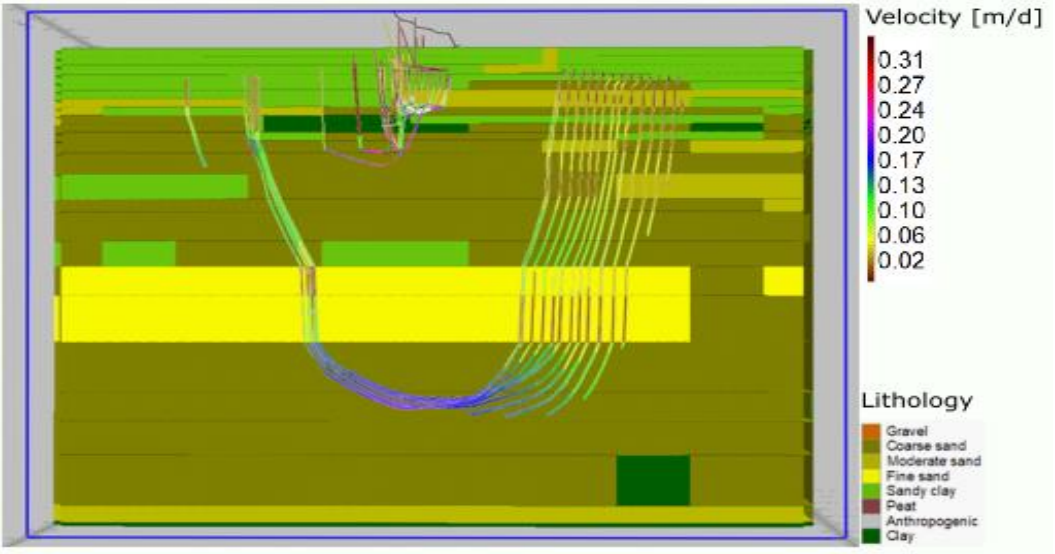

Figure 33: Front view of the flow lines around transect 155 with the lithology.

5.3 MAXIMUM HYDRAULIC HEAD DISTRIBUTION

5.3.1 CELLS WITH THE HIGHEST HYDRAULIC HEAD

Figure 34 shows the location of the highest hydraulic head in the confining layer (model layer 1) and in the upper aquifer (model layer 7).

The predictions of the 3D model shows a hydraulic head distribution high around the river with a decreases into the hinterland. Isolines are perpendicular to the watershed border. When comparing the obtained pattern of the distribution to Kurtulus & Flipo, (2011), and de Groot, (2016) and Zoutendijk, (2019), we inferred that this is a realistic pattern. The predictions of the 2D model show the same regional pattern as the 3D model, with the highest hydraulic head in and near the river, and a decrease into the hinterland.

Key factors that influence the maximum hydraulic head pattern are: i) the river stage, the maximum river stage is 6.8 m+NAP on 11-01-2018, ii) the fixed polder level (Figure 16), iii) and the influence of the hydraulic conductivity.

Between x-coordinate 154.000 and 155.000, inside the black dashed circle, a relative high hydraulic head can be found further away from the dike into the hinterland. This is the location where a dike breach has occurred in the past and this is expressed by higher hydraulic heads. These higher hydraulic heads are a result of high permeable sands that are washed behind the dike during the dike breach.

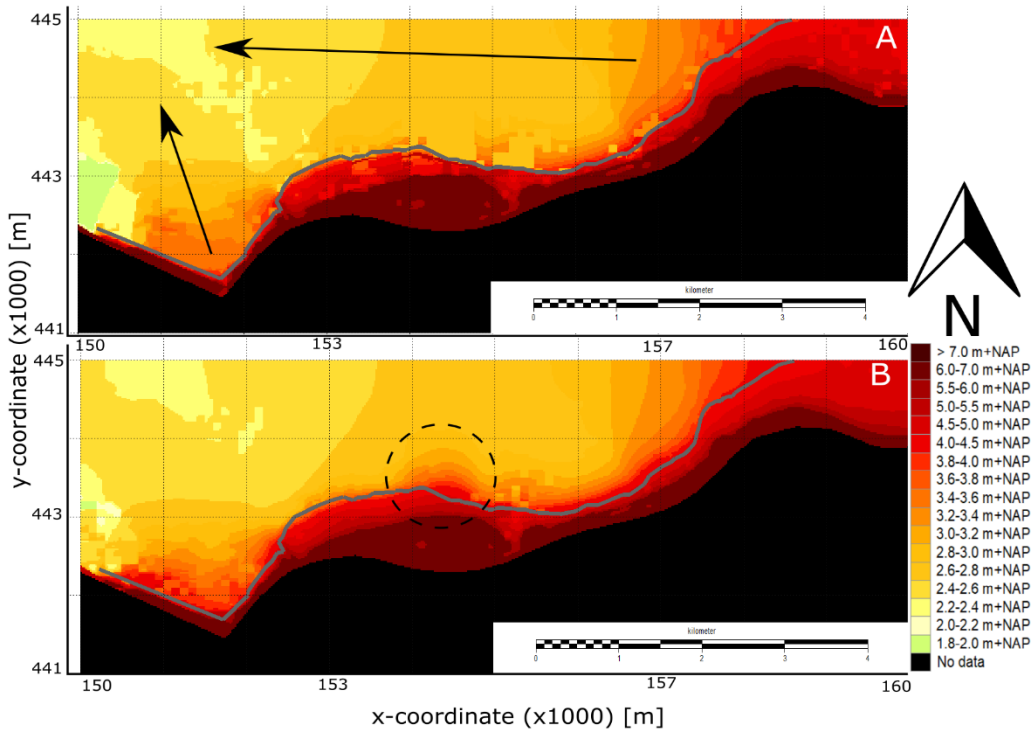

Figure 34: Top view. Map indication of the highest hydraulic head per model cell for the period of January 2018. A: for model layer 1 (confining layer), B: for model layer 7 (aquifer).

5.3.2 DAY WITH THE HIGHEST HYDRAULIC HEAD

Figure 35 shows the day of the highest hydraulic head in the confining layer (model layer 1) and in the upper aquifer (model layer 7). The day of the highest hydraulic head in the hinterland is the last day of the simulation, day 31, the 31st of January 2018. In the river the day of the highest hydraulic head is the day with the highest water level in the river, day 11, the 11th of January 2018. In the aquifer is visible that between x-coordinate 154.000 and 157.000 the highest hydraulic head occurs behind the dike on day 12 and 13 of the simulation, respectively the 12th and 13th of January 2018. While at all the other locations behind the dike the highest hydraulic head occurs on day 31.

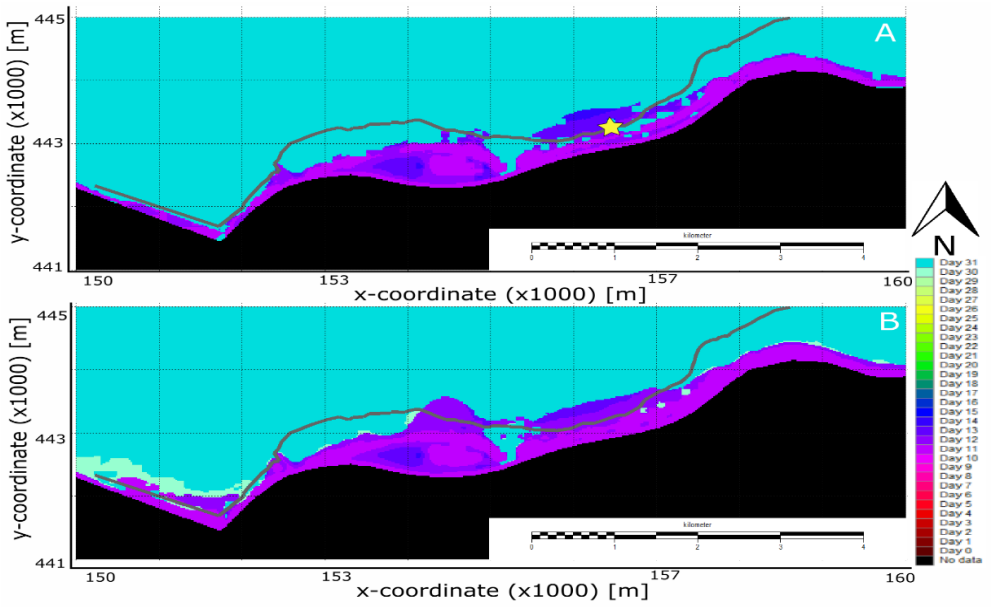

Figure 35: : Top view. Map indication on which day the highest hydraulic head was modelled per model cell. A: for model layer 1 (confining layer), B: for model layer 7 (aquifer). At the yellow star, which indicates the location of dike pole 40, two dike breaches have occurred in the past which are visible by the over-wash.

Concluded can be that an interesting area of interest has been chosen between x-coordinate 153.000 and 156.000.

5.4 DIFFERENCES IN HYDRAULIC HEAD DISTRIBUTION PER TIME STEP AND PER LAYER

In transect 153 the 2D model mainly overestimates the hydraulic head. The mean per model layer, per time step is shown in Figure 36. For more information see appendix C.

Because the hydraulic head in this transect is mainly overestimated in the 2D model, the mean shows where the small and large overestimations are. The overall overestimation in 2D increases on the days when the discharge in the river increases. This happens because more water enters the system and stays longer in the different layers then in the 3D model because the flowlines have a lower velocity than in the 3D model. The overall estimation in 2D increases in the layers that consist of sand, thus in the aquifer, and it increases again in the deepest layer which is impermeable. This happens because most flowlines will go vertical into the aquifer in the 2D model because the water flow along the easiest path. While in the 3D model the easiest path could also be horizontal. See Figure 33 for visualisation.

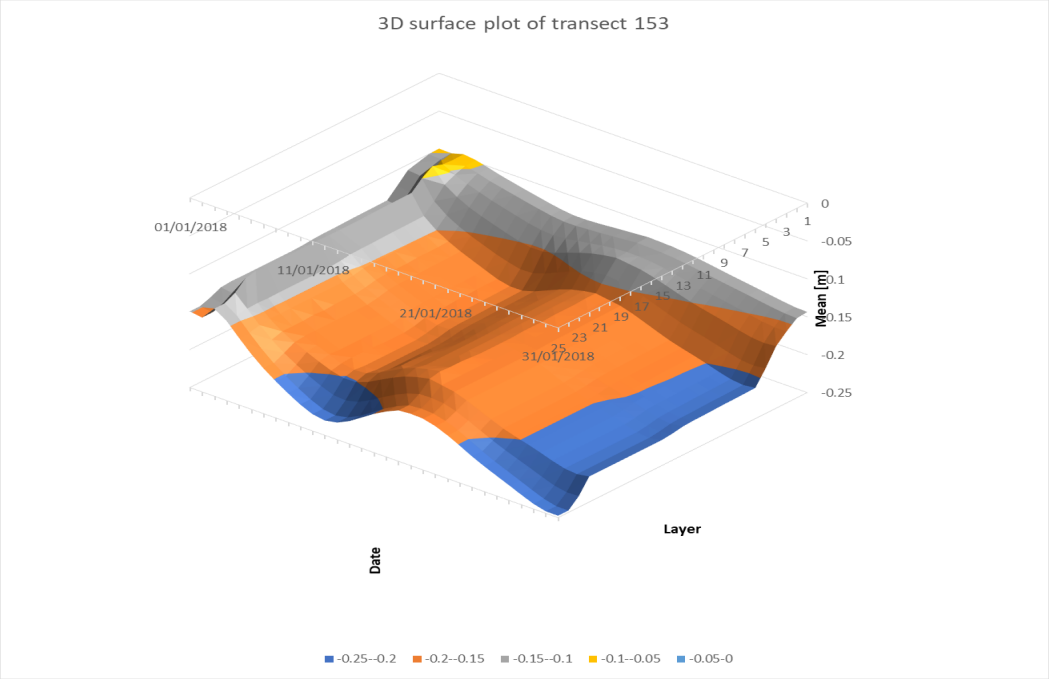

Figure 36: 3D surface plot of transect 153.

Transect 154 shows a large range in differences between the 2D and 3D model. The maximum overestimation is around 0.5 m and the maximum underestimation is -0.9 m. The largest over and underestimation occur on the days with highest discharge and in the layers which represent the aquifer. The large differences occur due to the local lithology and will be explored in section 5.6.

The other transects, 155 and 156, all have the means around the value of 0. The values of the mean tells you in this case if the hydraulic head has a tendency of over or underestimation in the 2D model. Because the mean is around the value of 0 there is no systematic error in the 2D model in these transects (Figure 37). These transects differ greatly in difference in hydraulic head between the 2D and 3D model on local scale. This will be clarified in section 5.7.

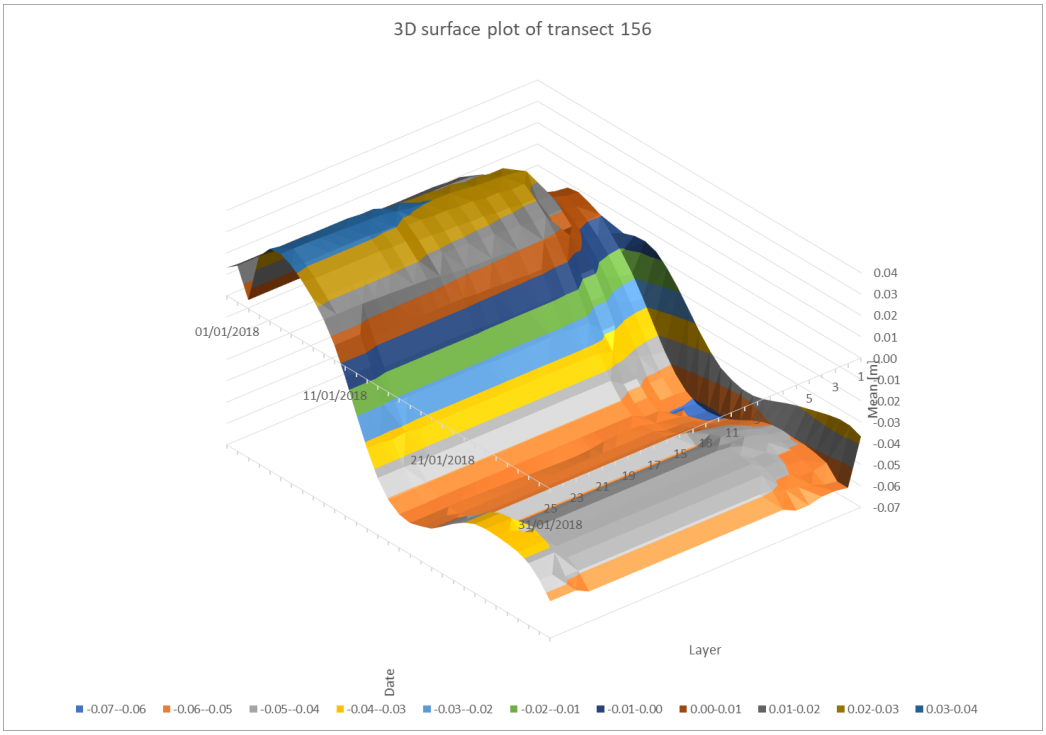

Figure 37: 3D surface plot of transect 156.

In transect 155, the maximum overestimation occur during days with high discharge, the maximum underestimation occurs on the days of the second discharge peak and in the first 9 layers. Transect 156 does not show this trend, the maximum overestimation is on all days and in all layers the same. The maximum underestimation occurs on days after high discharge events and in the first 6 layers, thus up until the aquifer.

5.5 HYDRAULIC HEAD DISTRIBUTION

As mentioned in the previous section the differences in the hydraulic head between the 2D and 3D model can show great changes locally. For dike stability assessments it is important that the values around the dike do not have underestimations in the 2D model.

5.5.1 HYDRAULIC HEAD DISTRIBUTION IN FORELAND (60M BEFORE DIKE)

Plot A (transect 153) in Figure 38 shows the hydraulic head in the confining layer and the aquifer, for both the 2D and the 3D model. In both layers, for both models, the hydraulic head follows the water level in the river over time, they show a damped down response to the river. The values of both layers are close together.

Plot B (transect 154) shows the hydraulic head values which do not follow the water level in the river in the confining layer and the level is constant. While the hydraulic head in the aquifer does shows a response to the river. The difference between the 2D and the 3D model increases when the water level in the river increases, the 2D model results in higher hydraulic head values.

Plot C (transect 155) shows an ever bigger response to the river in both the hydraulic head in the confining layer as in the aquifer, the head in the confining layer shows a delay towards the hydraulic head in the aquifer.

In plot D (transect 156) both layers show the same response to the water level in the river.

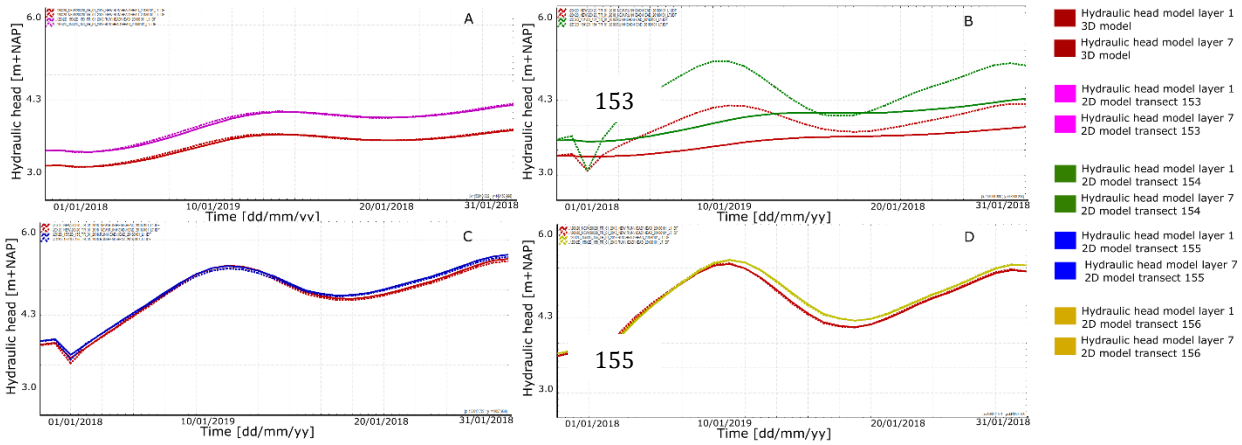

154

156

Figure 38: Time series. Hydraulic head distribution over time in model layer 1 and 7, in the foreland 60 metres before the dike. A) transect 153, B) transect 154, C) transect 155, D) transect 156. Dotted line represent model layer 7.

The differences between the transects in the foreland can be explained by the lithology. The lithology differs per transect (Figure 22, Figure 23, Figure 24, Figure 25). Transect 155, and 156 have the same lithology in the foreland, sandy clay on top of medium sand. Transect 153 also has sandy clay but then on top of coarse sand, leading to a higher hydraulic head in the 2D model. Transect 154 shows a different lithology with mainly very low permeable clay on top of coarse sand. This causes a difference between the confining layer and the aquifer and between the two models.

5.5.2 HYDRAULIC HEAD DISTRIBUTION UNDER THE DIKE

The plots for the hydraulic head distribution under the dike in Figure 39 show almost the same pattern as the hydraulic head distribution in the foreland in section 5.5.1. Plot A shows a damped

down response to the water level, and heads in the confining layer and aquifer show the same response.

Plot B shows that the head in the confining layer shows no response to the river stage while the hydraulic head in the aquifer does. The hydraulic head of the 2D model is always higher than the values for the 3D model.

Plot C shows that the head in the confining layer has a damped down response while the hydraulic head in the aquifer shows a high response to the river stage while in the foreland the head in the confining layer shows a higher response. The values for the 2D model are below those of the 3D model in the aquifer on days of high discharge.

Plot D shows that both hydraulic heads in the aquifer show a quick response to the river stage.

The dip at day 3 in the hydraulic head in the aquifer probably occurs due to the river stage before the weir, which also has a dip around the same day.

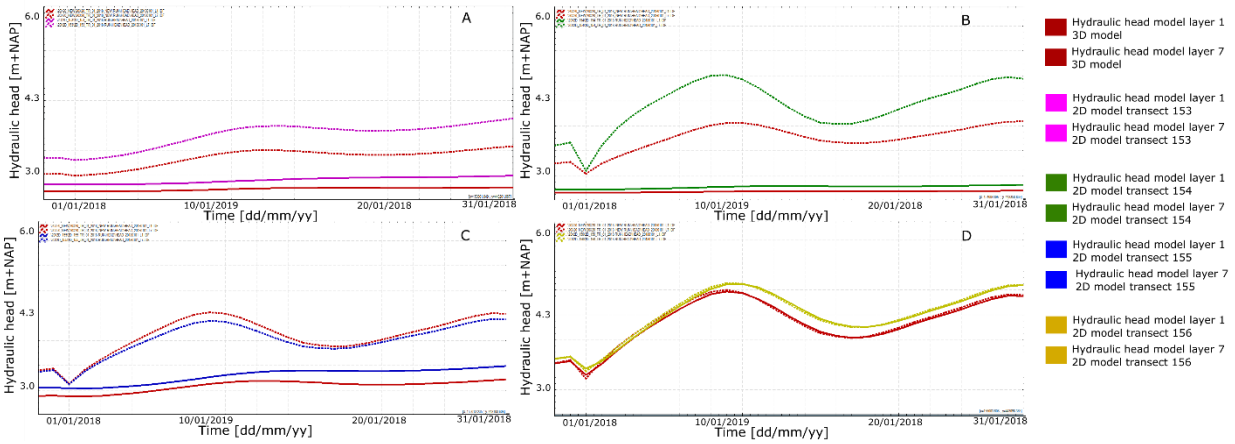

Figure 39: Time series. Hydraulic head distribution over time in model layer 1 and 7, under the dike. A) transect 153, B) transect 154, C) transect 155, D) transect 156. Dotted line represent model layer 7.

The differences between the transects under the dike can also be explained by the lithology. The lithology differs per transect (Figure 22, Figure 23, Figure 24, Figure 25). Especially in transect 153 and 155 does the lithology differ from the foreland. The sandy clay layer increases in thickness, and more clay can be found under the dike. This creates a difference between the hydraulic head in the confining layer and in the aquifer. And also between the two models.

The underestimation that can be found of the 2D model in transect 155 needs to be examined more closely, on local scale. This will be analysed in the next sections.

5.5.3 Hydraulic head distribution in hinterland (60m behind dike)

In the hinterland, shown in Figure 40, the head in the confining layer does not show any response to the river stage, only plot D shows a response. The response of the hydraulic head in the aquifer in the hinterland shows the same response as under the dike and in the foreland. Transect 153 has the lowest response and transect 155 and 156 show a high response.

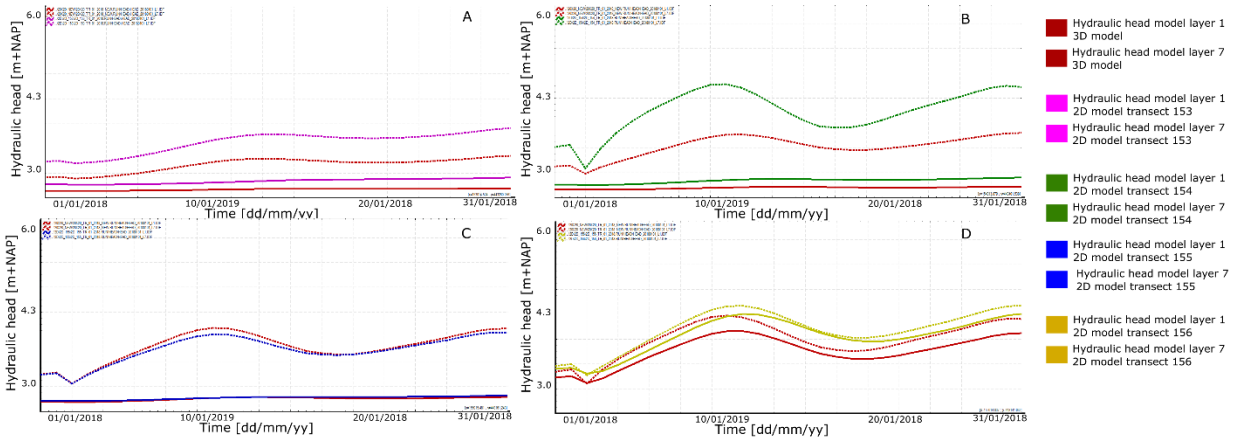

Figure 40: Time series. Hydraulic head distribution over time in model layer 1 and 7, in the hinterland 60 metres after the dike. A) transect 153, B) transect 154, C) transect 155, D) transect 156. Dotted line represent model layer 7.

The differences between the transects in the hinterland can also be explained by the lithology. The lithology differs per transect (Figure 22, Figure 23, Figure 24, Figure 25). All transects have the same lithology in the hinterland as under the dike, except for transect 156. A thicker layer of sandy clay can be found in the hinterland compared to the foreland and under the dike. This layer causes a difference between the hydraulic head in the confining layer and the aquifer. It also causes an increasing difference between the 2D and 3D model.

Transect 154 with x-coordinate 154.000 and transect 155 with x-coordinate 155.000 are chosen to display the results of in the following sections. There has been chosen for these transects because transect 154 shows a noticeable overestimation of the 2D model. Transect 155 shows an underestimation of the 2D model. Underestimations of the 2D model are important to explore because this could provide false safety if used for dike stability calculations. Both transects will be analysed and an explanation for the over and underestimations will be discussed in the following sections.

Transect 154 failed in the safety test on piping. Transect 155 failed on sliding of the landside, piping and the height of the dike was not sufficient. These transects are thus very interesting to take a more detailed look at.

5.6 HEADS IN TRANSECT 154

The focus will be on transect 154 in this section, because 154 has shown large overestimations in the 2D model in different layers at different timesteps. In this section the local differences will be explored and analysed.

5.6.1 HYDRAULIC HEAD IN THE AQUIFER

When the hydraulic head in the aquifer is so high during a high water event that the confining layer on top of the aquifer is pushed up behind the dike. Evidence for this phenomena are rips in the ground just behind the dike, in which water wells out. Rips itself are not a kind of dike failure but can lead to piping or sliding of the landside slope of the dike. It is thus an important feature to look at. That is why the hydraulic head in the aquifer is displayed here.

Figure 41 shows that the hydraulic head in the **first** (upper) aquifer is highest under the river and decreases into the hinterland. In the hinterland the drainage is set to 2.6 m+NAP. The green and blue lines show a delay in response after the river.

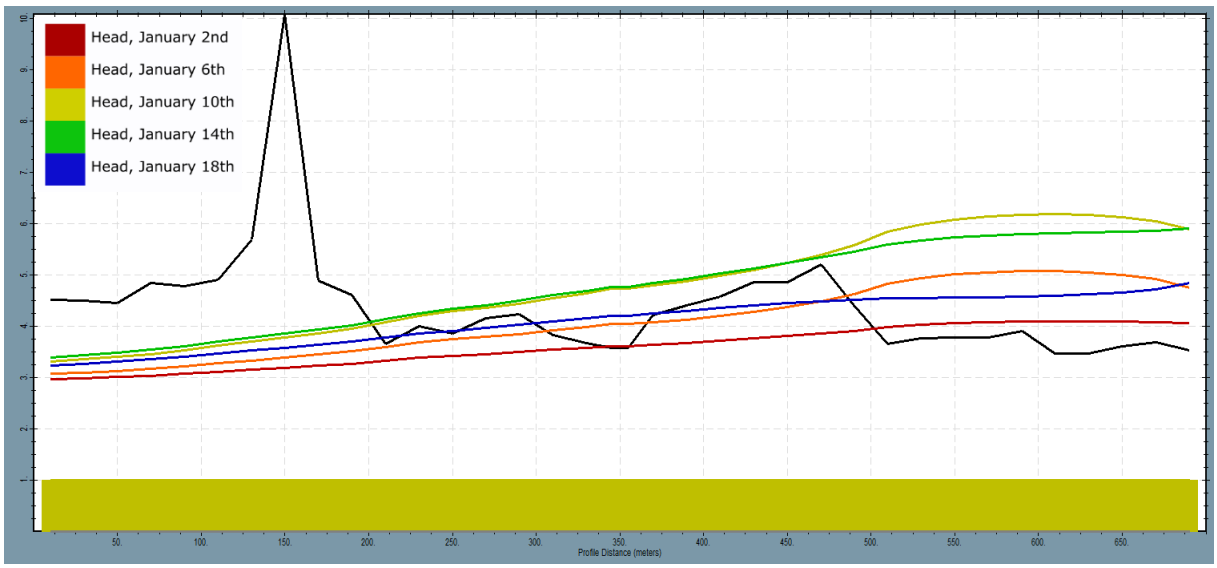

Figure 41: 3D model results. Cross-section of transect 154. Hydraulic head modelled in 3D, in the aquifer (starting from model layer 7) in transect 154. The black line is the surface of the transect 154. The yellow filled block is the location of the aquifer. Between 500m and 700m on the x-axis the river is located with conductance 100m2/d, and around 230m and 330m on the x-axis two canals are located with conductance 15 m2/d.

The figure with the difference between the model results of the 3D and the 2D model (Figure 42), shows large difference between the models, the y-axis ranges from +0.1 to -0.9 m. The figure shows at the right side of the transect (purple box) that the 2D model underestimates the hydraulic head, because the values are positive. Except for the blue line, the 18th of January, here the 2D model overestimates because the values are negative.

In the middle of the river at x=620, in the black circle in Figure 42, there is no difference between the 3D and the 2D model. On the left side of the river at x=500 you can see a turnaround in the difference between 3D and 2D compared to the right side of the river. Here the peak discharge in the river causes a higher hydraulic head in 2D while on the right side the 3D model shows a higher hydraulic head than the 2D model.

The further you move away from the river the higher the difference between 3D and 2D becomes. The 2D model results in higher hydraulic heads (-0.4 to -0.9), thus have a higher overestimation. Especially the days with the peak discharges, the orange, yellow and green line show large differences. These days have a difference of 0.65 m to 0.9 m in the hinterland, see the results in the black box.

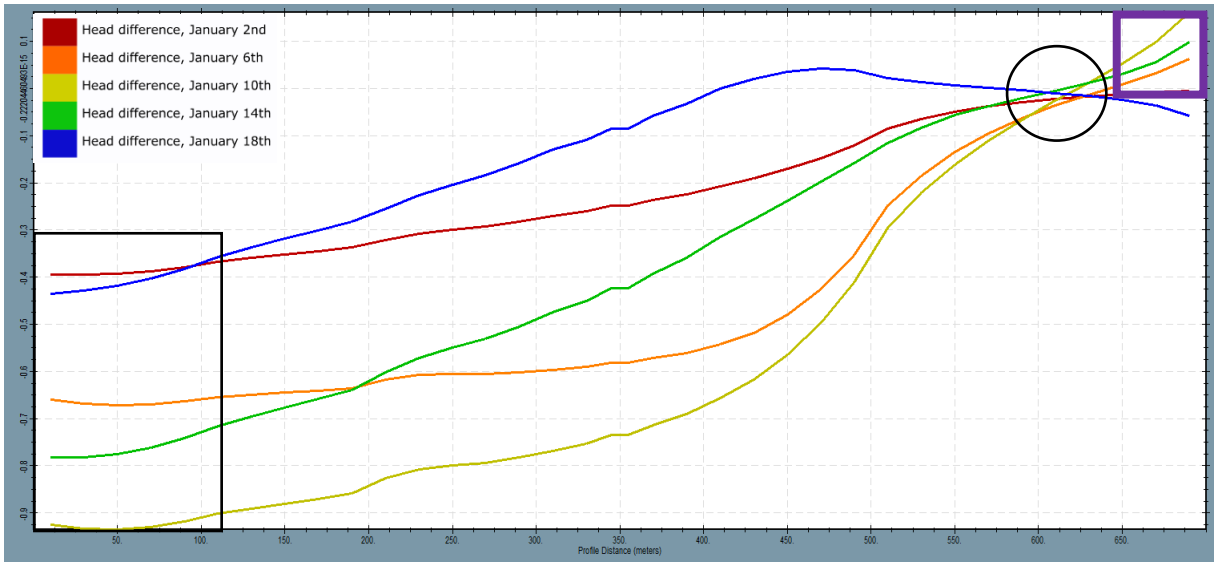

Figure 42: Difference (3D-2D) between the 3D model and 2D model in transect 154 in the aquifer, model layer 7.

The 2D model overestimates up to -0.9 m in the aquifer because of the occurrence of coarse sand from the river up until the hinterland. Coarse sand has a high hydraulic permeability of 25 [m/d]. Because water takes the easiest path all the water goes into the coarse sand layer in the 2D model. In the 3D model the water does not go down in a vertical line to the coarse sand layer in the aquifer but spreads out more to the left and right in the coarse sand layer. Leading to less water in the same model cell as the 2D model.

5.6.2 PRESSURE HEAD UNDERNEATH THE DIKE

The occurrence of uplift and heave and thus eventually piping, can be determined by the pressure head underneath the dike. The pressure head is calculated extracting the elevation head from the hydraulic head.

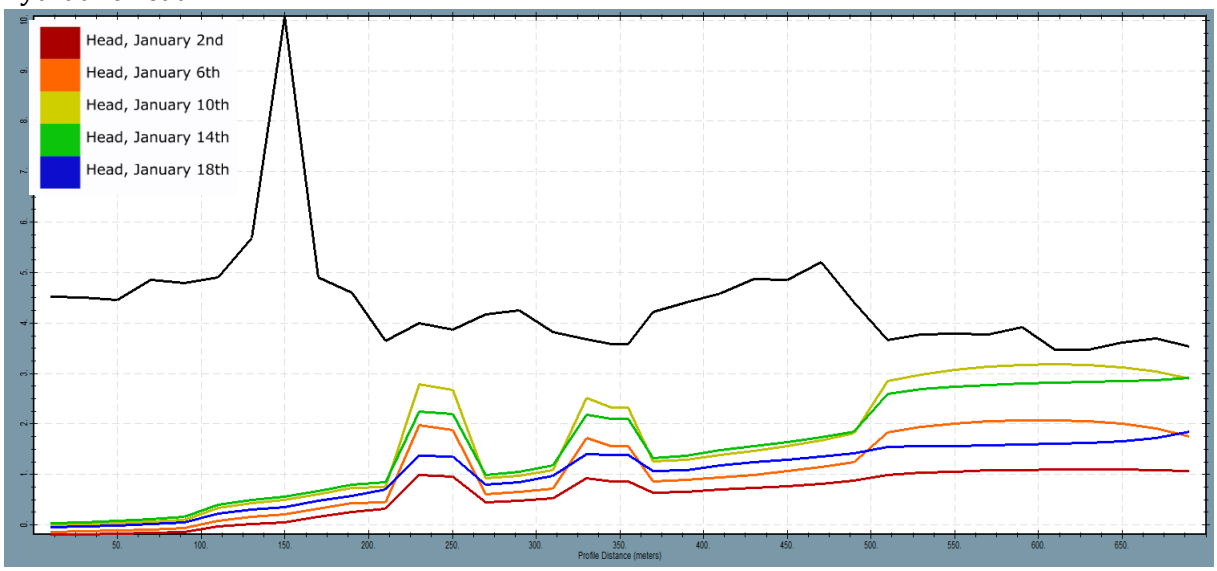

Figure 43: Pressure carried out on the confining layer (bottom model layer 4) of transect 154.
The black line is the surface of the transect 154. Between 500m and 700m on the x-axis the river is located with conductance 100m2/d, and around 230m and 330m on the x-axis two canals are located with conductance 15 m2/d.

Figure 43 depicts the 3D pressure head results, which range from 0.15 m to -0.7 m. The pressure is everywhere positive except for the 2nd and 6th of January (red and orange) in the hinterland. The pressure in the hinterland for all days lays very close together. The pressure increases at the places where the river and canals are situated. The higher the river stage the higher the pressure, but there is a delay after the peak discharge. The green and blue line have a higher pressure then the red and orange with almost the same river stage.

The difference in pressure (Figure 44) is high, just like the difference in hydraulic head (Figure 42). It ranges up to -0.7 m. Just as in Figure 42 there is almost no difference in the main river around x=620 m. At the location where the channels are located around x=230 and 330 the difference between the models is smaller than in the surrounding area, see the black circles. The peak discharges on the 6th, 10th and 14th of January show the largest difference where the 2D model results in higher overestimation. The days with almost the same river stage show almost the same difference between the models.

The 2D model underestimates the hydraulic heads in and around the river, during or after the peak discharge (purple box).

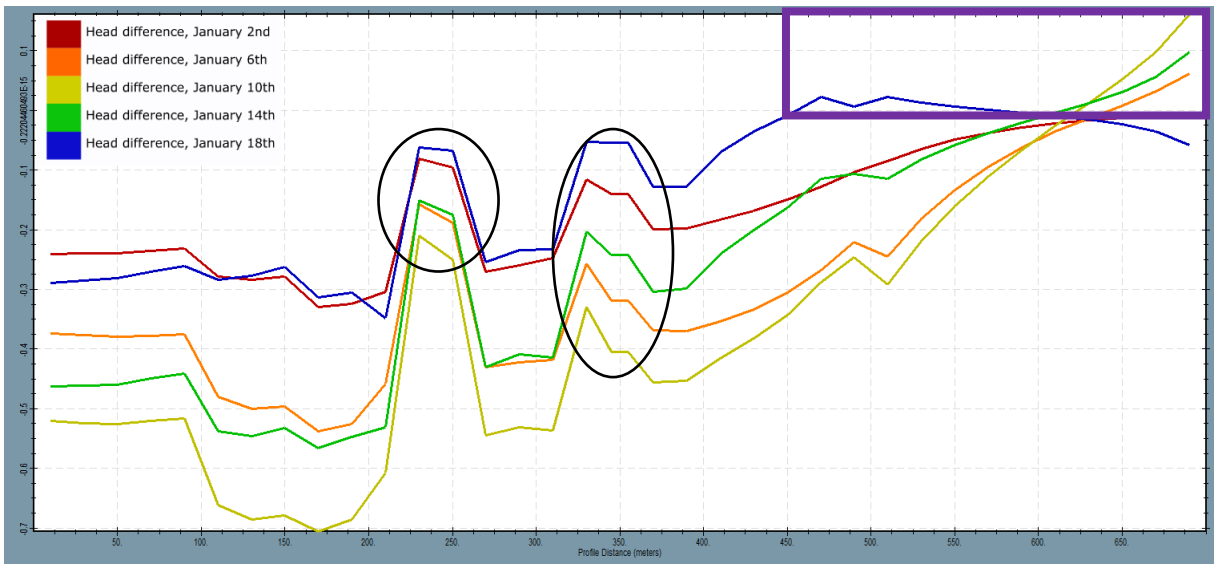

Figure 44: Difference in pressure (3D-2D) between the 3D and 2D model in transect 154.

The difference between the 2D and 3D model is lowest around the areas of water because the water stage is a fixed input. Meaning that there is less space for change in the subsurface under the water bodies. The 2D model overestimates, especially in the hinterland. The overestimation occurs because we look at the bottom of a very thick layer of clay, which has a hydraulic conductivity of 0.002 [m/d]. It is possible that water stays longer in the clay layer in the 2D model than in the 3D model, because the water velocity is slower. The 2D model underestimates at the right side of the river, no possible explanation has yet been found for this.

5.6.3 PRESSURE HEAD IN THE CONFINING LAYER

The occurrence of sliding of the land or water side of the dike can be determined by the pressure inside the dike, thus inside the confining layer. When the pressure increases in this layer and the friction decreases, the sliding can commence.

Figure 45 depicts the 3D pressure head results inside the confining layer. The pressure is positive on the locations of the river and negative where no water on the surface is present. The pressure in the layer under the dike and in the hinterland is for all the depicted days the same.

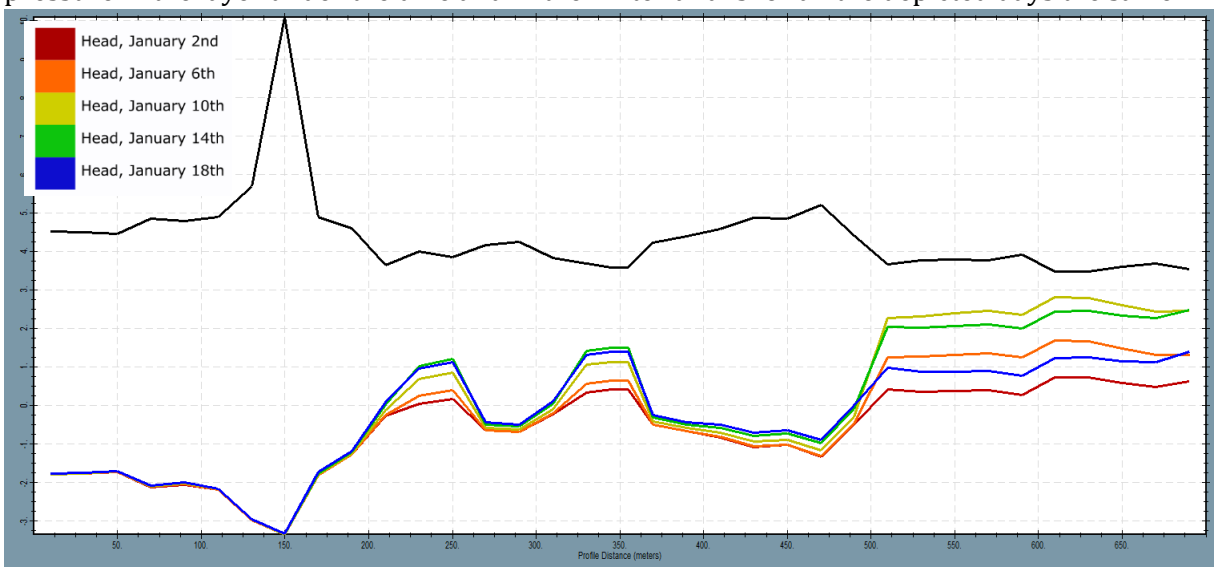

Figure 45: Pressure in the confining layer (bottom model layer 1) of transect 154.
The black line is the surface of the transect 154. Between 500m and 700m on the x-axis the river is located with conductance 100m2/d, and around 230m and 330m on the x-axis two canals are located with conductance 15 m2/d.

The difference in pressure in Figure 46 shows the same trend as the difference in pressure underneath the confining layer and hydraulic head (Figure 42 and Figure 44). It ranges up to -0.45

m, so the difference is smaller. There is almost no difference in the main river around x=620. At the location where the channels are located around x=230 and 330 the difference between the models is smaller than in the surrounding area, see the black circles. The difference with the pressure underneath the confining layer is that this figure shows that how longer the model runs the larger the differences between the 3D and 2D model becomes from x=0 to x=400.

The 2D model underestimates the hydraulic heads at the right side of the river (purple box).

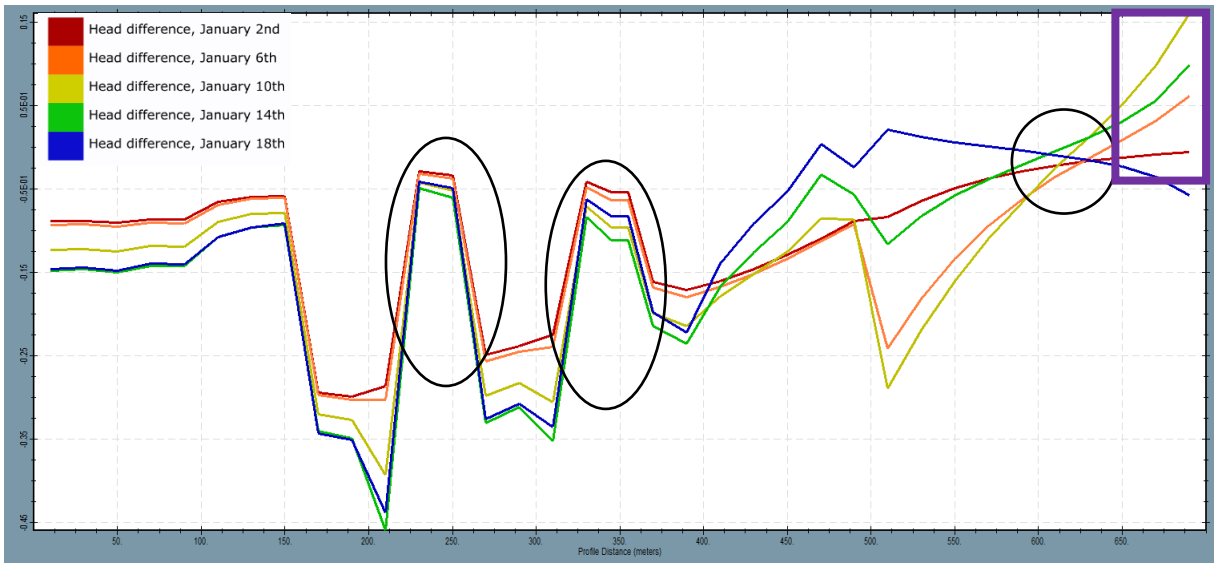

Figure 46: Difference (3D-2D) in pressure between the 3D and 2D model in transect 154.

Just like at the pressure underneath the dike the difference between the 2D and 3D model is lowest around the areas of water because the water stage is a fixed input. In the confining layer the difference is also low in the hinterland, because the water level in the polder level is also fixed and this is noticeable in the first model layer and not in model layer 4.

5.7 HEADS IN TRANSECT 155

The focus will be on transect 155 in this section, because this transect has shown underestimations in the 2D model in different layers at different timesteps. In this section the local differences will be explored and analysed.

5.7.1 HYDRAULIC HEAD IN THE AQUIFER

The hydraulic head in the **first** aquifer (Figure 47) is highest under the river and decreases into the hinterland. In the hinterland the drainage is set to 2.6 m+NAP. The green and blue line show a delay in response to the river stage, which is the same as in transect 154. The peak discharge provides the highest hydraulic head in the aquifer at the location of the river and the hinterland. Four days after the peak discharge, the hydraulic head under the side channels and in the hinterland is at its maximum.

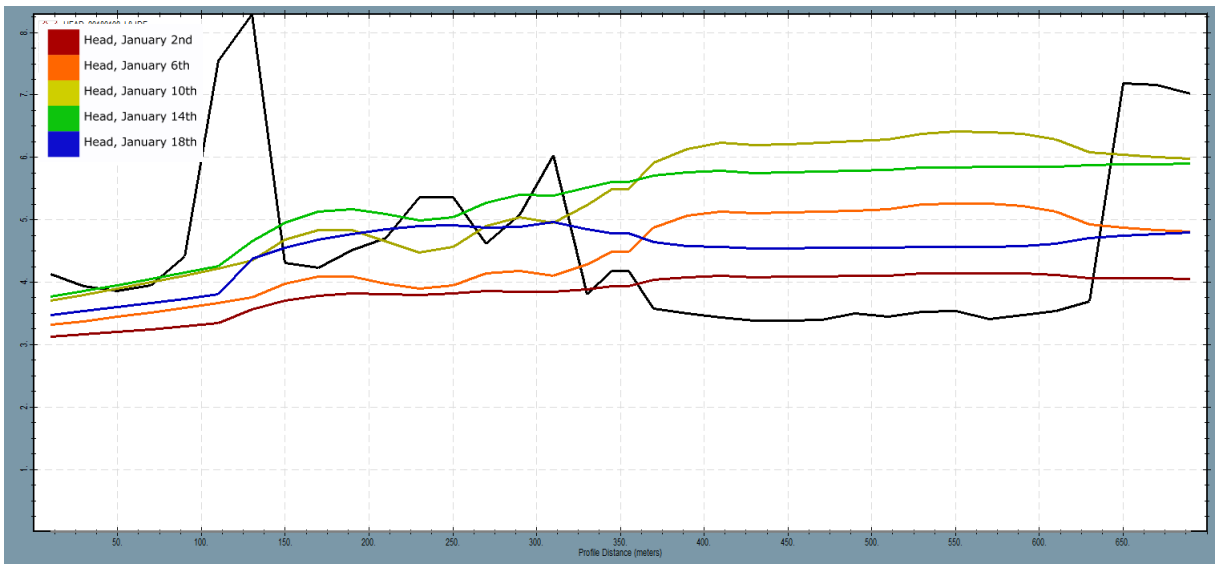

Figure 47: 3D model results. Cross-section of transect 155. Hydraulic head in the first aquifer (starting from model layer 6) in transect 155. The black line is the surface of the transect 155. Between 350 m and 600 m on the x-axis the river is located with conductance 100m2/d, and around 170m and 270m on the x-axis two canals are located with conductance 15m2/d.

The differences between the 3D and 2D model (Figure 48) range from -0.25 to 0.3 m. In the purple boxes the 2D model underestimates the hydraulic head. Especially the peak discharges at location x=650 result in underestimation in 2D of 0.3 m. Also between the two channels and the channels and in the hinterland occurs underestimation of the 2D model. This occurs during and after the peak discharge.

The hinterland at x=0 shows again that the days with the highest discharge cause a larger difference between 3D and 2D and days with lowest discharge cause the smallest difference.

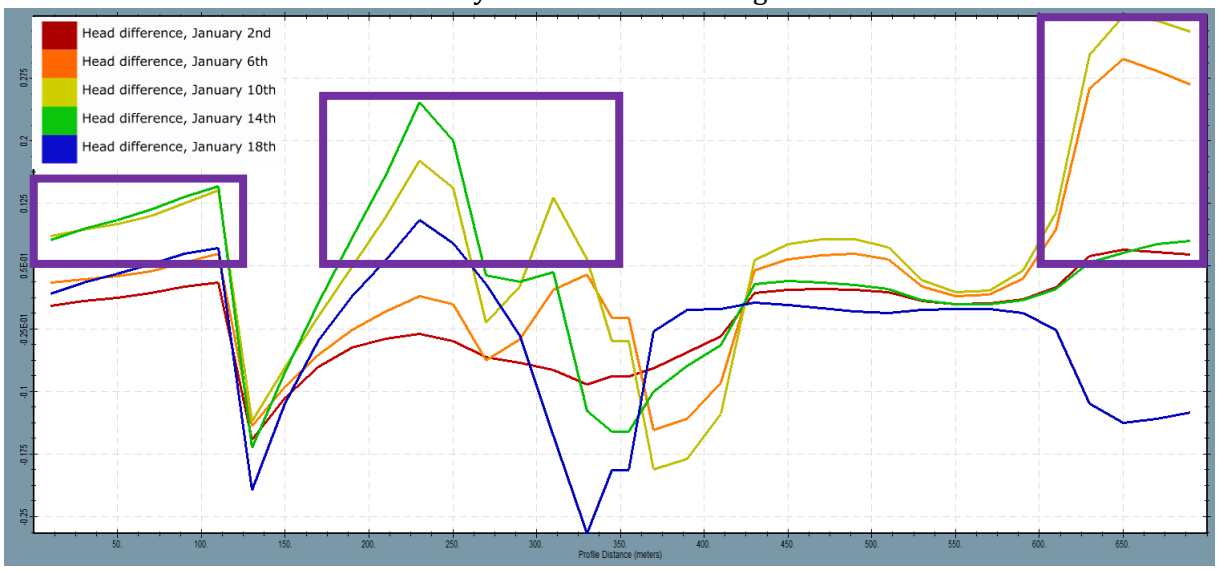

Figure 48: Difference (3D-2D) between the 2D model and 3D model in transect 155 in the first aquifer, model layer 8.

The 2D model underestimates on days with higher discharge (orange, yellow, green). The underestimations occur on locations just before or after a waterbody and in the hinterland. This could be because the water stays longer in the confining layer in the 2D model.

Figure 49 shows that the hydraulic head in the **second** aquifer is highest under the river and decreases into the hinterland. It shows the same pattern as in the first aquifer. The peak discharge provides the highest hydraulic head in the aquifer for all locations except in the hinterland.

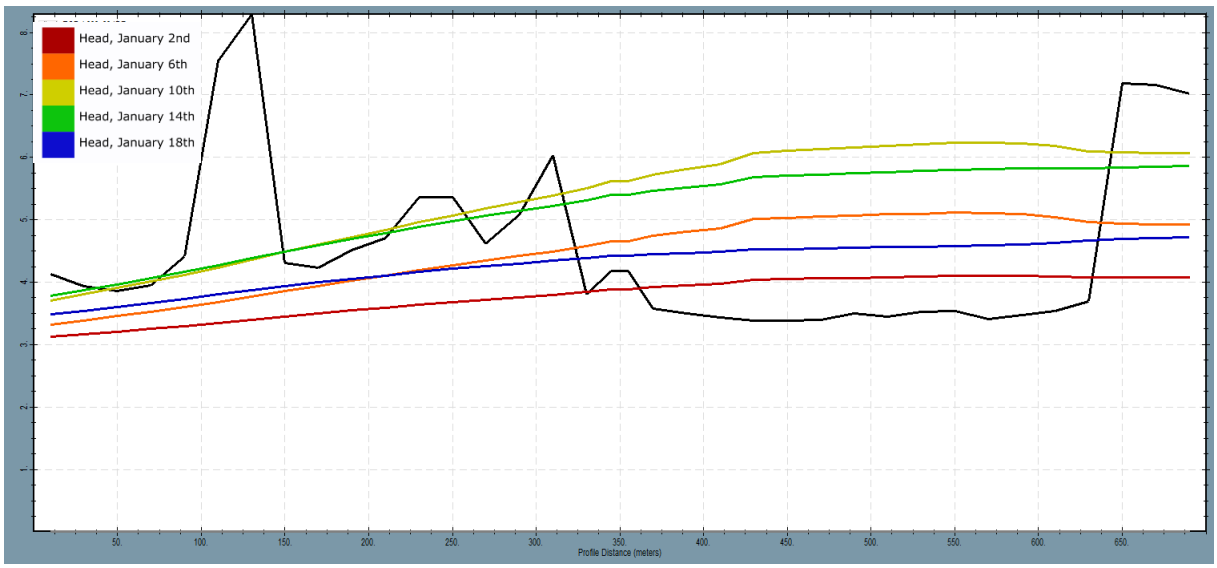

Figure 49: 2D view. Hydraulic head in the second aquifer (starting from model layer 11) in transect 155.
The black line is the surface of the transect 155. Between 350 m and 600 m on the x-axis the river is located with conductance 100m2/d, and around 170m and 270m on the x-axis two canals are located with conductance 15m2/d.

The differences between the 2D and 3D model (Figure 50) are larger and different than the differences in the first aquifer. The 2D model mainly underestimates in this aquifer, this can be seen in Figure 48. The y-axis ranges from +0.3 to -0.1. In the smaller dike with the height of 6 m+NAP around x=300, the 3D model produces higher hydraulic heads with for the days with the peak discharges (orange, yellow and green), see black circle. In the river the differences between 3D and 2D are smaller, there is only a noticeable difference of 0.1m on the days with the peak discharge.

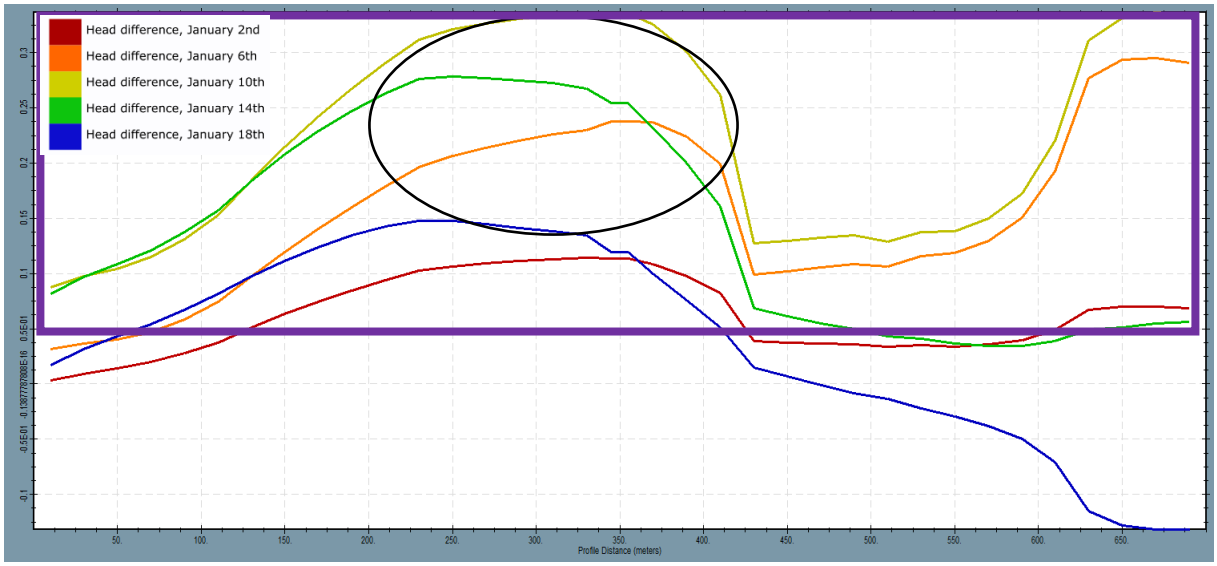

Figure 50: Difference (3D-2D) between the 2D model and 3D model in transect 155 in the second aquifer, model layer 11

Over the whole transect length the 2D model underestimates for all discharges. The second aquifer is located beneath a 2 metre thick impermeable clay layer with an hydraulic conductivity of 0.002 [m/d]. The water in the 2D model stays longer in this clay layer than in the 3D model, leading to less water in the second aquifer. The water in the 3D model probably moves around the clay layer down into the aquifer.

The other transects of 153 and 156 show negative differences, meaning that the 2D model overestimates. It shows in hinterland that the difference between 3D and 2D increases over time, see Appendix D.

5.7.2 PRESSURE HEAD UNDERNEATH THE DIKE

Just as at transect 154 the pressure is everywhere positive in Figure 51. Except for the hinterland, here all the days have a negative pressure. The pressure is highest on the location of the main river, and the pressure corresponds to the level of the river. A strong contrast can be seen between x=150 and 350 where the last days, green and blue, shows a strong delay to the river stage. The pressure on these days' increases while the river stage decreases.

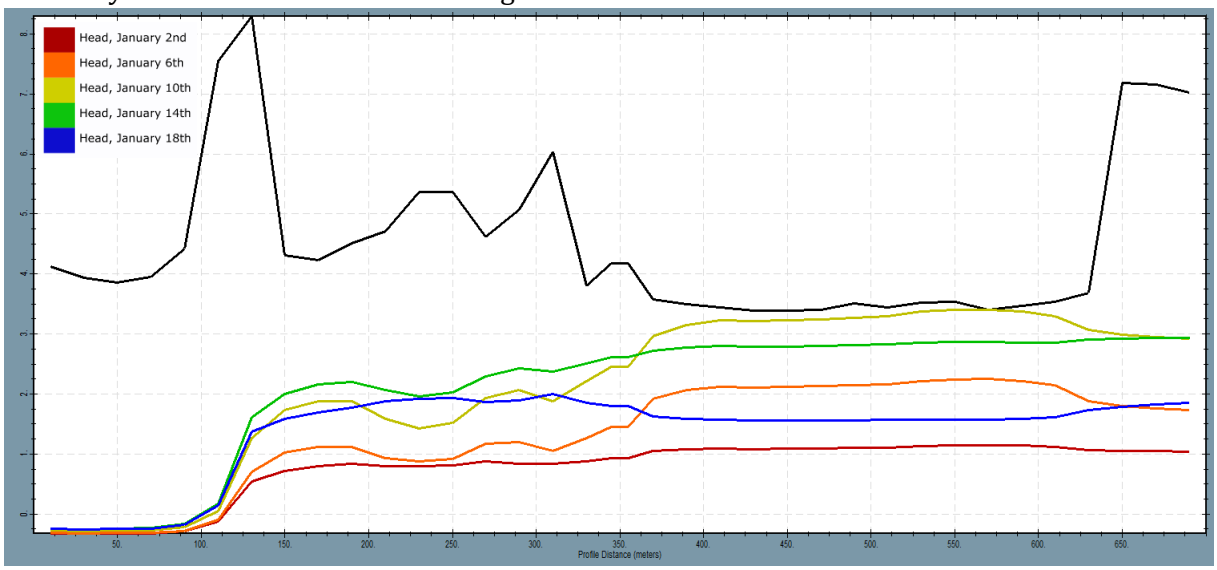

Figure 51: Pressure carried out on the confining layer (bottom model layer 4) of transect 155.
The black line is the surface of the transect 155. Between 350 m and 600 m on the x-axis the river is located with conductance 100m2/d, and around 170m and 270m on the x-axis two canals are located with conductance 15m2/d.

The difference in pressure is just like the difference in hydraulic head high at the right side of the transect in the black box in Figure 52. The differences at the location of the river are not noticeable. At x=330, the last day (blue) shows a difference of -0.25 m, see the black circle. The difference in the hinterland is very low (-0.025) and the lines are very close together. The locations of overestimations are almost the same as the locations in the first aquifer, and they have the same rate of overestimation (Figure 48).

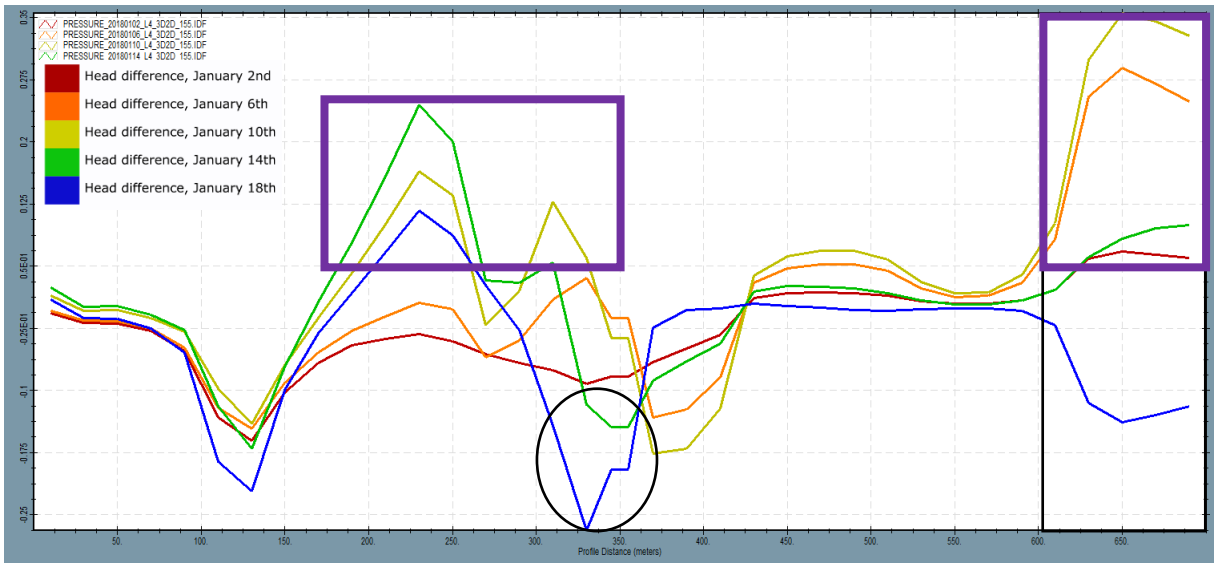

Figure 52: Difference (3D-2D) in pressure between the 3D and 2D model in transect 155.

The pressure at the bottom of the confining layer is underestimated in the 2D model at the same locations as the first aquifer, before or after waterbodies. This happens because of the same reason, the water stays longer in the confining layer in the 2D model. In the hinterland the 2D model

does not underestimate, this could be because the polder has a fixed water level, therefore there is little room for change between the two models.

5.7.3 PRESSURE HEAD IN THE CONFINING CLAY LAYER

Figure 53 depicts the 3D model results inside the confining layer. The pressure is positive on the location where the river and canals are present, at the other locations the pressure is negative.

The difference in pressure (Figure 54) between the two models is almost identical to the pressure difference at the bottom of the confining layer (Figure 52).

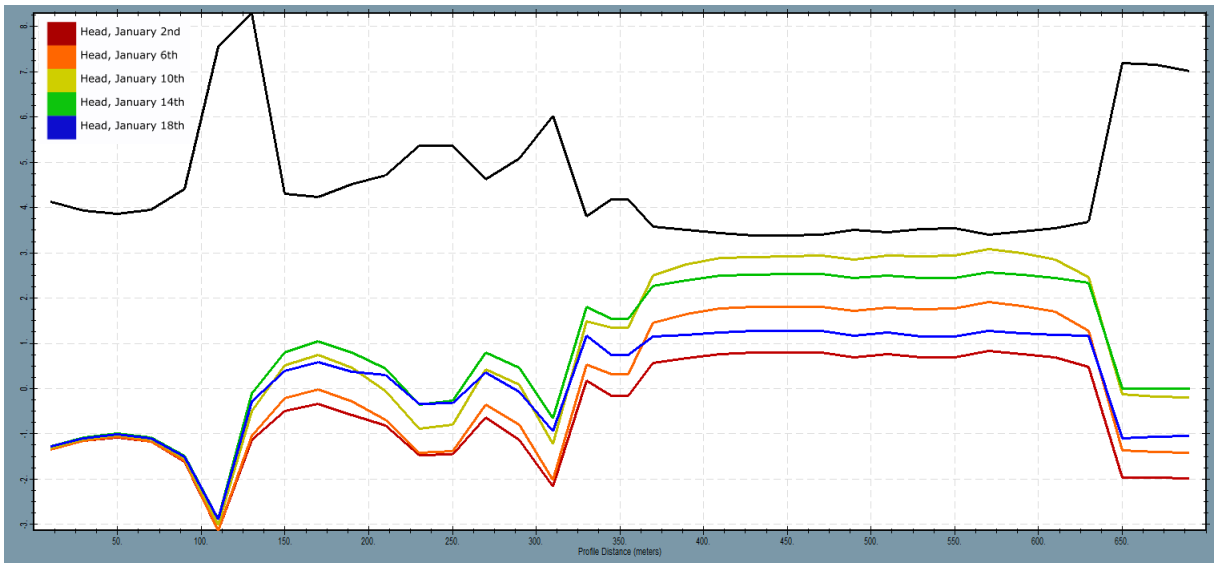

Figure 53: Pressure in the confining layer (bottom model layer 1) of transect 155.
The black line is the surface of the transect 155. Between 350 m and 600 m on the x-axis the river is located with conductance 100m2/d, and around 170m and 270m on the x-axis two canals are located with conductance 15m2/d.

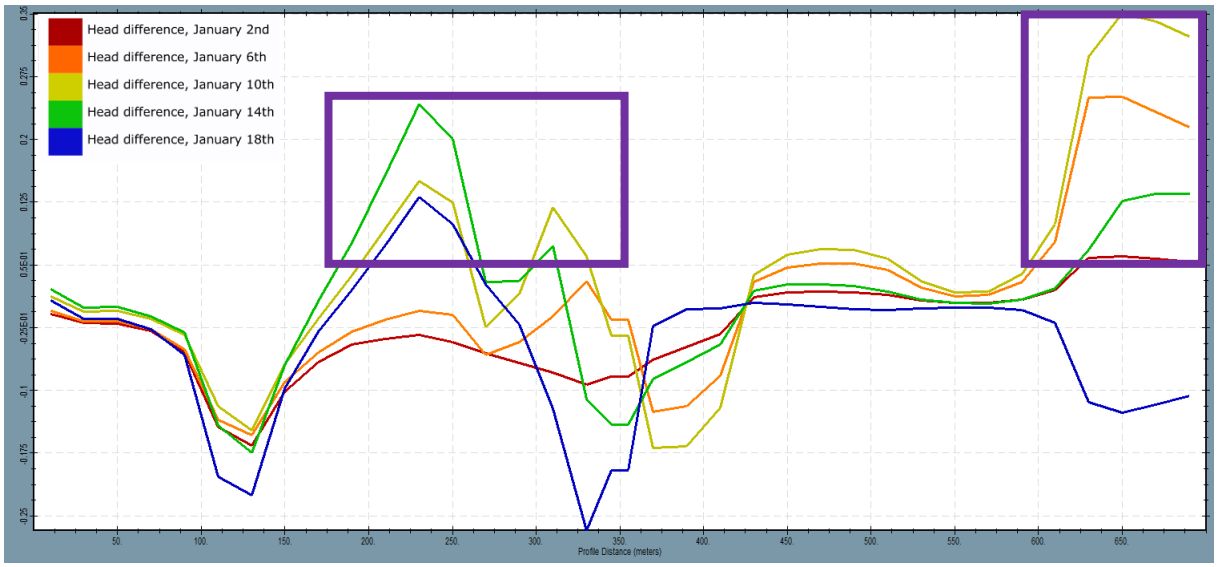

Figure 54: Difference in pressure between the 3D and 2D model in transect 155.

The pressure in the confining layer is underestimated in the 2D model at the same locations as the pressure under the confining layer. This happens for the same reasons.

6 DISCUSSION

This research investigated the groundwater flow conditions around and underneath river dikes with a highly heterogeneous subsurface. This investigation was done to examine the difference between a 3D and 2D model and to see if a 3D model gives a better representation of the hydraulic head prediction in response to the influence of heterogeneity for dike stability assessments.

6.1 DISCUSSION OF THE RESULTS

To summarize the results, I have grouped the difference between the models (positive and negative) per location in their dependency for discharge, and/or time, and /or depth. Discharge dependent is when the water level in the river has influence on the behaviour of the head difference between 2D and 3D. Time dependent is when the behaviour of the head difference between 2D and 3D is dependent on the length of the model run. Depth dependent is when the difference between 2D and 3D differs also per model layer. A positive difference means that 3D has higher value for the head compared to 2D, negative is when 3D has lower values for the head compared to 2D. The dependencies are depicted in Table 4. See appendix F for the detailed analysis.

Table 4: Dependencies for different locations.

		Discharge	Time	Discharge & time
River		9	0	0
	Depth	0	0	0
River side		7	0	3
	Depth	0	0	0
Foreland		4	3	2
	Depth	1	1	0
Channels		5	1	1
	Depth	2	0	0
Dike		3	4	2
	Depth	2	1	0
Hinterland		3	4	2
	Depth	0	0	0

As shown in Figure 41 till Figure 54 and Table 4, the difference (positive and negative) in hydraulic head of the 3D and 2D model has a dependency on the location of the measurement. The river is the location with the minimal difference between the 2D and 3D model, of 0.05 m. The difference is minimal because the model has a limitation in the direction the water can flow from the river package, the water can only flow out at the bottom of a model cell, not at the sides (Vermeulen & Minnema, 2019). Also both models have the same input for water stage. Therefore, the values for the hydraulic head at the location of the river are fairly constant.

While the middle of the river has a bottom which is flat, the sides of the river are modelled as cascading. This means that at different depths the bottom of the cells is located. While the water can only flow out of the bottom of the cell this does not have a large effect on the hydraulic head on the sides of the river because of the cascading pattern. This leads to increasing differences, positive and negative, between the 3D and 2D model for the hydraulic and pressure head, ranging from -0.1 m to 0.3 m. This happens because the water flows out of the bottom of the cells at different depths and will then be able to go further down or left, right or up.

The direction of the flow in the 3D and 2D model is determined by the permeability of the different soil types. While in the 3D model the water can flow around very impermeable soils such as clay, the water must go through such a layer in a 2D model because it cannot enter a cell left or right

as these cells do not exist. The flow is much slower in these impermeable clay layers, than in the permeable sand layers.

Figure 41 till Figure 54 illustrate that there is an increase in difference between the hydraulic head values for the 3D and 2D model away from the river to the hinterland. Less cases become discharge dependent and more cases become time and depth dependent. Time and depth dependency have to do with the lithology of the subsurface as the groundwater can move around impermeable layers in the 3D model, while in the 2D model this is not possible. As Lee et al. (2017) states, the probability of having high hydraulic conductivity areas (areas of sand) connected in regions increases in 3D. This impacts flow and transport of water. If high hydraulic conductivity regions are well connected in the 2D model, it could be possible that the 2D and 3D flow patterns are comparable. Otherwise the gradient, slope and angle of the hydraulic head distribution are different in a 2D model than a 3D model. Creating different hydraulic head patterns.

More importantly in this research are the locations of the underestimation of the 2D model. Dike stability assessments use 2D models for their calculations and ultimately recommendations for the safety of a dike. To analyse this the models have been compared per timestep, per layer. See appendix C.

The underestimation in the 2D model occurs in all transects, mainly in transect 154 and 155 it is clearly visible because the underestimation at certain locations in the transect is higher than 0.2 m. The underestimation reaches 0.5 m. Underestimation is for most part discharge and depth dependent. Especially transect 155 has more locations where underestimation occurs. Most critical underestimations are those near the dike, because dike stability assessments use the values for the hydraulic head on these locations. In transect 155 the underestimation increases drastically in the second aquifer. This is proof that underestimation of the 2D model arises due to lithology, especially clay has a lot of influence on the hydraulic head. The second aquifer of transect 155 is located underneath an impermeable clay layer with an hydraulic conductivity of 0.002 [m/d].

Van den Boer et al. (2014) states that poor predictions in 2D models arise from the assumption that erosion, especially piping, can be described in two dimensions. This could be a reason for the over and underestimations.

6.2 Model performance

The results indicate that there are strong differences between the 3D groundwater model and 2D groundwater model. However, the 3D model does not show fit the empirical values from the piezometers of HDSR. Although the pattern of the distribution follows the same pattern as the piezometer measurements, the values of the 3D model are on average 0.37 m below the empirical values. The values of the 3D model do not fit the empirical values as a result of not calibrated input parameters such as horizontal and vertical permeability, storage and specific yield. Also the river and drainage conductance are untested.

It has to be taken into account that the underestimations of the 2D model are thus even more off from the empirical piezometer values than the 3D model.

6.3 Recommendations

Model evaluation is the first step that needs to be taken to enhance the model performance. This includes model calibration, validation and uncertainty assessment. The addition of these factors will lead to more realistic hydraulic head predictions.

To revise and enhance the claims that are made in the results, different scenarios should be run to examine the effects of different high water stages and durations. See appendix E for these scenarios.

The input parameters that are at least required for a groundwater investigation are: a sufficient amount of model layers, the vertical and horizontal permeability, storage coefficient, and specific yield. If the amount of model layers is increased, a more detailed model is obtained with respect to resulted heads and budget terms, but this will also increase the computation time. A balance needs to be found between results and computation time.

Furthermore, it is important to work with the finest available resolution. Only then the model will give the most accurate output for hydraulic heads and budget terms.

7 CONCLUSION

To investigate the behaviour of groundwater flow under the dike between Wijk van Duurstede and Amerongen and to explore if there is a change in terms of representing the hydraulic heads under the dike and the resulting groundwater flow paths under normal conditions and during high water events between 3D and 2D modelling, two groundwater models of different dimensions have been created. The models simulated the hydraulic head distribution in several lithological layers. These results were analysed and compared for the 3D and 2D model. The hydraulic head distribution shows different behaviour in terms of dimensions:

- The behaviour changes with the distance from the river. A higher difference between the models is observed in the hinterland compared to the river.
- The higher the discharge, the more the behaviour can change around the river as well.
- The depth at which the results are observed show a higher difference deeper into the subsurface.
- The longer the model runs the higher the differences can become. This is mainly in the hinterland.

In terms of underestimation of the 2D model, which can provide false safety if used for dike stability assessments, the following findings were observed:

- Underestimation is highest in the aquifer on days with the high discharge.
- Impermeable clay with an hydraulic conductivity of 0.002 [m/d] has influence on the underestimation of the 2D model.

This research demonstrate that a 3D groundwater model is an effective way to predict hydraulic head distributions in heterogeneous subsurface near river dikes. It is more effective than a 2D model when you look at regional patterns. A 2D groundwater model is effective for determining local patterns, for example at the groundwater flow in the confining layer or the subsurface below the waterbodies with fixed input parameters. So unless information on the flow pattern close to a 3D flow phenomenon (like piping) is needed, 3D modelling might not be necessary.

Furthermore, the 3D model was often below the empirical values of the piezometers, the underestimations of the 2D model are further below the empirical values. In addition the 2D model has a larger range in values for the hydraulic head. Where for example the hydraulic head in the aquifer ranges from 3 m+NAP to 3.9 m+NAP in the 3D model, ranges the head in the 2D model in the same aquifer from 3 m+NAP to 4.7 m+NAP (Figure 38, plot B).

Concluded can be that a 2D groundwater model mainly overestimates which is OK for dike stability assessments. But the influence of the lithology on the underestimation of the 2D model has not yet been thoroughly determined therefore 3D groundwater model gives a better representation of the hydraulic head prediction in response to the influence in heterogeneity near and under river dikes than a 2D model. This is an important conclusion for dike stability assessments. It is recommended to use 3D groundwater models for future dike stability assessments.

8 REFERENCES

Allersma, H. G. B., & Rohe, A. (2003). Centrifuge tests on the failure of dikes caused by uplift pressure. *International Journal of Physical Modelling in Geotechnics*, *3*(1), 45–53. https://doi.org/10.1680/ijpmg.2003.030104

Berendsen, H. J. A., & Stouthamer, E. (2002). Paleogeographic evolution and avulsion history of the Holocene Rhine-Meuse delta, The Netherlands. *Netherlands Journal of Geosciences - Geologie En Mijnbouw*, *81*(1), 97–112. https://doi.org/10.1017/S0016774600020606

Brandl, H., & Szabo, M. (2013). Hydraulic failure of flood protection dykes. *18th International Conference on Soil Mechanics and Geotechnical Engineering: Challenges and Innovations in Geotechnics, ICSMGE 2013*, *4*, 3289–3292.

Cohen, K. (1994). *Zand in banen: zanddieptekaarten van het rivierengebied en het IJsseldal in de provincies Gelderland en Overijssel*. www.gelderland.nl/wateratlas

Deltares report , http://nhi.nu/nl/files/3114/3635/4839/1220056-004-ZWS-0003-r-Waterkwaliteitsmodellering_-_DEF.pdf , 2015

de Groot, J. (2016). *3D groundwater flow in heterogeneous subsurfaces underneath dikes*.

Dorst, P. H. (2019). *Modelling the phreatic surface in regional flood defences*. http://repository.tudelft.nl/

Finsbury et al., http://webissimo.developpement-durable.gouv.fr/IMG/pdf/A_The_International_Dike_Handbook_C731__cle7f8a33.pdf , 2013

Ge, S. & Gorelick, S. M. (2015). Groundwater and Surface Water. *Encyclopedia of Atmospheric Sciences: Second Edition*, 209–216. https://doi.org/10.1016/B978-0-12-382225-3.00171-7

Gouw, M. J. P., & Erkens, G. (2007). Architecture of the Holocene Rhine-Meuse delta (the Netherlands) - A result of changing external controls. *Netherlands Journal of Geosciences - Geologie En Mijnbouw*, *86*(1), 23–54. https://doi.org/10.1017/S0016774600021302

Harbaugh, A. (2005). MODFLOW-2005, the U.S. Geological Survey modular ground-water model. *U.S. Geological Survey Techniques and Methods*, *6-A16*.

HDSR, https://www.hdsr.nl/beleid-plannen/peilbesluiten-0/ , 2019

HDSR, https://www.hdsr.nl/beleid-plannen/sterke-lekdijk/wijk-duurstede/, n.d.

Hoffmans, G., & Van Rijn, L. (2018). Hydraulic approach for predicting piping in dikes. *Journal of Hydraulic Research*, *56*(2), 268–281. https://doi.org/10.1080/00221686.2017.1315747

Kurtulus, B., & Flipo, N. (2011). *Hydraulic head interpolation using ANFIS-model selection and sensitivity analysis*. https://doi.org/10.1016/j.cageo.2011.04.019

Lambert, J. W. M., Vastenburg, E., & Roelofsen, F. J. (2015). A model, describing the influence of water management alternatives on dike stability. *Proceedings of the International Association of Hydrological Sciences*, *372*, 515–518. https://doi.org/10.5194/piahs-372-515-2015

Lee, S. Y., Carle, S. F., & Fogg, G. E. (2007). Geologic heterogeneity and a comparison of two geostatistical models: Sequential Gaussian and transition probability-based geostatistical simulation. Advances in water resources, 30(9), 1914-1932.

Maurits Zoutendijk. (2019). *On the rise of the groundwater table due to infiltration of surface water*.

Oudhouten, https://www.oudhouten.nl/nieuwe-tijd/dijkdoorbraak-lekdijk/

Pham-Van, S., Hinkelmann, R., Nehrig, M., & Martinez, I. (2011). A comparison of model concepts and experiments for seepage processes through a dike with a fault zone. *Engineering Applications of Computational Fluid Mechanics*, *5*(1), 149–158. https://doi.org/10.1080/19942060.2011.11015359

Polanco, L., & Rice, J. (2014). Reliability-based evaluation of the effects of geometry on levee

underseepage potential. *Geotechnical Special Publication*, *234 GSP*, 860–871. https://doi.org/10.1061/9780784413272.084

Roover, S. De. (2015). Modelling the Jakarta groundwater system : A Sensitivity Analysis Modelling the Jakarta groundwater system : A Sensitivity Analysis. In *Deltares Universiteit Twente*.

Schweckendiek, T., Vrouwenvelder, A. C. W. M., & Calle, E. O. F. (2014). Updating piping reliability with field performance observations. *Structural Safety*. https://doi.org/10.1016/j.strusafe.2013.10.002

Slijkhuis, K., Gelder, P. Van, & Vrijling, J. K. (2001). Optimal dike height under statistical-, construction-and damage uncertainty. *Citg.Tudelft.Nl*, *7*, 1137–1140. http://www.citg.tudelft.nl/fileadmin/Faculteit/CiTG/Over_de_faculteit/Afdelingen/Afdeling_Waterbouwkunde/sectie_waterbouwkunde/people/personal/gelder/publications/papers/doc/paper12.pdf

Sloff, K., Van Spijk, A., Stouthamer, E., & Sieben, A. (2013). Understanding and managing the morphology of branches incising into sand-clay deposits in the Dutch Rhine Delta. *International Journal of Sediment Research*, *28*(2), 127–138. https://doi.org/10.1016/S1001-6279(13)60025-6

Stoop, N. M. (2018). *The effects of anisotropy and heterogeneity in the piping sensitive layer*.

Stouthamer, E., & Van Asselen, S. (2015). Potential of Holocene deltaic sequences for subsidence due to peat compaction. *Proceedings of the International Association of Hydrological Sciences*, *372*(1), 173–178. https://doi.org/10.5194/piahs-372-173-2015

Van Der Most, H., Tánczos, I., De Bruijn, K. M., & Wagenaar, D. (n.d.). *NEW, RISK-BASED STANDARDS FOR FLOOD PROTECTION IN THE NETHERLANDS*.

Vandenboer, K., van Beek, V., & Bezuijen, A. (2014). 3D finite element method (FEM) simulation of groundwater flow during backward erosion piping. *Frontiers of Structural and Civil Engineering*, *8*(2), 160–166. https://doi.org/10.1007/s11709-014-0257-7

Vermeulen, P., Hong, N., Dinh, N., & Nam, G. (2013). Groundwater modeling for the Mekong Delta using iMOD. *20th International Congress on Modelling Anf Simultation*, *December*, 2499–2505. http://www.mssanz.org.au/modsim2013/L4/vermeulen.pdf

Vermeulen, P. T. M., & Minnema, B. (2019). IMOD User Manual version 4.4. *Deltares*, 580.

Winkels, T. G., Dirkx, W. J., Stouthamer, E., Cohen, K. M., & Middelkoop, H. (2018). *Subsurface heterogeneity at different spatial scales: Impact on piping hazard zones in the Netherlands*.

APPENDIX

APPENDIX A

Table 5: Permeability values [m/d] in different sources.

Lithology	***Stoop, 2018*** **Permeability [m/d]**	***Yu et al., 2012*** **Permeability moderate sorted [m/d]**	***Sanchez et al., 2012*** **Permeability [m/d]**	***Smedema &Rycroft, 1983*** **Permeability [m/d]**	***Forster et al., 2017*** **Permeability [m/d]**
Anthropogenic					
Peat	0.35		0.147		0.002 – 0.5
Clay	0.002	0.011	0.01	0.002 – 0.2	0.00001 – 0.0001
Sandy clay	0.5	0.5	0.123	0.5 – 2	0.1 – 1
Fine sand	2	5.4	0.65	1 – 3	1 – 10
Medium sand	5	24.6	5.640	1 – 5	1 – 10
Coarse sand	25	32.9		10 – 50	10 – 100
Gravel	250	142			100 – 1000
Shells					

APPENDIX B

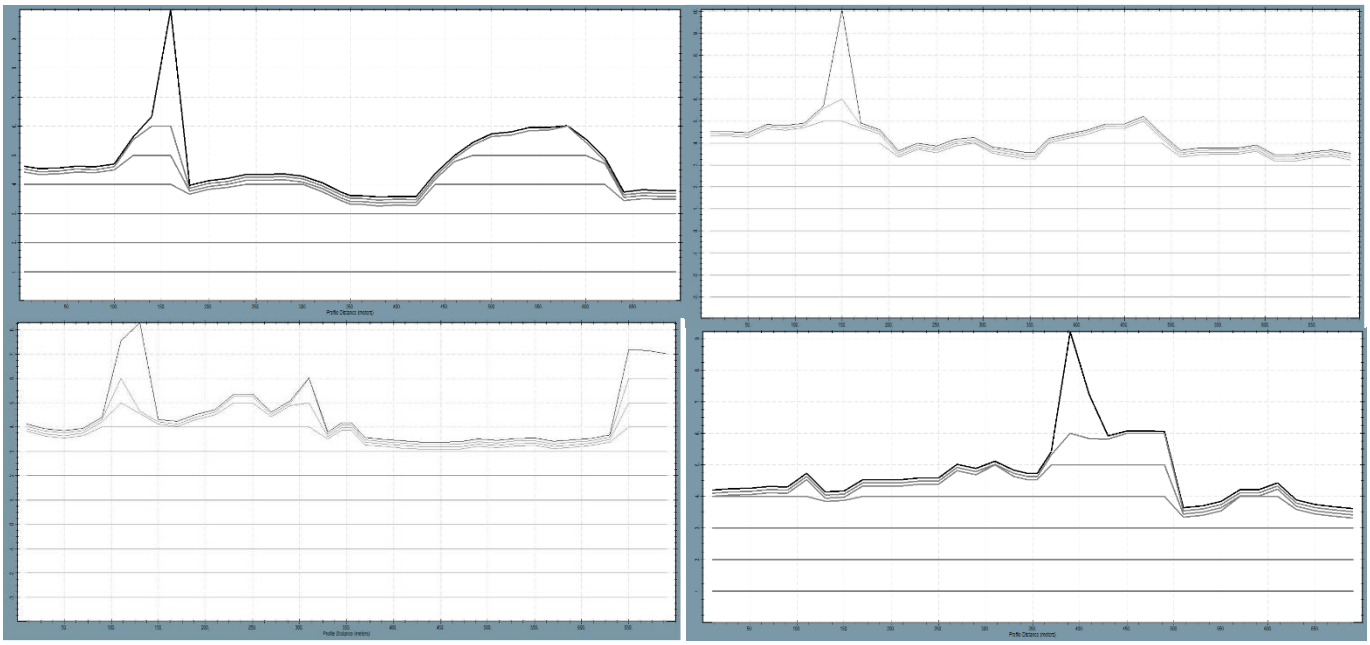

Figure 55: Transects with AHN and model layers. A) transect 153 with coordinates X: 153000 Y: 443350-442650. B) transect 154 with coordinates X: 154000 Y: 443500-442800. C) transect 155 with coordinates X: 155000 Y: 443220-442520. D) transect 156 with coordinates X: 156000 Y: 443500-442800

APPENDIX C

	153	Layer			1	2	3	4	5	6	7	8	9	10	11	12	13	14	15	16	17	18	19	20	21	22	23	24	25
Am. Ben.	Timestep	Mean			-0.12	-0.12	-0.13	-0.14	-0.16	-0.17	-0.17	-0.17	-0.17	-0.18	-0.18	-0.18	-0.18	-0.18	-0.18	-0.18	-0.18	-0.18	-0.18	-0.18	-0.18	-0.18	-0.19	-0.20	-0.20
			Max		0.03	0.03	0.03	0.09	0.09	0.09	0.09	0.09	0.09	0.09	0.09	0.09	0.09	0.08	0.07	0.07	0.07	0.07	0.07	0.07	0.07	0.05	0.01	0.01	0.01
				Min	-0.49	-0.49	-0.49	-0.55	-0.55	-0.55	-0.55	-0.55	-0.55	-0.55	-0.55	-0.55	-0.55	-0.54	-0.54	-0.54	-0.53	-0.53	-0.53	-0.53	-0.56	-0.58	-0.72	-0.84	-0.84
4.1	43101.00	-0.13	0.00	-0.36	-0.10	-0.10	-0.10	-0.11	-0.12	-0.13	-0.13	-0.13	-0.13	-0.13	-0.13	-0.14	-0.14	-0.14	-0.14	-0.14	-0.14	-0.14	-0.14	-0.14	-0.14	-0.14	-0.14	-0.15	-0.15
4.2	43102.00	-0.13	0.00	-0.37	-0.10	-0.10	-0.11	-0.11	-0.12	-0.14	-0.14	-0.14	-0.14	-0.14	-0.14	-0.14	-0.14	-0.14	-0.14	-0.14	-0.14	-0.14	-0.14	-0.14	-0.14	-0.14	-0.15	-0.15	-0.15
4.7	43103.00	-0.11	0.09	-0.29	-0.10	-0.10	-0.10	-0.09	-0.10	-0.11	-0.11	-0.11	-0.11	-0.11	-0.11	-0.11	-0.11	-0.11	-0.11	-0.11	-0.11	-0.11	-0.11	-0.11	-0.11	-0.12	-0.13	-0.13	-0.13
5.0	43104.00	-0.13	0.04	-0.32	-0.10	-0.10	-0.10	-0.11	-0.12	-0.14	-0.14	-0.14	-0.14	-0.14	-0.14	-0.14	-0.14	-0.14	-0.14	-0.14	-0.14	-0.14	-0.14	-0.14	-0.14	-0.14	-0.14	-0.15	-0.14
5.4	43105.00	-0.15	0.03	-0.42	-0.10	-0.10	-0.11	-0.12	-0.14	-0.15	-0.15	-0.15	-0.15	-0.15	-0.15	-0.15	-0.15	-0.16	-0.16	-0.16	-0.16	-0.16	-0.16	-0.16	-0.16	-0.16	-0.16	-0.16	-0.16
5.7	43106.00	-0.16	0.02	-0.51	-0.11	-0.11	-0.12	-0.13	-0.15	-0.16	-0.16	-0.16	-0.16	-0.16	-0.16	-0.16	-0.16	-0.17	-0.17	-0.17	-0.17	-0.17	-0.17	-0.17	-0.17	-0.17	-0.17	-0.18	-0.18
5.9	43107.00	-0.16	0.01	-0.59	-0.11	-0.11	-0.12	-0.13	-0.15	-0.17	-0.17	-0.17	-0.17	-0.17	-0.17	-0.17	-0.17	-0.17	-0.18	-0.18	-0.18	-0.18	-0.18	-0.18	-0.18	-0.18	-0.18	-0.19	-0.19
6.2	43108.00	-0.17	0.00	-0.67	-0.11	-0.11	-0.12	-0.14	-0.16	-0.17	-0.17	-0.17	-0.17	-0.17	-0.18	-0.18	-0.18	-0.18	-0.18	-0.18	-0.18	-0.18	-0.18	-0.18	-0.18	-0.18	-0.19	-0.20	-0.20
6.4	43109.00	-0.18	0.00	-0.73	-0.12	-0.12	-0.13	-0.14	-0.17	-0.18	-0.18	-0.18	-0.18	-0.18	-0.18	-0.18	-0.18	-0.19	-0.19	-0.19	-0.19	-0.19	-0.19	-0.19	-0.19	-0.19	-0.20	-0.21	-0.21
6.7	43110.00	-0.18	-0.01	-0.79	-0.12	-0.12	-0.13	-0.15	-0.17	-0.19	-0.19	-0.19	-0.19	-0.19	-0.19	-0.19	-0.19	-0.19	-0.20	-0.20	-0.20	-0.19	-0.19	-0.19	-0.19	-0.20	-0.21	-0.22	-0.22
6.7	43111.00	-0.19	-0.01	-0.83	-0.12	-0.12	-0.14	-0.15	-0.17	-0.19	-0.19	-0.19	-0.19	-0.19	-0.19	-0.19	-0.19	-0.20	-0.20	-0.20	-0.20	-0.20	-0.20	-0.20	-0.20	-0.20	-0.22	-0.23	-0.23
6.5	43112.00	-0.19	-0.01	-0.84	-0.12	-0.13	-0.14	-0.15	-0.17	-0.19	-0.19	-0.19	-0.19	-0.19	-0.19	-0.19	-0.19	-0.20	-0.20	-0.20	-0.20	-0.20	-0.20	-0.20	-0.20	-0.20	-0.22	-0.23	-0.23
6.2	43113.00	-0.18	-0.01	-0.82	-0.12	-0.13	-0.14	-0.15	-0.17	-0.18	-0.19	-0.19	-0.19	-0.19	-0.19	-0.19	-0.19	-0.19	-0.19	-0.19	-0.19	-0.19	-0.19	-0.19	-0.19	-0.19	-0.21	-0.23	-0.23
5.7	43114.00	-0.18	0.00	-0.78	-0.12	-0.13	-0.13	-0.14	-0.16	-0.18	-0.18	-0.18	-0.18	-0.18	-0.18	-0.18	-0.18	-0.18	-0.18	-0.18	-0.18	-0.18	-0.18	-0.18	-0.18	-0.19	-0.21	-0.22	-0.22
5.3	43115.00	-0.17	0.00	-0.71	-0.12	-0.12	-0.13	-0.14	-0.15	-0.17	-0.17	-0.17	-0.17	-0.17	-0.17	-0.17	-0.17	-0.17	-0.18	-0.18	-0.18	-0.18	-0.18	-0.18	-0.17	-0.18	-0.20	-0.21	-0.21
4.9	43116.00	-0.16	0.00	-0.63	-0.12	-0.12	-0.13	-0.13	-0.15	-0.17	-0.17	-0.17	-0.17	-0.17	-0.17	-0.17	-0.17	-0.17	-0.17	-0.17	-0.17	-0.17	-0.17	-0.17	-0.17	-0.17	-0.19	-0.20	-0.20
4.7	43117.00	-0.16	0.00	-0.57	-0.12	-0.12	-0.13	-0.13	-0.14	-0.16	-0.16	-0.16	-0.16	-0.16	-0.16	-0.16	-0.16	-0.16	-0.16	-0.16	-0.16	-0.16	-0.16	-0.16	-0.16	-0.17	-0.18	-0.19	-0.19
4.5	43118.00	-0.16	0.00	-0.52	-0.12	-0.12	-0.13	-0.13	-0.14	-0.16	-0.16	-0.16	-0.16	-0.16	-0.16	-0.16	-0.16	-0.16	-0.16	-0.16	-0.16	-0.16	-0.16	-0.16	-0.16	-0.16	-0.18	-0.18	-0.18
4.6	43119.00	-0.16	0.00	-0.48	-0.12	-0.12	-0.13	-0.13	-0.14	-0.16	-0.16	-0.16	-0.16	-0.16	-0.16	-0.16	-0.16	-0.16	-0.16	-0.16	-0.16	-0.16	-0.16	-0.16	-0.16	-0.16	-0.17	-0.18	-0.18
4.7	43120.00	-0.16	0.00	-0.47	-0.12	-0.12	-0.13	-0.13	-0.15	-0.16	-0.16	-0.16	-0.16	-0.17	-0.17	-0.17	-0.17	-0.17	-0.17	-0.17	-0.17	-0.17	-0.17	-0.17	-0.17	-0.17	-0.18	-0.18	-0.18
4.9	43121.00	-0.17	0.00	-0.48	-0.12	-0.12	-0.13	-0.13	-0.15	-0.17	-0.17	-0.17	-0.17	-0.17	-0.17	-0.17	-0.17	-0.17	-0.17	-0.17	-0.17	-0.17	-0.17	-0.17	-0.17	-0.17	-0.18	-0.19	-0.19
5.2	43122.00	-0.17	0.01	-0.50	-0.12	-0.12	-0.13	-0.14	-0.16	-0.17	-0.18	-0.18	-0.18	-0.18	-0.18	-0.18	-0.18	-0.18	-0.18	-0.18	-0.18	-0.18	-0.18	-0.18	-0.18	-0.18	-0.19	-0.19	-0.19
5.4	43123.00	-0.18	0.01	-0.54	-0.13	-0.13	-0.14	-0.14	-0.16	-0.18	-0.18	-0.18	-0.18	-0.18	-0.18	-0.18	-0.18	-0.19	-0.19	-0.19	-0.19	-0.19	-0.19	-0.19	-0.19	-0.19	-0.19	-0.20	-0.20
5.6	43124.00	-0.18	0.00	-0.58	-0.13	-0.13	-0.14	-0.15	-0.17	-0.19	-0.19	-0.19	-0.19	-0.19	-0.19	-0.19	-0.19	-0.19	-0.19	-0.19	-0.19	-0.19	-0.19	-0.19	-0.19	-0.19	-0.20	-0.21	-0.21
5.8	43125.00	-0.19	0.00	-0.63	-0.13	-0.13	-0.14	-0.15	-0.17	-0.19	-0.19	-0.19	-0.19	-0.19	-0.19	-0.19	-0.19	-0.20	-0.20	-0.20	-0.20	-0.20	-0.20	-0.20	-0.20	-0.20	-0.21	-0.22	-0.22
5.9	43126.00	-0.19	0.00	-0.67	-0.13	-0.13	-0.14	-0.16	-0.18	-0.20	-0.20	-0.20	-0.20	-0.20	-0.20	-0.20	-0.20	-0.20	-0.20	-0.20	-0.20	-0.20	-0.20	-0.20	-0.20	-0.20	-0.21	-0.22	-0.22
6.1	43127.00	-0.20	-0.01	-0.70	-0.14	-0.14	-0.15	-0.16	-0.18	-0.20	-0.20	-0.20	-0.20	-0.20	-0.20	-0.20	-0.20	-0.21	-0.21	-0.21	-0.21	-0.21	-0.21	-0.21	-0.21	-0.21	-0.22	-0.23	-0.23
6.3	43128.00	-0.20	-0.01	-0.74	-0.14	-0.14	-0.15	-0.16	-0.19	-0.21	-0.21	-0.21	-0.21	-0.21	-0.21	-0.21	-0.21	-0.21	-0.21	-0.21	-0.21	-0.21	-0.21	-0.21	-0.21	-0.21	-0.23	-0.24	-0.24
6.5	43129.00	-0.21	-0.01	-0.78	-0.14	-0.14	-0.15	-0.17	-0.19	-0.21	-0.21	-0.21	-0.21	-0.21	-0.21	-0.21	-0.21	-0.22	-0.22	-0.22	-0.22	-0.22	-0.22	-0.22	-0.22	-0.22	-0.23	-0.24	-0.24
6.4	43130.00	-0.21	-0.01	-0.80	-0.14	-0.14	-0.16	-0.17	-0.19	-0.21	-0.21	-0.21	-0.21	-0.21	-0.21	-0.21	-0.21	-0.22	-0.22	-0.22	-0.22	-0.22	-0.22	-0.22	-0.22	-0.22	-0.24	-0.25	-0.25
6.2	43131.00	-0.21	-0.01	-0.80	-0.14	-0.15	-0.16	-0.17	-0.19	-0.21	-0.21	-0.21	-0.21	-0.21	-0.21	-0.21	-0.21	-0.21	-0.22	-0.22	-0.22	-0.22	-0.22	-0.22	-0.22	-0.22	-0.24	-0.25	-0.25

Figure 56: Data difference 2D and 3D model transect 153.

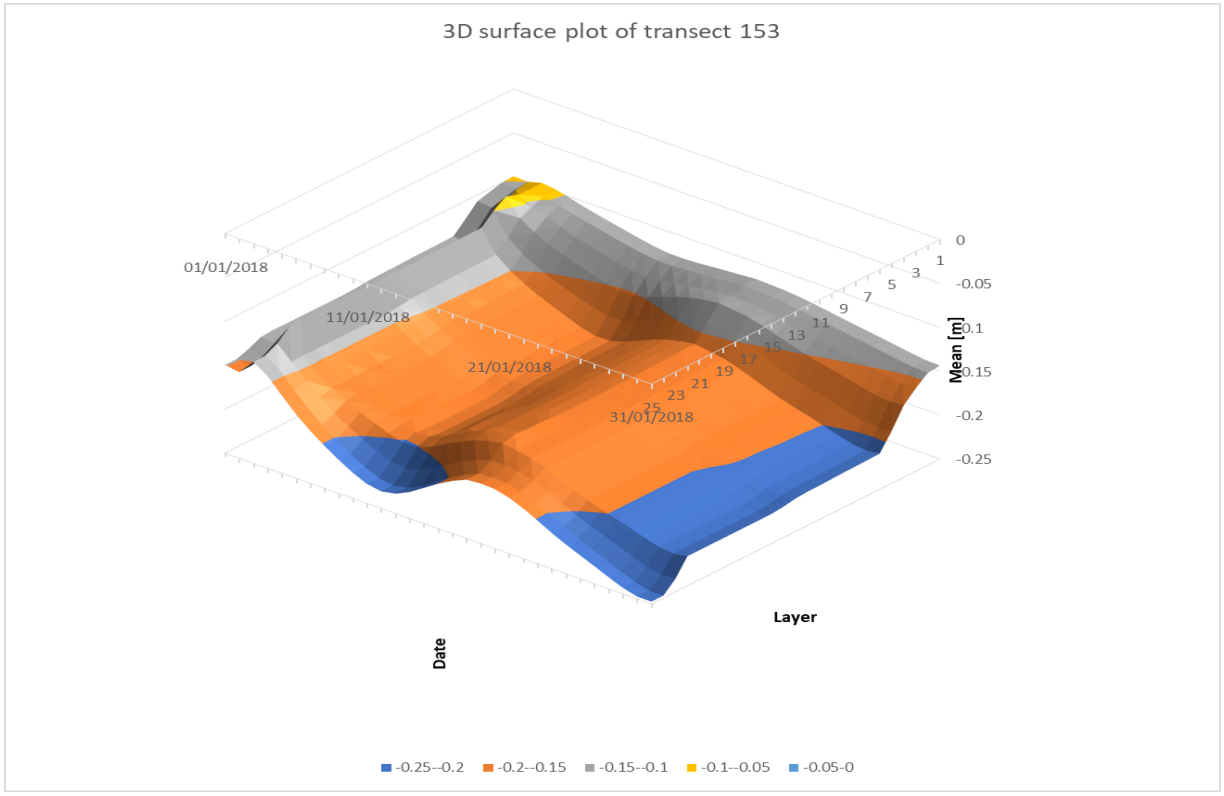

154		Layer			1	2	3	4	5	6	7	8	9	10	11	12	13	14	15	16	17	18	19	20	21	22	23	24	25
Am. Ben.	Timestep	Mean			-0.101	-0.105	-0.112	-0.173	-0.262	-0.296	-0.305	-0.305	-0.305	-0.306	-0.306	-0.306	-0.307	-0.308	-0.31	-0.31	-0.312	-0.315	-0.317	-0.317	-0.317	-0.314	-0.3	-0.3	-0.3
			Max		0.51	0.51	0.51	0.51	0.51	0.51	0.51	0.51	0.51	0.51	0.51	0.51	0.52	0.52	0.52	0.52	0.52	0.52	0.53	0.53	0.53	0.53	0.53	0.53	0.53
				Min	-0.514	-0.515	-0.515	-0.719	-0.954	-0.958	-0.962	-0.962	-0.962	-0.962	-0.962	-0.962	-0.962	-0.962	-0.959	-0.959	-0.948	-0.923	-0.91	-0.906	-0.905	-0.905	-0.9	-0.9	-0.9
4.1	01/01/2018	-0.19	0.00	-0.37	-0.10	-0.102	-0.105	-0.135	-0.178	-0.196	-0.201	-0.201	-0.201	-0.201	-0.201	-0.201	-0.201	-0.201	-0.201	-0.201	-0.201	-0.201	-0.201	-0.201	-0.201	-0.208	-0.21	-0.2	-0.2
4.2	02/01/2018	-0.19	0.02	-0.4	-0.10	-0.101	-0.105	-0.138	-0.186	-0.205	-0.21	-0.21	-0.21	-0.21	-0.211	-0.211	-0.211	-0.211	-0.211	-0.211	-0.211	-0.211	-0.211	-0.211	-0.211	-0.216	-0.21	-0.21	-0.21
4.7	03/01/2018	-0.13	0.15	-0.3	-0.11	-0.106	-0.106	-0.102	-0.108	-0.121	-0.125	-0.125	-0.125	-0.125	-0.125	-0.125	-0.125	-0.125	-0.125	-0.125	-0.125	-0.125	-0.125	-0.125	-0.125	-0.138	-0.16	-0.17	-0.17
5.0	04/01/2018	-0.19	0.02	-0.35	-0.10	-0.106	-0.11	-0.139	-0.182	-0.197	-0.201	-0.201	-0.201	-0.201	-0.201	-0.201	-0.201	-0.201	-0.201	-0.201	-0.201	-0.201	-0.201	-0.201	-0.201	-0.204	-0.19	-0.19	-0.18
5.4	05/01/2018	-0.23	0.14	-0.54	-0.10	-0.101	-0.107	-0.161	-0.233	-0.253	-0.259	-0.259	-0.259	-0.259	-0.259	-0.259	-0.259	-0.259	-0.259	-0.259	-0.259	-0.259	-0.259	-0.259	-0.259	-0.258	-0.23	-0.22	-0.22
5.7	06/01/2018	-0.26	0.24	-0.67	-0.09	-0.092	-0.1	-0.171	-0.263	-0.289	-0.296	-0.296	-0.296	-0.297	-0.297	-0.297	-0.297	-0.297	-0.297	-0.297	-0.297	-0.297	-0.297	-0.297	-0.297	-0.295	-0.27	-0.25	-0.25
5.9	07/01/2018	-0.28	0.33	-0.76	-0.08	-0.084	-0.093	-0.174	-0.28	-0.311	-0.32	-0.32	-0.32	-0.32	-0.32	-0.32	-0.32	-0.32	-0.32	-0.32	-0.32	-0.32	-0.32	-0.32	-0.32	-0.319	-0.29	-0.27	-0.27
6.2	08/01/2018	-0.3	0.40	-0.83	-0.07	-0.077	-0.087	-0.175	-0.292	-0.328	-0.338	-0.338	-0.338	-0.338	-0.338	-0.338	-0.338	-0.338	-0.338	-0.338	-0.338	-0.338	-0.338	-0.338	-0.338	-0.338	-0.31	-0.29	-0.29
6.4	09/01/2018	-0.31	0.46	-0.89	-0.07	-0.071	-0.082	-0.177	-0.303	-0.343	-0.354	-0.354	-0.354	-0.354	-0.354	-0.354	-0.354	-0.354	-0.354	-0.354	-0.354	-0.354	-0.354	-0.354	-0.354	-0.354	-0.32	-0.3	-0.3
6.7	10/01/2018	-0.32	0.51	-0.94	-0.06	-0.067	-0.078	-0.178	-0.312	-0.356	-0.367	-0.368	-0.368	-0.369	-0.369	-0.369	-0.369	-0.369	-0.369	-0.369	-0.369	-0.369	-0.369	-0.369	-0.369	-0.369	-0.34	-0.32	-0.31
6.7	11/01/2018	-0.33	0.53	-0.96	-0.06	-0.065	-0.076	-0.178	-0.316	-0.362	-0.375	-0.375	-0.375	-0.375	-0.375	-0.375	-0.375	-0.375	-0.375	-0.375	-0.375	-0.375	-0.375	-0.375	-0.375	-0.378	-0.35	-0.33	-0.33
6.5	12/01/2018	-0.32	0.51	-0.94	-0.06	-0.065	-0.077	-0.174	-0.308	-0.356	-0.369	-0.369	-0.369	-0.369	-0.369	-0.369	-0.369	-0.369	-0.369	-0.369	-0.369	-0.369	-0.369	-0.369	-0.369	-0.375	-0.35	-0.33	-0.33
6.2	13/01/2018	-0.31	0.46	-0.88	-0.07	-0.071	-0.081	-0.168	-0.291	-0.339	-0.352	-0.352	-0.352	-0.352	-0.352	-0.352	-0.352	-0.352	-0.352	-0.352	-0.352	-0.352	-0.352	-0.352	-0.352	-0.362	-0.34	-0.33	-0.33
5.7	14/01/2018	-0.29	0.37	-0.78	-0.08	-0.08	-0.089	-0.161	-0.268	-0.313	-0.325	-0.326	-0.326	-0.327	-0.327	-0.327	-0.327	-0.327	-0.327	-0.327	-0.327	-0.327	-0.327	-0.327	-0.327	-0.34	-0.33	-0.33	-0.33
5.3	15/01/2018	-0.27	0.25	-0.67	-0.09	-0.092	-0.099	-0.155	-0.243	-0.286	-0.297	-0.297	-0.297	-0.297	-0.297	-0.297	-0.297	-0.297	-0.297	-0.297	-0.297	-0.297	-0.297	-0.297	-0.297	-0.314	-0.32	-0.32	-0.32
4.9	16/01/2018	-0.25	0.12	-0.57	-0.10	-0.106	-0.111	-0.153	-0.224	-0.262	-0.272	-0.272	-0.272	-0.272	-0.272	-0.272	-0.272	-0.272	-0.272	-0.272	-0.272	-0.272	-0.272	-0.272	-0.272	-0.291	-0.3	-0.3	-0.3
4.7	17/01/2018	-0.24	0.08	-0.5	-0.12	-0.118	-0.123	-0.155	-0.212	-0.246	-0.255	-0.255	-0.255	-0.255	-0.255	-0.255	-0.255	-0.255	-0.255	-0.255	-0.255	-0.255	-0.255	-0.255	-0.255	-0.274	-0.29	-0.29	-0.29
4.5	18/01/2018	-0.24	0.06	-0.45	-0.13	-0.129	-0.132	-0.158	-0.207	-0.237	-0.245	-0.245	-0.245	-0.246	-0.246	-0.246	-0.246	-0.246	-0.246	-0.246	-0.246	-0.246	-0.246	-0.246	-0.246	-0.264	-0.28	-0.28	-0.28
4.6	19/01/2018	-0.24	0.02	-0.44	-0.13	-0.136	-0.139	-0.166	-0.215	-0.243	-0.255	-0.255	-0.255	-0.255	-0.255	-0.255	-0.255	-0.255	-0.255	-0.255	-0.255	-0.255	-0.255	-0.255	-0.255	-0.267	-0.28	-0.28	-0.28
4.7	20/01/2018	-0.24	0.01	-0.45	-0.14	-0.139	-0.143	-0.173	-0.224	-0.251	-0.258	-0.258	-0.258	-0.258	-0.258	-0.258	-0.258	-0.258	-0.258	-0.258	-0.258	-0.258	-0.258	-0.258	-0.258	-0.273	-0.28	-0.28	-0.28
4.9	21/01/2018	-0.26	0.01	-0.49	-0.14	-0.14	-0.145	-0.182	-0.24	-0.267	-0.275	-0.275	-0.275	-0.275	-0.275	-0.275	-0.275	-0.275	-0.275	-0.275	-0.275	-0.275	-0.275	-0.275	-0.275	-0.287	-0.29	-0.29	-0.29
5.2	22/01/2018	-0.27	0.01	-0.55	-0.14	-0.138	-0.144	-0.19	-0.258	-0.287	-0.294	-0.295	-0.295	-0.295	-0.296	-0.296	-0.296	-0.296	-0.296	-0.296	-0.296	-0.296	-0.296	-0.296	-0.296	-0.305	-0.3	-0.3	-0.3
5.4	23/01/2018	-0.29	0.01	-0.62	-0.13	-0.135	-0.141	-0.196	-0.275	-0.305	-0.314	-0.314	-0.314	-0.314	-0.314	-0.314	-0.314	-0.314	-0.314	-0.314	-0.314	-0.314	-0.314	-0.314	-0.314	-0.323	-0.31	-0.31	-0.31
5.6	24/01/2018	-0.3	0.01	-0.68	-0.13	-0.13	-0.137	-0.2	-0.289	-0.322	-0.331	-0.331	-0.331	-0.331	-0.331	-0.331	-0.331	-0.331	-0.331	-0.331	-0.331	-0.331	-0.331	-0.331	-0.331	-0.339	-0.33	-0.32	-0.32
5.8	25/01/2018	-0.31	0.06	-0.73	-0.12	-0.124	-0.132	-0.201	-0.298	-0.333	-0.343	-0.343	-0.343	-0.343	-0.343	-0.343	-0.343	-0.343	-0.343	-0.343	-0.343	-0.343	-0.343	-0.343	-0.343	-0.351	-0.34	-0.33	-0.33
5.9	26/01/2018	-0.32	0.11	-0.76	-0.12	-0.119	-0.128	-0.201	-0.304	-0.342	-0.352	-0.353	-0.353	-0.353	-0.354	-0.354	-0.354	-0.354	-0.354	-0.354	-0.354	-0.354	-0.354	-0.354	-0.354	-0.361	-0.35	-0.34	-0.34
6.1	27/01/2018	-0.33	0.15	-0.8	-0.11	-0.115	-0.124	-0.202	-0.311	-0.352	-0.362	-0.362	-0.362	-0.362	-0.362	-0.362	-0.362	-0.362	-0.362	-0.362	-0.362	-0.362	-0.362	-0.362	-0.362	-0.371	-0.35	-0.34	-0.34
6.3	28/01/2018	-0.33	0.19	-0.85	-0.11	-0.111	-0.121	-0.204	-0.32	-0.363	-0.374	-0.374	-0.374	-0.374	-0.374	-0.374	-0.374	-0.374	-0.374	-0.374	-0.374	-0.374	-0.374	-0.374	-0.374	-0.382	-0.36	-0.35	-0.35
6.5	29/01/2018	-0.34	0.23	-0.88	-0.10	-0.108	-0.118	-0.205	-0.327	-0.372	-0.383	-0.383	-0.383	-0.383	-0.383	-0.383	-0.383	-0.383	-0.383	-0.383	-0.383	-0.383	-0.383	-0.383	-0.383	-0.392	-0.37	-0.36	-0.36
6.4	30/01/2018	-0.34	0.23	-0.89	-0.10	-0.106	-0.116	-0.203	-0.326	-0.372	-0.385	-0.385	-0.385	-0.386	-0.387	-0.387	-0.387	-0.387	-0.387	-0.387	-0.387	-0.387	-0.387	-0.387	-0.387	-0.395	-0.38	-0.36	-0.36
6.2	31/01/2018	-0.34	0.22	-0.86	-0.10	-0.106	-0.116	-0.198	-0.316	-0.363	-0.375	-0.375	-0.375	-0.375	-0.375	-0.375	-0.375	-0.375	-0.375	-0.375	-0.375	-0.375	-0.375	-0.375	-0.375	-0.387	-0.37	-0.36	-0.36

Figure 57: Data difference 2D and 3D model transect 154.

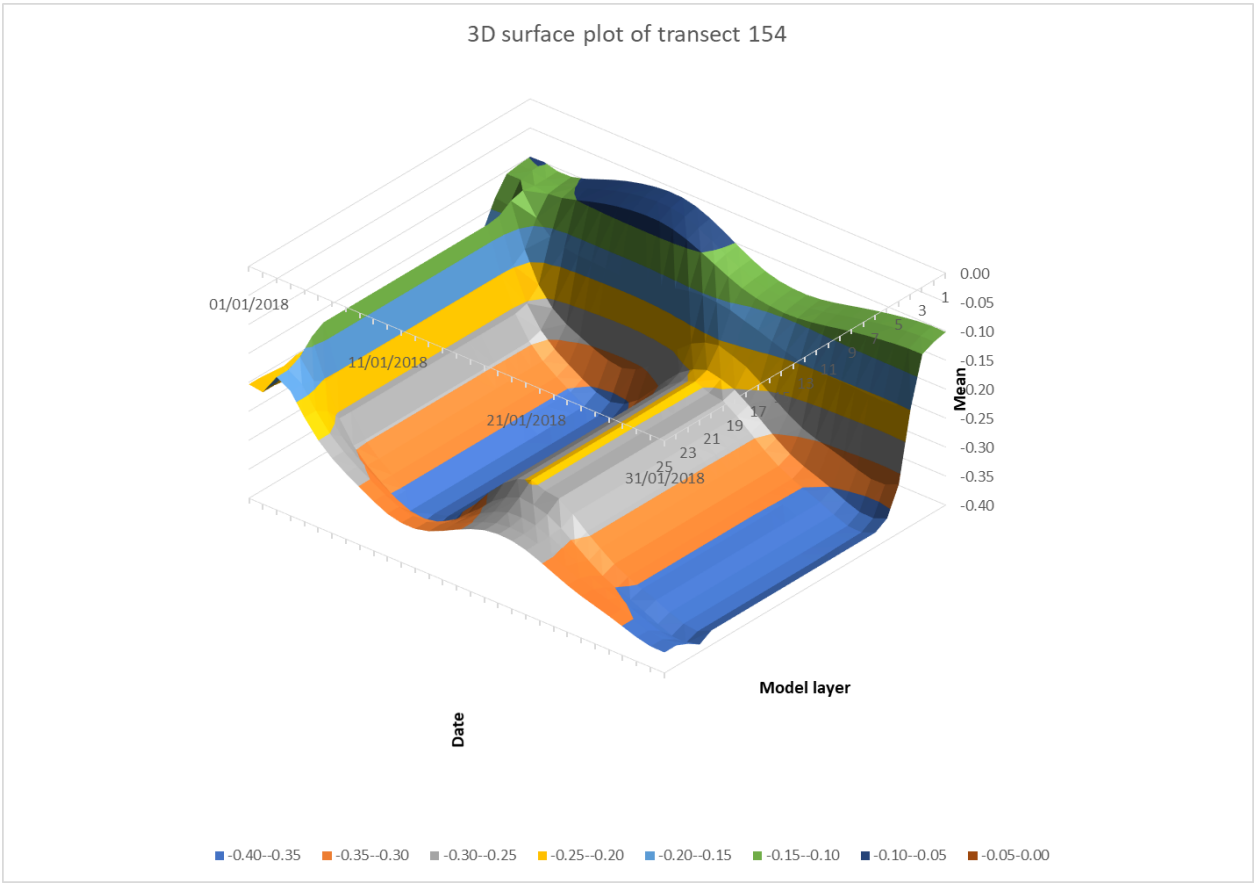

Figure 58: 3D surface plot of transect 154.

155		Layer			1.00	2.00	3.00	4.00	5.00	6.00	7.00	8.00	9.00	10.00	11.00	12.00	13.00	14.00	15.00	16.00	17.00	18.00	19.00	20.00	21.00	22.00	23.00	24.00	25.00
Am. Ben.	Timestep	Mean			-0.03	-0.03	-0.03	-0.03	-0.03	-0.04	-0.03	-0.03	-0.03	-0.01	0.00	0.01	0.01	0.01	0.01	0.01	0.01	0.01	0.01	0.01	0.01	0.01	0.01	0.01	0.01
			Max		0.35	0.35	0.35	0.36	0.36	0.36	0.35	0.35	0.34	0.34	0.34	0.34	0.34	0.34	0.34	0.34	0.34	0.34	0.34	0.34	0.33	0.33	0.33	0.33	0.33
				Min	-0.28	-0.27	-0.27	-0.27	-0.27	-0.27	-0.27	-0.27	-0.27	-0.18	-0.18	-0.18	-0.18	-0.18	-0.18	-0.18	-0.18	-0.18	-0.18	-0.18	-0.18	-0.17	-0.17	-0.17	-0.17
4.1	01/01/2018	-0.02	0.10	-0.17	-0.03	-0.03	-0.03	-0.03	-0.03	-0.03	-0.03	-0.03	-0.03	-0.02	-0.01	-0.01	-0.01	-0.01	-0.01	-0.01	-0.01	-0.01	-0.01	-0.01	-0.01	-0.01	-0.01	-0.01	-0.01
4.2	02/01/2018	-0.02	0.11	-0.17	-0.03	-0.03	-0.03	-0.03	-0.03	-0.03	-0.03	-0.03	-0.03	-0.02	-0.01	-0.01	-0.01	-0.01	-0.01	-0.01	-0.01	-0.01	-0.01	-0.01	-0.01	-0.01	0.00	0.00	0.00
4.7	03/01/2018	-0.05	0.04	-0.19	-0.04	-0.04	-0.04	-0.04	-0.04	-0.04	-0.04	-0.04	-0.05	-0.05	-0.05	-0.05	-0.05	-0.05	-0.05	-0.05	-0.05	-0.05	-0.05	-0.05	-0.05	-0.05	-0.05	-0.05	-0.05
5.0	04/01/2018	-0.01	0.14	-0.16	-0.03	-0.03	-0.03	-0.03	-0.03	-0.03	-0.03	-0.03	-0.03	-0.01	0.00	0.00	0.00	0.00	0.00	0.00	0.00	0.00	0.00	0.00	0.00	0.00	0.00	0.00	0.00
5.4	05/01/2018	0.01	0.25	-0.16	-0.02	-0.02	-0.02	-0.02	-0.02	-0.02	-0.02	-0.02	-0.02	0.00	0.02	0.02	0.02	0.02	0.02	0.02	0.02	0.02	0.02	0.02	0.02	0.02	0.03	0.03	0.03
5.7	06/01/2018	0.02	0.30	-0.15	-0.02	-0.02	-0.02	-0.02	-0.02	-0.02	-0.02	-0.02	-0.01	0.01	0.03	0.04	0.04	0.04	0.04	0.04	0.04	0.04	0.04	0.04	0.04	0.04	0.04	0.04	0.04
5.9	07/01/2018	0.03	0.33	-0.16	-0.01	-0.01	-0.01	-0.01	-0.01	-0.01	-0.01	-0.01	0.00	0.02	0.04	0.04	0.04	0.05	0.05	0.05	0.05	0.05	0.05	0.05	0.05	0.05	0.05	0.05	0.05
6.2	08/01/2018	0.03	0.34	-0.17	-0.01	-0.01	-0.01	-0.01	-0.01	-0.01	-0.01	-0.01	0.00	0.03	0.04	0.05	0.05	0.05	0.05	0.05	0.05	0.05	0.05	0.05	0.05	0.05	0.06	0.06	0.06
6.4	09/01/2018	0.04	0.36	-0.18	-0.01	-0.01	-0.01	-0.01	-0.01	-0.01	0.00	0.00	0.01	0.03	0.05	0.06	0.06	0.06	0.06	0.06	0.06	0.06	0.06	0.06	0.06	0.06	0.06	0.06	0.06
6.7	10/01/2018	0.04	0.36	-0.19	-0.01	-0.01	-0.01	0.00	-0.01	-0.01	0.00	0.00	0.01	0.03	0.05	0.06	0.06	0.06	0.06	0.06	0.07	0.07	0.07	0.07	0.07	0.07	0.07	0.07	0.07
6.7	11/01/2018	0.04	0.34	-0.20	-0.01	-0.01	0.00	0.00	0.00	0.00	0.00	0.00	0.01	0.03	0.05	0.06	0.06	0.06	0.06	0.06	0.06	0.06	0.06	0.06	0.06	0.06	0.07	0.07	0.07
6.5	12/01/2018	0.03	0.34	-0.19	-0.01	-0.01	-0.01	-0.01	-0.01	-0.01	0.00	0.00	0.01	0.03	0.05	0.05	0.05	0.05	0.05	0.05	0.05	0.05	0.05	0.05	0.05	0.05	0.06	0.06	0.06
6.2	13/01/2018	0.02	0.31	-0.16	-0.01	-0.01	-0.01	-0.01	-0.01	-0.01	-0.01	-0.01	0.00	0.01	0.03	0.03	0.03	0.04	0.04	0.04	0.04	0.04	0.04	0.04	0.04	0.04	0.04	0.04	0.04
5.7	14/01/2018	0.00	0.28	-0.17	-0.02	-0.02	-0.02	-0.02	-0.02	-0.02	-0.02	-0.02	-0.01	0.00	0.01	0.01	0.01	0.02	0.02	0.02	0.02	0.02	0.02	0.02	0.02	0.02	0.02	0.02	0.02
5.3	15/01/2018	-0.01	0.24	-0.19	-0.03	-0.03	-0.03	-0.03	-0.03	-0.03	-0.03	-0.03	-0.02	-0.01	-0.01	0.00	0.00	0.00	0.00	0.00	0.00	0.00	0.00	0.00	0.00	0.00	0.00	0.00	0.00
4.9	16/01/2018	-0.03	0.21	-0.23	-0.03	-0.03	-0.03	-0.03	-0.03	-0.03	-0.03	-0.03	-0.03	-0.03	-0.02	-0.02	-0.02	-0.02	-0.02	-0.02	-0.02	-0.02	-0.02	-0.02	-0.02	-0.02	-0.02	-0.02	-0.02
4.7	17/01/2018	-0.03	0.17	-0.26	-0.04	-0.04	-0.04	-0.04	-0.04	-0.04	-0.04	-0.04	-0.04	-0.04	-0.03	-0.03	-0.03	-0.03	-0.03	-0.03	-0.03	-0.03	-0.03	-0.03	-0.03	-0.03	-0.03	-0.03	-0.03
4.5	18/01/2018	-0.04	0.15	-0.27	-0.04	-0.04	-0.04	-0.04	-0.05	-0.05	-0.05	-0.05	-0.05	-0.04	-0.04	-0.04	-0.04	-0.04	-0.04	-0.04	-0.04	-0.04	-0.04	-0.04	-0.04	-0.04	-0.04	-0.04	-0.04
4.6	19/01/2018	-0.04	0.14	-0.26	-0.05	-0.05	-0.05	-0.05	-0.05	-0.05	-0.05	-0.05	-0.05	-0.04	-0.04	-0.04	-0.04	-0.04	-0.04	-0.04	-0.04	-0.04	-0.04	-0.04	-0.04	-0.04	-0.03	-0.03	-0.03
4.7	20/01/2018	-0.04	0.14	-0.25	-0.05	-0.05	-0.05	-0.05	-0.05	-0.05	-0.05	-0.05	-0.05	-0.04	-0.04	-0.03	-0.03	-0.03	-0.03	-0.03	-0.03	-0.03	-0.03	-0.03	-0.03	-0.03	-0.03	-0.03	-0.03
4.9	21/01/2018	-0.04	0.15	-0.25	-0.05	-0.05	-0.05	-0.05	-0.05	-0.05	-0.05	-0.05	-0.05	-0.04	-0.03	-0.03	-0.03	-0.03	-0.03	-0.03	-0.03	-0.03	-0.03	-0.03	-0.03	-0.03	-0.02	-0.02	-0.02
5.2	22/01/2018	-0.03	0.17	-0.26	-0.05	-0.05	-0.05	-0.05	-0.05	-0.06	-0.05	-0.05	-0.05	-0.03	-0.02	-0.02	-0.02	-0.02	-0.02	-0.02	-0.02	-0.02	-0.02	-0.02	-0.02	-0.02	-0.02	-0.02	-0.02
5.4	23/01/2018	-0.02	0.20	-0.26	-0.04	-0.04	-0.04	-0.04	-0.04	-0.04	-0.04	-0.04	-0.04	-0.03	-0.01	-0.01	-0.01	-0.01	-0.01	-0.01	-0.01	-0.01	-0.01	-0.01	-0.01	-0.01	-0.01	-0.01	-0.01
5.6	24/01/2018	-0.02	0.22	-0.27	-0.04	-0.04	-0.04	-0.04	-0.04	-0.04	-0.04	-0.04	-0.04	-0.02	-0.01	0.00	0.00	0.00	0.00	0.00	0.00	0.00	0.00	0.00	0.00	0.00	0.00	0.00	0.00
5.8	25/01/2018	-0.01	0.23	-0.27	-0.04	-0.04	-0.04	-0.04	-0.04	-0.04	-0.04	-0.04	-0.04	-0.02	0.00	0.00	0.00	0.00	0.00	0.00	0.00	0.00	0.00	0.00	0.00	0.00	0.00	0.01	0.01	0.01
5.9	26/01/2018	-0.01	0.25	-0.27	-0.04	-0.04	-0.04	-0.04	-0.04	-0.05	-0.04	-0.04	-0.03	-0.01	0.00	0.01	0.01	0.01	0.01	0.01	0.01	0.01	0.01	0.01	0.01	0.01	0.01	0.01	0.01
6.1	27/01/2018	-0.01	0.26	-0.27	-0.04	-0.04	-0.04	-0.04	-0.04	-0.04	-0.04	-0.04	-0.03	-0.01	0.01	0.01	0.01	0.01	0.01	0.01	0.01	0.01	0.01	0.01	0.01	0.01	0.02	0.02	0.02
6.3	28/01/2018	0.00	0.28	-0.27	-0.04	-0.04	-0.03	-0.03	-0.03	-0.03	-0.03	-0.03	-0.03	-0.01	0.01	0.02	0.02	0.02	0.02	0.02	0.02	0.02	0.02	0.02	0.02	0.02	0.02	0.02	0.02
6.5	29/01/2018	0.00	0.30	-0.27	-0.03	-0.03	-0.03	-0.03	-0.03	-0.03	-0.03	-0.03	-0.03	0.00	0.01	0.02	0.02	0.02	0.02	0.02	0.02	0.02	0.02	0.02	0.02	0.02	0.03	0.03	0.03
6.4	30/01/2018	0.00	0.30	-0.28	-0.03	-0.03	-0.03	-0.03	-0.04	-0.04	-0.04	-0.04	-0.03	0.01	0.01	0.02	0.02	0.02	0.02	0.02	0.02	0.02	0.02	0.02	0.02	0.02	0.02	0.02	0.02
6.2	31/01/2018	-0.01	0.28	-0.28	-0.04	-0.04	-0.04	-0.04	-0.04	-0.04	-0.04	-0.04	-0.03	-0.01	0.00	0.01	0.01	0.01	0.01	0.01	0.01	0.01	0.01	0.01	0.01	0.01	0.01	0.01	0.01

Figure 59: Data difference 2D and 3D model transect 155.

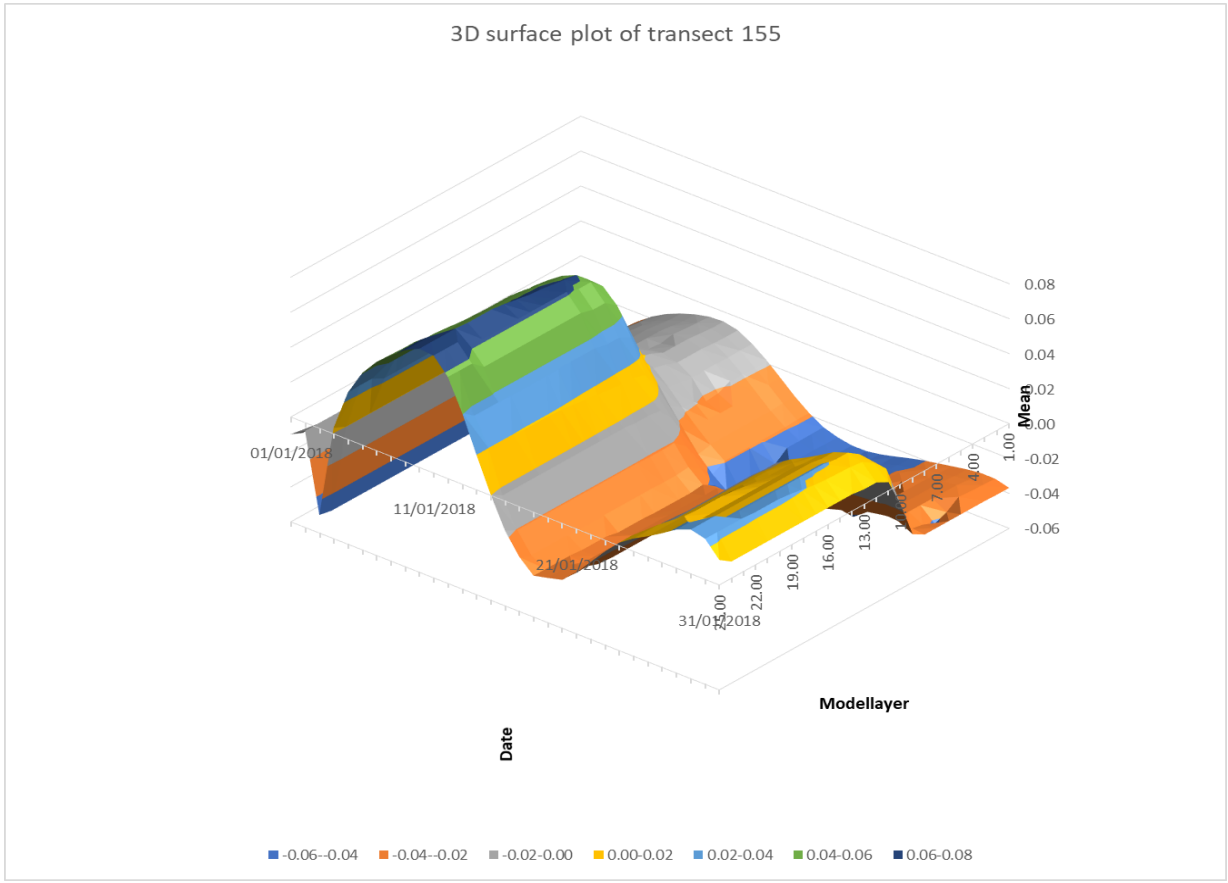

Figure 60: 3D surface plot of transect 155.

	156	Layer			1	2	3	4	5	6	7	8	9	10	11	12	13	14	15	16	17	18	19	20	21	22	23	24	25
Am. Ben.	Timestep	Mean			-0.036	-0.036	-0.035	-0.033	-0.029	-0.025	-0.023	-0.022	-0.022	-0.022	-0.022	-0.022	-0.022	-0.022	-0.021	-0.021	-0.02	-0.02	-0.02	-0.019	-0.019	-0.019	-0.02	-0.02	-0.02
			Max		0.189	0.189	0.189	0.189	0.19	0.19	0.19	0.19	0.19	0.19	0.19	0.19	0.19	0.19	0.19	0.19	0.191	0.191	0.191	0.191	0.191	0.191	0.191	0.191	0.191
				Min	-0.411	-0.388	-0.38	-0.366	-0.349	-0.332	-0.315	-0.307	-0.307	-0.306	-0.306	-0.306	-0.305	-0.305	-0.304	-0.303	-0.303	-0.302	-0.302	-0.301	-0.3	-0.3	-0.3	-0.3	-0.3
4.1	01/01/2018	0.01	0.19	-0.17	-0.03	-0.01	-0.01	-0.01	0.00	0.00	0.01	0.01	0.01	0.01	0.01	0.01	0.01	0.01	0.01	0.01	0.01	0.01	0.01	0.01	0.01	0.01	0.01	0.01	0.01
4.2	02/01/2018	0.01	0.19	-0.17	-0.03	-0.01	-0.01	0.00	0.00	0.01	0.01	0.01	0.01	0.01	0.01	0.01	0.01	0.01	0.01	0.01	0.02	0.02	0.02	0.02	0.02	0.02	0.02	0.02	0.02
4.7	03/01/2018	0.00	0.19	-0.18	-0.04	-0.01	-0.01	-0.01	0.00	0.00	0.00	0.00	0.01	0.01	0.00	0.00	0.00	0.00	0.00	0.00	0.00	0.00	0.00	0.00	0.00	0.00	0.00	0.00	0.00
5.0	04/01/2018	0.02	0.19	-0.15	-0.03	0.00	0.00	0.00	0.01	0.01	0.02	0.02	0.02	0.02	0.02	0.02	0.02	0.02	0.02	0.02	0.03	0.03	0.03	0.03	0.03	0.03	0.03	0.03	0.03
5.4	05/01/2018	0.03	0.19	-0.14	-0.02	0.00	0.00	0.01	0.02	0.02	0.03	0.03	0.03	0.03	0.03	0.03	0.03	0.03	0.03	0.03	0.03	0.03	0.03	0.03	0.03	0.03	0.03	0.03	0.03
5.7	06/01/2018	0.03	0.19	-0.14	-0.02	0.01	0.01	0.01	0.02	0.02	0.03	0.03	0.03	0.03	0.03	0.03	0.03	0.03	0.03	0.03	0.03	0.03	0.03	0.03	0.03	0.03	0.03	0.03	0.03
5.9	07/01/2018	0.02	0.19	-0.15	-0.01	0.00	0.00	0.01	0.01	0.01	0.02	0.02	0.03	0.03	0.03	0.03	0.03	0.03	0.03	0.03	0.03	0.03	0.03	0.03	0.03	0.03	0.03	0.03	0.03
6.2	08/01/2018	0.02	0.19	-0.17	-0.01	0.00	0.00	0.00	0.01	0.01	0.02	0.02	0.02	0.02	0.02	0.02	0.02	0.02	0.02	0.02	0.03	0.03	0.03	0.03	0.03	0.03	0.03	0.03	0.03
6.4	09/01/2018	0.01	0.19	-0.20	-0.01	-0.01	0.00	0.00	0.01	0.01	0.02	0.02	0.02	0.02	0.02	0.02	0.02	0.02	0.02	0.02	0.02	0.02	0.02	0.02	0.02	0.02	0.02	0.02	0.02
6.7	10/01/2018	0.01	0.19	-0.23	-0.01	-0.01	-0.01	-0.01	0.00	0.01	0.01	0.01	0.01	0.01	0.01	0.01	0.01	0.01	0.01	0.01	0.01	0.01	0.01	0.02	0.02	0.02	0.02	0.02	0.02
6.7	11/01/2018	0.00	0.19	-0.27	-0.01	-0.02	-0.02	-0.01	-0.01	-0.01	0.00	0.00	0.00	0.00	0.00	0.00	0.00	0.00	0.00	0.00	0.00	0.00	0.00	0.00	0.00	0.00	0.01	0.01	0.01
6.5	12/01/2018	-0.01	0.19	-0.30	-0.01	-0.03	-0.03	-0.02	-0.02	-0.02	-0.01	-0.01	-0.01	-0.01	-0.01	-0.01	-0.01	-0.01	-0.01	-0.01	-0.01	-0.01	-0.01	-0.01	-0.01	-0.01	-0.01	-0.01	-0.01
6.2	13/01/2018	-0.02	0.19	-0.34	-0.01	-0.04	-0.04	-0.03	-0.03	-0.03	-0.02	-0.02	-0.02	-0.02	-0.02	-0.02	-0.02	-0.02	-0.02	-0.02	-0.02	-0.02	-0.02	-0.02	-0.02	-0.02	-0.02	-0.02	-0.02
5.7	14/01/2018	-0.04	0.19	-0.38	-0.02	-0.05	-0.04	-0.04	-0.04	-0.04	-0.03	-0.03	-0.03	-0.03	-0.03	-0.03	-0.03	-0.03	-0.03	-0.03	-0.03	-0.03	-0.03	-0.03	-0.03	-0.03	-0.03	-0.03	-0.03
5.3	15/01/2018	-0.05	0.19	-0.40	-0.03	-0.05	-0.05	-0.05	-0.05	-0.05	-0.04	-0.04	-0.04	-0.04	-0.04	-0.04	-0.04	-0.04	-0.04	-0.04	-0.04	-0.04	-0.04	-0.04	-0.04	-0.04	-0.04	-0.04	-0.04
4.9	16/01/2018	-0.05	0.19	-0.41	-0.03	-0.06	-0.06	-0.06	-0.05	-0.05	-0.05	-0.05	-0.05	-0.05	-0.05	-0.05	-0.05	-0.05	-0.05	-0.05	-0.05	-0.05	-0.05	-0.05	-0.05	-0.05	-0.05	-0.05	-0.05
4.7	17/01/2018	-0.06	0.19	-0.41	-0.04	-0.06	-0.06	-0.06	-0.06	-0.06	-0.05	-0.05	-0.05	-0.05	-0.05	-0.05	-0.05	-0.05	-0.05	-0.05	-0.05	-0.05	-0.05	-0.05	-0.05	-0.05	-0.05	-0.05	-0.05
4.5	18/01/2018	-0.06	0.19	-0.39	-0.04	-0.06	-0.06	-0.06	-0.06	-0.06	-0.06	-0.05	-0.05	-0.06	-0.06	-0.06	-0.06	-0.06	-0.06	-0.06	-0.06	-0.06	-0.06	-0.06	-0.06	-0.06	-0.06	-0.06	-0.06
4.6	19/01/2018	-0.06	0.19	-0.37	-0.05	-0.06	-0.06	-0.06	-0.06	-0.06	-0.06	-0.06	-0.06	-0.06	-0.06	-0.06	-0.06	-0.06	-0.06	-0.06	-0.06	-0.06	-0.06	-0.06	-0.06	-0.06	-0.05	-0.05	-0.05
4.7	20/01/2018	-0.05	0.19	-0.36	-0.05	-0.06	-0.06	-0.06	-0.06	-0.06	-0.05	-0.05	-0.05	-0.05	-0.05	-0.05	-0.05	-0.05	-0.05	-0.05	-0.05	-0.05	-0.05	-0.05	-0.05	-0.05	-0.05	-0.05	-0.05
4.9	21/01/2018	-0.05	0.19	-0.34	-0.05	-0.06	-0.06	-0.05	-0.05	-0.05	-0.05	-0.05	-0.05	-0.05	-0.05	-0.05	-0.05	-0.05	-0.05	-0.05	-0.05	-0.05	-0.05	-0.05	-0.05	-0.05	-0.05	-0.05	-0.05
5.2	22/01/2018	-0.05	0.19	-0.33	-0.05	-0.05	-0.05	-0.05	-0.05	-0.05	-0.05	-0.05	-0.05	-0.05	-0.05	-0.05	-0.05	-0.05	-0.05	-0.05	-0.05	-0.05	-0.05	-0.05	-0.05	-0.05	-0.05	-0.04	-0.04
5.4	23/01/2018	-0.04	0.19	-0.32	-0.04	-0.05	-0.05	-0.05	-0.05	-0.05	-0.05	-0.05	-0.05	-0.05	-0.05	-0.05	-0.05	-0.05	-0.05	-0.05	-0.05	-0.05	-0.05	-0.05	-0.05	-0.05	-0.04	-0.04	-0.04
5.6	24/01/2018	-0.04	0.19	-0.31	-0.04	-0.05	-0.05	-0.05	-0.05	-0.05	-0.05	-0.05	-0.05	-0.05	-0.05	-0.05	-0.05	-0.05	-0.05	-0.05	-0.05	-0.05	-0.05	-0.05	-0.05	-0.05	-0.04	-0.04	-0.04
5.8	25/01/2018	-0.04	0.19	-0.31	-0.04	-0.05	-0.05	-0.05	-0.04	-0.04	-0.04	-0.04	-0.04	-0.04	-0.04	-0.04	-0.04	-0.04	-0.04	-0.04	-0.04	-0.04	-0.04	-0.04	-0.04	-0.04	-0.04	-0.04	-0.04
5.9	26/01/2018	-0.04	0.19	-0.32	-0.04	-0.05	-0.05	-0.05	-0.05	-0.04	-0.04	-0.04	-0.04	-0.04	-0.04	-0.04	-0.04	-0.04	-0.04	-0.04	-0.04	-0.04	-0.04	-0.04	-0.04	-0.04	-0.04	-0.04	-0.04
6.1	27/01/2018	-0.04	0.19	-0.32	-0.04	-0.05	-0.05	-0.05	-0.05	-0.05	-0.04	-0.04	-0.04	-0.04	-0.04	-0.04	-0.04	-0.04	-0.04	-0.04	-0.04	-0.04	-0.04	-0.04	-0.04	-0.04	-0.04	-0.04	-0.04
6.3	28/01/2018	-0.04	0.19	-0.33	-0.04	-0.05	-0.05	-0.05	-0.05	-0.05	-0.04	-0.04	-0.04	-0.04	-0.04	-0.04	-0.04	-0.04	-0.04	-0.04	-0.04	-0.04	-0.04	-0.04	-0.04	-0.04	-0.04	-0.04	-0.04
6.5	29/01/2018	-0.05	0.19	-0.34	-0.03	-0.05	-0.05	-0.05	-0.05	-0.05	-0.05	-0.05	-0.05	-0.05	-0.05	-0.05	-0.05	-0.05	-0.05	-0.05	-0.05	-0.05	-0.05	-0.05	-0.05	-0.05	-0.05	-0.04	-0.04
6.4	30/01/2018	-0.05	0.19	-0.36	-0.03	-0.06	-0.06	-0.05	-0.05	-0.05	-0.05	-0.05	-0.05	-0.05	-0.05	-0.05	-0.05	-0.05	-0.05	-0.05	-0.05	-0.05	-0.05	-0.05	-0.05	-0.05	-0.05	-0.05	-0.05
6.2	31/01/2018	-0.06	0.19	-0.38	-0.04	-0.06	-0.06	-0.06	-0.06	-0.06	-0.06	-0.06	-0.06	-0.06	-0.06	-0.06	-0.06	-0.06	-0.06	-0.06	-0.06	-0.06	-0.06	-0.06	-0.06	-0.06	-0.05	-0.05	-0.05

Figure 61: Data difference 2D and 3D model transect 156.

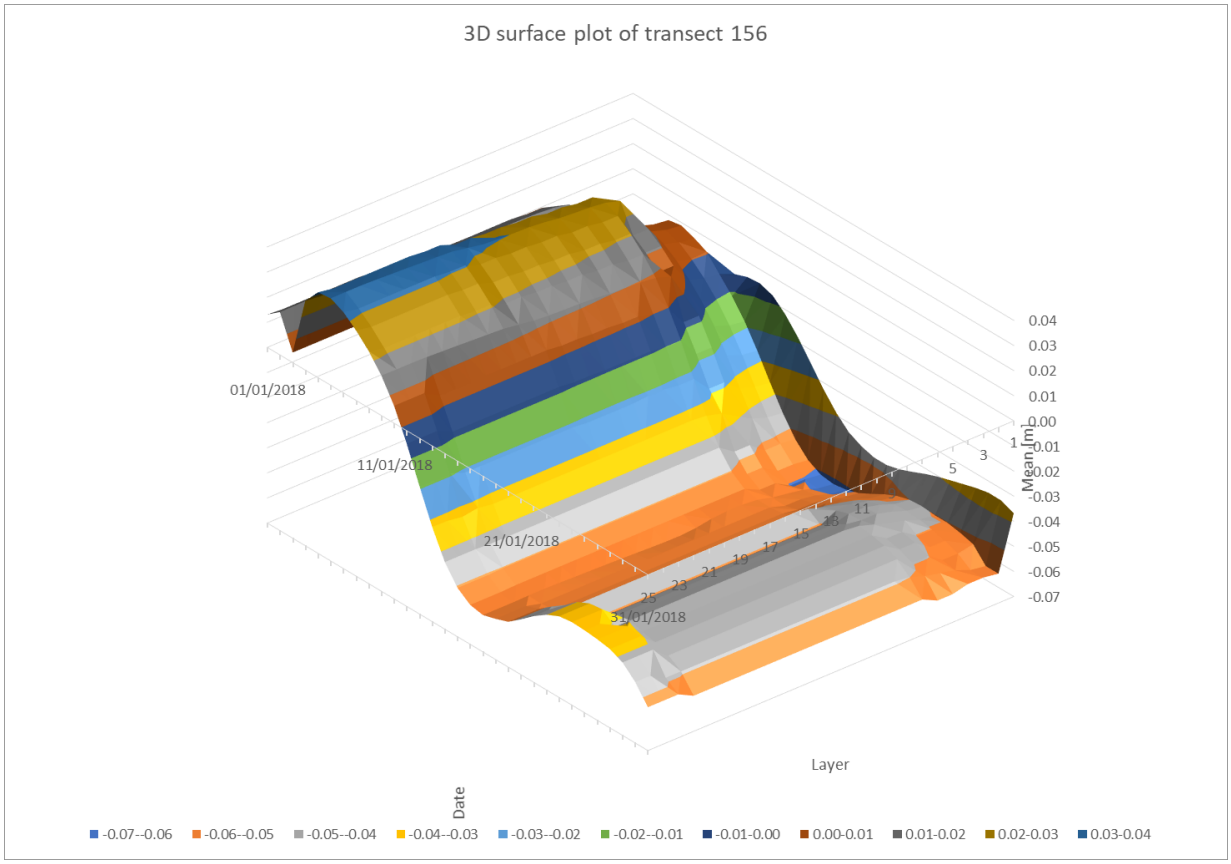

APPENDIX D

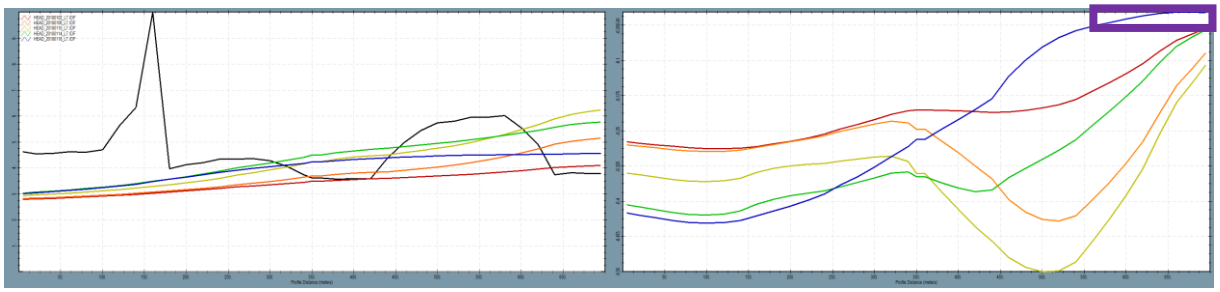

Figure 62: 2D view. Hydraulic head in upper aquifer (model layer 7) in transect 153. The difference between the hydraulic head values of the 3D and 2D model. y-axis in metres.

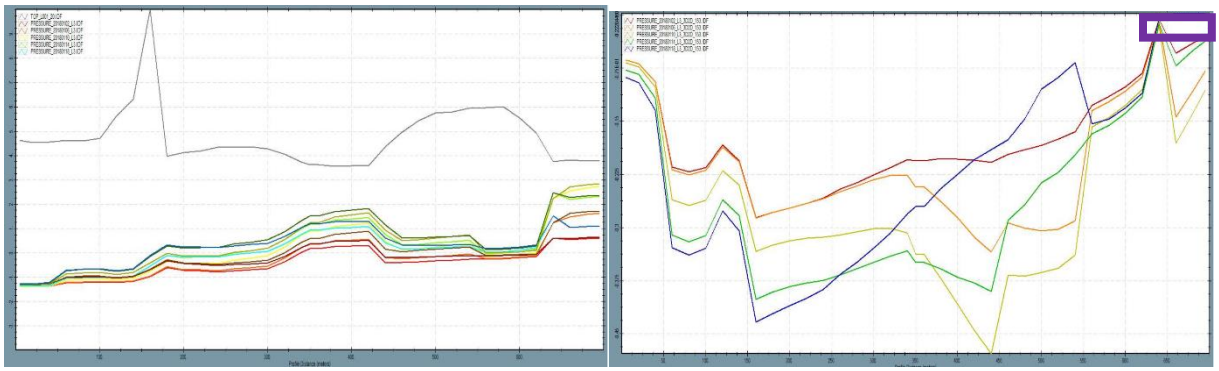

Figure 63: 2D view. Pressure underneath the dike (model layer 3) in transect 153. Light colours = 3D and dark colours = 2D. The difference between the hydraulic head values of the 3D and 2D model. y-axis in metres.

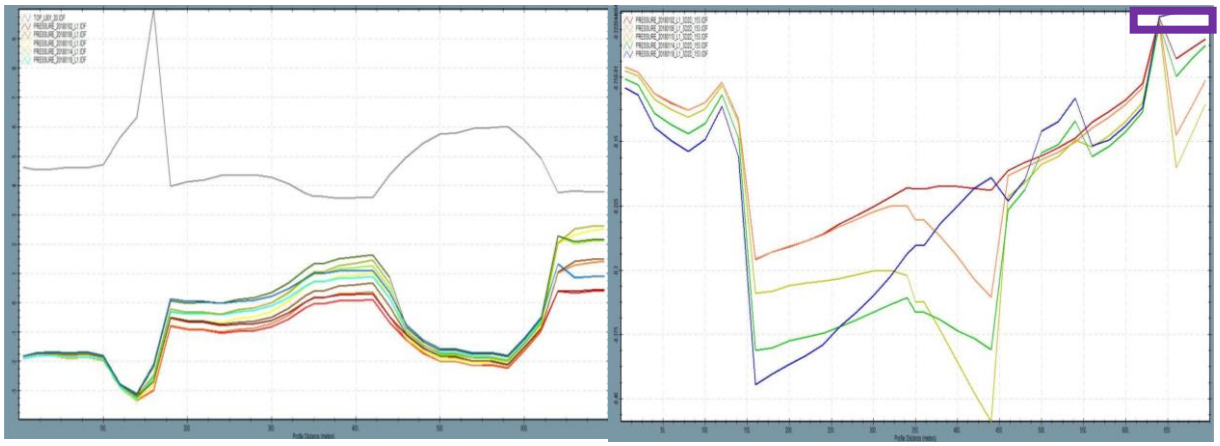

Figure 64: 2D view. Pressure in the confining layer (model layer 1) in transect 153. Light colours = 3D and dark colours = 2D. The difference between the hydraulic head values of the 3D and 2D model. y-axis in metres.

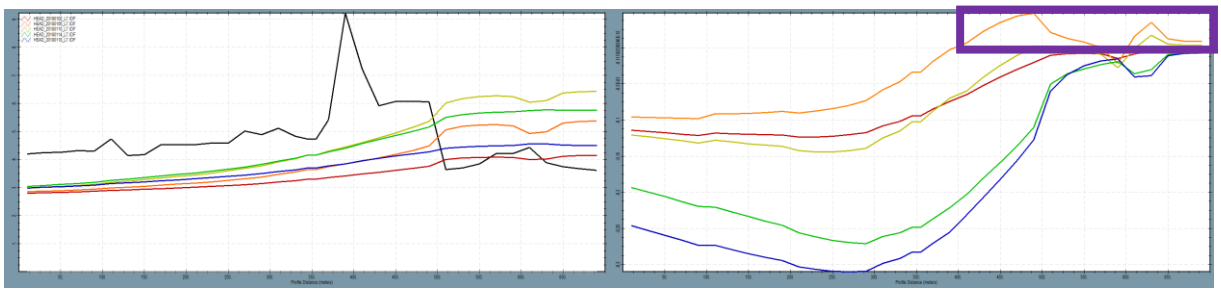

Figure 65: Hydraulic head in upper aquifer (model layer 7) in transect 156. The difference between the hydraulic head values of the 3D and 2D model. y-axis in metres.

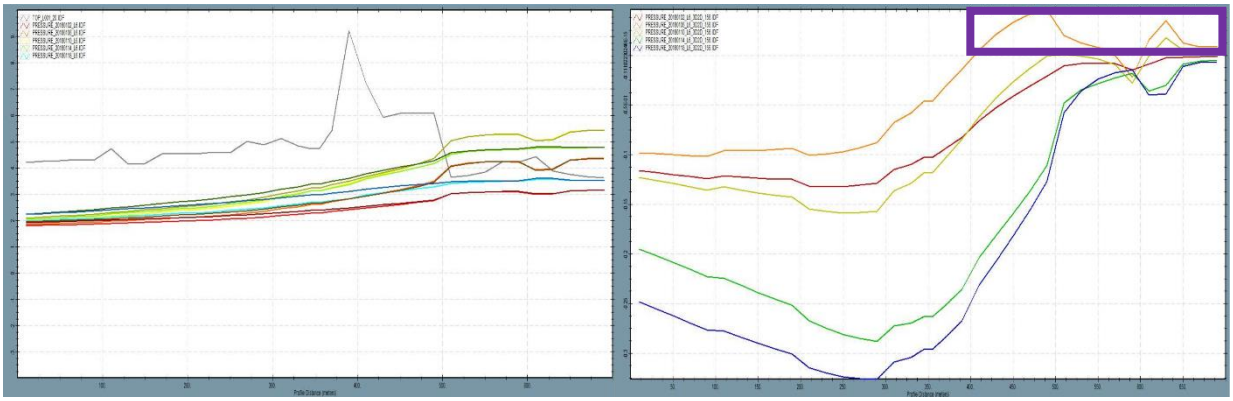

Figure 66: 2D view. Pressure underneath the dike (model layer 6) in transect 156. Light colours = 3D and dark colours = 2D. The difference between the hydraulic head values of the 3D and 2D model. y-axis in metres.

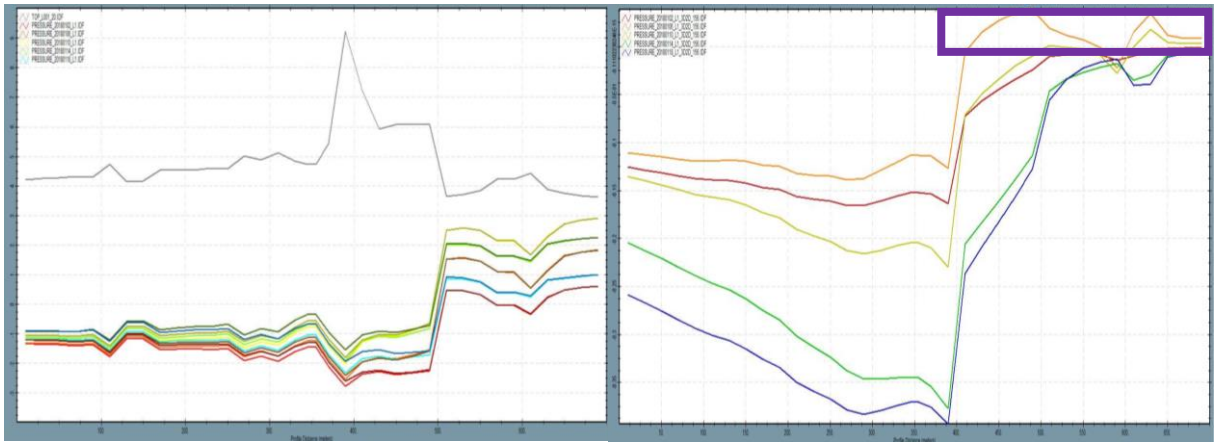

Figure 67: 2D view. Pressure in the confining layer (model layer 1) in transect 156. Light colours = 3D and dark colours = 2D.
The difference between the hydraulic head values of the 3D and 2D model. y-axis in metres.

APPENDIX E

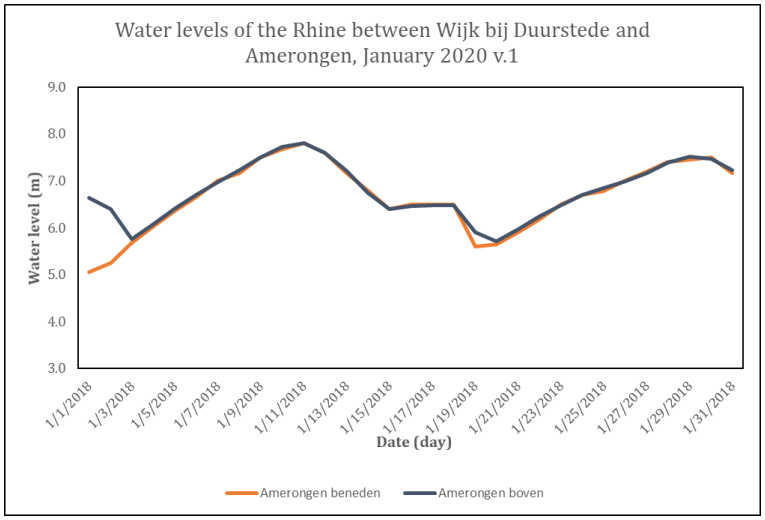

Figure 68: Water stage fictive scenario, water stage is 1 m higher than the real scenario of 2018

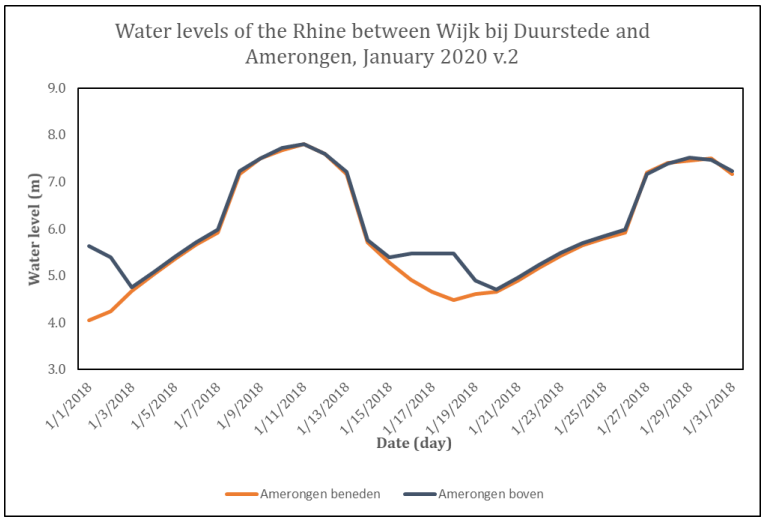

Figure 69: Water stage fictive scenario, water stage 1 m higher than the real scenario of 2018 at the peak discharges in the middle and end of the month.

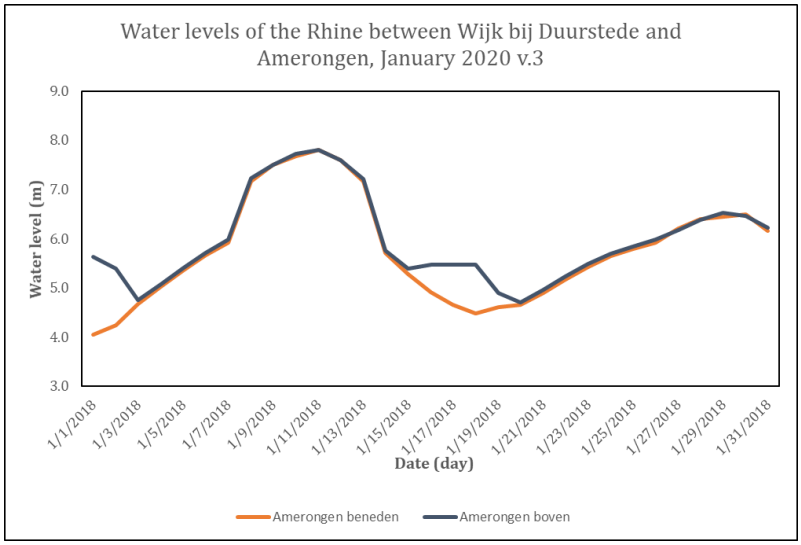

Figure 70: Water stage fictive scenario, water stage 1 m higher than the real scenario of 2018 at the peak discharge in the middle of the month.

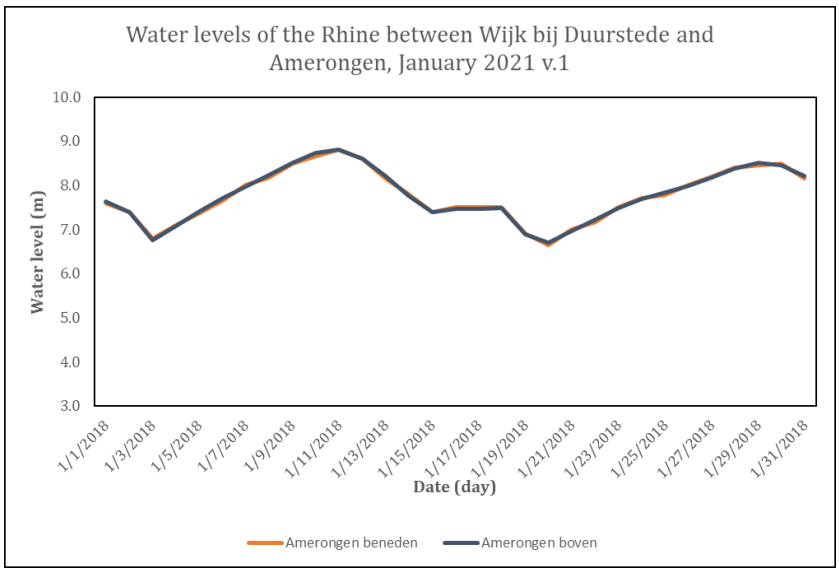

Figure 71: Water stage fictive scenario, water stage is 2 m higher than the real scenario of 2018.

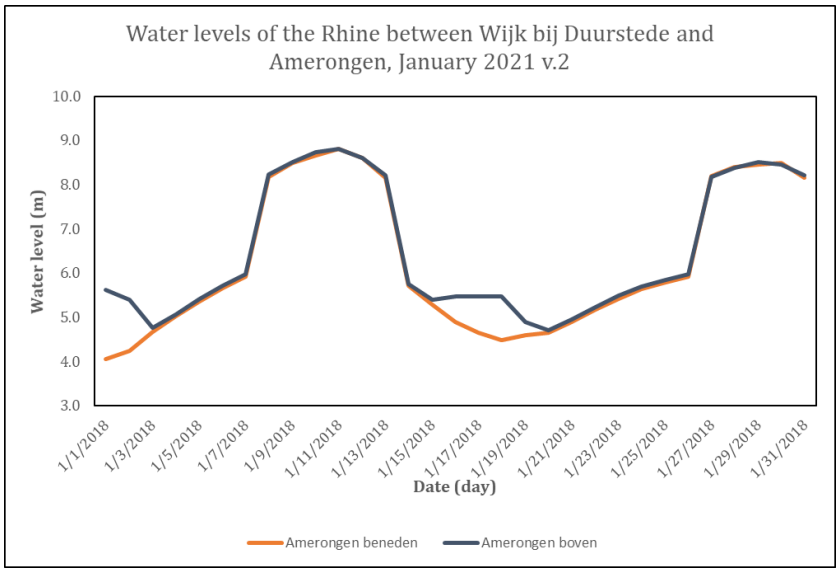

Figure 72: Water stage fictive scenario, water stage 2 m higher than the real scenario of 2018 at the peak discharges in the middle and end of the month.

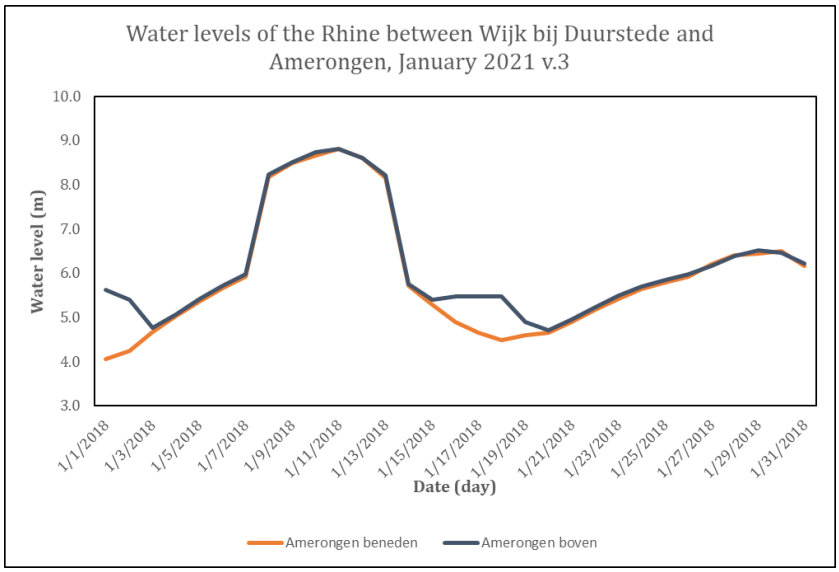

Figure 73: Water stage fictive scenario, water stage 2 m higher than the real scenario of 2018 at the peak discharge in the middle of the month.

APPENDIX F

Table 6: Table of the indication per location per transect if the difference between 2D and 3D are time, depth, or discharge dependent.

Aquifer		Transect 153							Transect 154							Transect 155 upper							Transect 155 lower							Transect 156						
		Difference							Difference							Difference							Difference							Difference						
Head		---	--	-	0	+	++	+++	---	--	-	0	+	++	+++	---	--	-	0	+	++	+++	---	--	-	0	+	++	+++	---	--	-	0	+	++	+++
River	Time dependent																																			
	Depth dependent																										x									
	Discharge dependent			x								x							x								x						x			
River side	Time dependent																							x							x					
	Depth dependent																																			
	Discharge dependent		x								x		x					x			x							x						x		
Foreland land	Time dependent																x			x	x											x	x			
	Depth dependent																																			
	Discharge dependent	x								x																		x						x		
Foreland Channels	Time dependent																	x																		
	Depth dependent																											x								
	Discharge dependent		x							x																		x								
Dike	Time dependent		x														x														x					
	Depth dependent																									x										
	Discharge dependent									x																x						x				
Hinterland	Time dependent		x																x												x					
	Depth dependent																									x										
	Discharge dependent								x																	x						x				

Confining layer		Transect 153							Transect 154							Transect 155														Transect 156						
		Difference							Difference							Difference														Difference						
Pressure		---	--	-	0	+	++	+++	---	--	-	0	+	++	+++	---	--	-	0	+	++	+++								---	--	-	0	+	++	+++
River	Time dependent																																			
	Depth dependent																																			
	Discharge dependent			x								x							x														x			
River side	Time dependent																																x			
	Depth dependent																																			
	Discharge dependent				x						x		x					x			x													x		
Foreland land	Time dependent		x	x													x			x	x											x	x			
	Depth dependent			x						x	x																									
	Discharge dependent									x	x																							x		
Foreland Channels	Time dependent																	x																		
	Depth dependent										x																										
	Discharge dependent		x								x							x																		
Dike	Time dependent			x													x														x					
	Depth dependent			x					x																												
	Discharge dependent								x																							x				
Hinterland	Time dependent			x															x												x					
	Depth dependent								x																												
	Discharge dependent								x																							x				